2009

Cell Size Control And Asymmetric Cell Fates In Start Of The Saccharomyces cerevisiae Cell Cycle

Talia, Stefano Di

Cell size control and asymmetric cell fates in Start of the *Saccharomyces cerevisiae* cell cycle

A Thesis Presented to the Faculty of

The Rockefeller University

in Partial Fulfillment of the Requirements for

the degree of Doctor of Philosophy

by

Stefano Di Talia

June 2009

Cell size control and asymmetric cell fates in Start of the *Saccharomyces cerevisiae* cell cycle

Stefano Di Talia, Ph.D.
The Rockefeller University 2009

Understanding the molecular and biophysical mechanisms that couple the process of cell growth to cell division is one of the major challenges of modern cell biology. *Saccharomyces cerevisiae* (budding yeast) has been an important model organism to study the coupling between cell growth and cell division. The insights obtained from studies of this unicellular organism have been pivotal for related studies in animal systems.

The classical picture that emerged from studies in budding yeast was that cell cycle commitment in G1, at a point called Start, requires growth to a critical cell size. This deterministic model did not address how cell size control can be achieved despite the stochasticity of elementary cellular processes. Furthermore, no clear connection between the commitment at Start and the molecular network controlling the G1/S transition was known.

We developed a novel framework for analyzing the precision of cell size control, by combining single-cell time-lapse imaging of fluorescently labeled cells and rigorous mathematical analysis. This allowed us to quantify the contributions of size control and molecular noise to temporal variability of the G1 phase. Comparing wild-type and mutant strains bearing multiple fluorescent cell cycle markers, we found that Start regulatory dynamics can be decomposed into a size sensing module and a completely

independent timing module. We identified inactivation of the Whi5 repressor as marking the boundary between the two modules and showed that different G1 cyclins, *CLN3* vs. *CLN1* and *CLN2*, control the two modules. We also showed how positive feedback of G1 cyclins *CLN1* and *CLN2* on their own transcription ensures a fast transition between the two modules and a coherent commitment to cell cycle progression.

Difference in cell size at birth is not the only determinant of the differential regulation of Start between mother and daughter cell. Using single-cell analysis, microarrays and chromatin immuno-precipitations we have shown that cell-type specific difference in regulation of Start is also due to regulation of the G1 cyclin *CLN3* by daughter-specific transcription factors Ace2 and Ash1. This work demonstrates how asymmetric localization of cell-fate determinants results in cell-type-specific regulation of the cell cycle in budding yeast.

Questa tesi e’ dedicata alla mia famiglia

Acknowledgements

I am indebted to Professors Frederick Cross and Eric Siggia for their continuous guidance and for many stimulating discussions. Their original insights and approach to science have contributed greatly to my scientific maturity and will continue to inspire me in the future.

I thank my former colleagues Drs. James Bean and Jan Skotheim for enjoyable and productive collaborations that have inspired many of the results I have obtained in the last years.

I thank Dr. Hongyin Wang and Professor Bruce Futcher for a recent collaboration.

I acknowledge discussions with Professors Paul Nurse and Tim Ryan, who have served as members of my thesis committee in the last few years. Their encouragement and suggestions have been crucial for the success of my experimental projects.
I thank Professor Marcelo Magnasco for much good advice and for convincing me to apply to the graduate program of The Rockefeller University.

I thank all the past and current members of the Cross lab who have been wonderful colleagues and have contribute to my scientific maturity. In particular, my thanks go to our lab manager Lea Schroeder for being always helpful and kind and to Jonathan Robbins and Benjamin Drapkin for endless discussions about many aspects of cell cycle control and science in general.

I would like to thank my family for their unconditioned love and support and their ability to be close to me even when far away geographically.

The work presented in this thesis would have not been possible without the love and help of my fiancée Veronica Lubkov.

TABLE OF CONTENTS

LIST OF FIGURES

LIST OF TABLES

Chapter 1: Introduction

Overview. Cells are the basic units of life and their ability to grow and reproduce is at the basis of most biological processes. Cell reproduction occurs by an elaborate series of events, the cell cycle, whereby cells duplicate their chromosomes and distribute them into two newly born cells (Morgan, 2007). The discrete chromosomal processes of duplication and segregation are often coupled to the processes of cell growth (Morgan, 2007). How cells coordinate these processes remains poorly understood (Morgan, 2007). Unicellular organisms, such as *Saccharomyces cerevisiae* (budding yeast), provide ideal experimental models to reveal the basic principles of the coordination of growth and division (Jorgensen and Tyers, 2004). In budding yeast, the rate of cell proliferation is determined by the rate of cell growth and not by the processes of DNA replication and mitosis that can happen on shorter time scales than cell mass doubling time (Johnston et al., 1977). At the core of the mechanism linking the rate of growth to cell division could be the reliance on critical cell size for cell cycle progression (Nurse, 1975). Cell size control imposes that cells cannot traverse a cell cycle transition until they have achieved a critical size. In budding yeast, this point, occurring in the G1 phase, has been indicated as Start and represents a point of commitment to the cell cycle with respect to cell growth/size control and mating factor treatment (Johnston et al., 1977). Pre-Start cells rapidly respond to changes in nutrient conditions and to the presence of pheromone, while post-Start cells are insensitive to nutrient limitation or pheromone with respect to cell cycle progression (Johnston et al., 1977).

Cell size control and cell cycle variability. In budding yeast division is asymmetrical, yielding a bigger mother and a smaller daughter that spends a longer period of time in the G1 phase (Hartwell and Unger, 1977). This delay may be in part determined by cell size or translation rate, as smaller cells spend a longer time in G1 (Hartwell and Unger, 1977; Johnston et al., 1977).

The requirement for a critical size, however, cannot be interpreted deterministically, as the timing of G1 shows substantial variability that is independent of cell size (Lord and Wheals, 1981; Nurse, 1980). This variability may come from molecular noise: noise due to small numbers of key regulatory molecules (Schroedinger, 1944; Spudich and Koshland, 1976). Recently, many studies have shown that gene expression is a noisy process that can generate cell-cell variability. Various insights on the origin of gene expression noise have been obtained (Samoilov et al., 2006). Despite these insights it is unclear what effects noise has on the precision of natural eukaryotic circuits and on the cell cycle in particular. In Chapter 3, we present an analysis decomposing G1 variability into size-dependent variability, which is due to size control and variable cell size at birth, and size-independent variability, which is most likely due to molecular noise in gene expression (Di Talia et al., 2007).

Control of Start and the G1 phase. Genetic and biochemical analyses have decomposed the control of the G1 phase into a cascade of events culminating in activation of budding and S-phase (Jorgensen and Tyers, 2004; Wittenberg and Reed, 2005). The G1/S transition is initiated by the G1 cyclin Cln3 that in complex with the

cyclin-dependent kinase, Cdc28, activates the transcription factors SBF and MBF (Cross, 1995; Dirick et al., 1995; Stuart and Wittenberg, 1995; Tyers et al., 1993). Once active, SBF and MBF activate the expression of more than 100 genes (G1/S regulon) (Spellman et al., 1998). The G1/S regulon, which contains two additional G1 cyclins, *CLN1* and *CLN2*, contributes to DNA replication, budding and spindle pole body duplication (Cross, 1995; Dirick et al., 1995). To reset the cycle, the expression of SBF and MBF is shut off by mitotic cyclins and Nrm1 (Amon et al., 1993; de Bruin et al., 2006). The activation by Cln3 of the G1/S regulon requires the phosphorylation of promoter-bound protein complexes, including SBF/MBF and the transcriptional inhibitor Whi5 (Costanzo et al., 2004; de Bruin et al., 2004; Wijnen et al., 2002).

Cln3 initiates the cell cycle in a dosage-dependent manner and plays an important role in the control of cell size (Cross, 1988, 1995; Nash et al., 1988). Overexpression or deletion of *CLN3* result in small or large cell size respectively (Cross, 1988, 1989; Nash et al., 1988). Whi5 is one of the main targets on Cln3 activity as indicated by the fact that the small cell size phenotype of the *whi5* mutant is largely epistatic to the large cell size phenotype of the *cln3* mutant (Costanzo et al., 2004; de Bruin et al., 2004). Furthermore, Whi5 inactivation seems to be rate limiting for SBF/MBF activation (Costanzo et al., 2004; de Bruin et al., 2004).

G1 cyclins Cln1 and Cln2 also bind with the CDK Cdc28 and drive activation of B-type cyclins, bud emergence and spindle pole body duplication, culminating in the transition

from the G1 to the S phase (Cross, 1995; Dirick et al., 1995). Genetic evidence suggests that Cln1 and Cln2 may drive these events directly (Cross, 1995).

Asymmetric transcriptional programs. Asymmetric cell division in budding yeast yields a larger mother and a smaller daughter cell, which transcribe different genes due to daughter-specific transcription factors, Ace2 and Ash1 (Bobola et al., 1996; Colman-Lerner et al., 2001; Sil and Herskowitz, 1996). It has been shown that daughters are slower to pass Start than mothers even when both are equally large (Lord and Wheals, 1983). This finding points to an additional source of asymmetry, other than cell size, in Start control. In Chapter 4, we show that differential gene expression in mothers and daughters provides such asymmetry.

Daughter-specific localization of Ash1 is achieved through active transport of *ASH1* mRNA to the bud tip and consequent preferential accumulation of Ash1 in the daughter nucleus (Cosma, 2004). Asymmetric localization of Ace2 is due to the Mob2-Cbk1 complex (Colman-Lerner et al., 2001; Mazanka et al., 2008; Weiss et al., 2002), which prevents nuclear export of Ace2 from the daughter nucleus immediately after mitotic exit (Colman-Lerner et al., 2001; Mazanka et al., 2008; Weiss et al., 2002). Ash1 represses expression of the *HO* endonuclease gene responsible for mating type switching (Bobola et al., 1996; Sil and Herskowitz, 1996), thus restricting *HO* expression to mother cells. The transcription factor Ace2 also accumulates specifically in daughter nuclei, where it activates a number of genes (Colman-Lerner et al., 2001).

Coupling observations on asymmetric gene expression and asymmetric G1 control, Ace2 was proposed to cause a daughter-specific G1 delay (Laabs et al., 2003). In that work, it was also proposed that Ace2-dependent delay, due to indirect repression of *CLN3*, is the only determinant of the differences in G1 regulation in mothers and daughters, and that cell size does not play a role in the regulation of G1 (Laabs et al., 2003). This interpretation is incompatible with classical models of Start control and with our analysis presented in Chapter 3 showing that small cells display efficient size control. By analyzing the interaction between daughter-specific transcriptional programs, cell size control, and irreversible commitment to the cell cycle at Start in Chapter 4 we will clarify how asymmetric localization of cell fates determinants results in cell-type-specific regulation of the cell cycle in budding yeast.

Chapter 2: Materials and Methods

Strain and plasmid constructions. Standard methods were used throughout. All strains are of the W303 background. The plasmid pSD03 (pRS403-*CLN2*) was obtained by cloning the SmaI-SfoI fragment containing *CLN2* genomic DNA obtained from the Yep24-*CLN2* 2μ plasmid (J. Mc Kinney unpublished data) at the SmaI site in pRS403. The *CLN2* genomic fragment started 1.4 Kb upstream of *CLN2* open reading frame and ended about 8Kb downstream. A homologous recombination pop-out of the Ty1 (retrotransposon) downstream of *CLN2* was found in the original Yep24-*CLN2* 2μ plasmid. pSD03 was integrated at the *HIS3* locus by BglII digestion. Strain SD27-1-1A was confirmed by Southern blot analysis to have five duplicative integrations of pSD03. The plasmid pJB06T (pRS404-*ACT1pr-DSRED*) was obtained as follows. The *ACT1pr* (~500 bp upstream of *ACT1* open reading frame) was inserted into pTY24 (obtained from NCRR Yeast Resource Center, University of Washington) just upstream of *DSRED* coding sequence. The BamHI-BglII fragment containing *ACT1pr-DSRED* was then inserted at the BamHI site in pRS404. Plasmid pSD02 (pRS406-*ACT1pr-DSRED*) was obtained by cloning the BglI fragment containing *ACT1pr-DSRED* obtained from pJB06T into the BglI fragment containing *URA3* obtained from pRS406. pSD02 was integrated at the *URA3* locus by NcoI digestion. Tetraploid SD-tet was constructed as follows. SD06-A-4A and SD06-B-5D were mated by cell-to-cell mating using a micromanipulator, followed by isolation of the resulting diploid SD09. Mating type switching was induced in SD09 cells, transformed with a 2μ plasmid carrying *GAL-HO* (pJH132, kind gift from Jim Haber), by plating cells on galactose for 4 hours. Purified

single colonies were tested for mating type. Diploids homozygous at the mating locus (a/a and α/α) and that lost the *GAL-HO* plasmid were subsequently mated by micromanipulation to obtain the tetraploid SD-tet. This strain was confirmed to be a true 4N strain by sporulation and dissection of tetrads. Most tetrads gave 4 viable spores; from a few tetrads in which all 4 spores were non-maters, all the progeny were sporulated, yielding on subsequent tetrad analysis haploid MATa or MATα segregants with high viability.

Strain SD20-1A was confirmed by Southern blot analysis to have two duplicative integrations of pSD02. All the other strains that carry pSD02 were obtained by crosses with SD20-1A or with strains derived from it so they also have two duplicative integrations of pSD02. We observed that strains transformed with one copy of pJB06T or two copies of pSD02 behave identically with the only difference that the average intensity of the second reporter is two times larger than the average intensity of the first one, as expected by difference in copy number. A *MYO1-GFP* strain was backcrossed at least 5 times to W303 to obtain the strains used in this paper.

Plasmid pSD07 was constructed by inserting *CLN3* (amplified from yeast genome by PCR) in the pRS405-*CYC1pr* (kind gift of Nicolas Buchler) by XbaI and SalI digestion. Plasmids pSD08, pSD09 and pSD10 were constructed by replacing the *CYC1pr* promoter with the *CDC28pr, ACT1pr* and *ADH1pr*. *ACT1pr* and *CDC28pr* were obtained by PCR amplification of yeast genome, while *ADH1pr* was obtained from pRS405-*ADH1pr* (kind gift of Nicolas Buchler). Plasmid pSD13 was obtained from pSD08 by substituting the

BglII fragment containing the *LEU2* gene with the BglI fragment containing the *HIS3* gene. Plasmid pSD14 was built from plasmid pMM99 (pRS414-*CLN3-9xMYC*, kind gift of Mary Miller) by replacing the BglI fragment containing the *TRP1* gene with the BglI fragment containing the *HIS3* gene, followed by SalI and SwaI digestion and blunt end ligation. Plasmid pSD15 was obtained by subcloning a fragment containing the mutated *CLN3* promoter and part of *CLN3* ORF (kind gift of Adam Rosenbrock and Bruce Futcher) in FC101. Mutations of the Ash1 binding sites on the *CLN3* promoter were introduced by PCR splice overlap of FC101 or pSD15. The PCR reactions were inserted in plasmids pSD16 and pSD17 by XbaI and BclI digestion.

All the strains expressing *CLN3-9xMYC* were generated by transforming in yeast plasmid pSD14 after EcoRI digestion. These strains carry *CLN3-9xMYC* and a truncated not functional *CLN3*. Strains carrying mutations of the Ace2/Swi5 and Ash1 binding sites were generated by transforming in strains SD15-8A and SD15-6C plasmids pSD15, pSD16 and pSD17 after HpaI digestion. Pop-outs were selected on 5'-FOA plates and PCR of the *CLN3* promoter region were analyzed by sequencing.

Mutations of the Ace2/Swi5 and Ash1 putative binding sites on the *CLN3* promoter. We identified in the *CLN3* promoter 3 putative Ace2/Swi5 binding and 2 sites that are over-represented in Ace2 and Swi5 regulated genes (data not shown). We also found 8 putative Ash1 binding sites on the same promoter. We introduced the following mutations of the Ace2/Swi5 putative binding sites (ATG +1): GCCAGCG mutated to GCtAaCG (-1183), TGCTGGC mutated to TGtTaGC (-1016), GGCTGAC mutated to GGtcaAC (-1001), TGCTGAT mutated to TGtTaAT (-766), CCCAGCC

mutated to CCtAaCC (-701). We introduced the following mutations of the Ash1 putative binding sites (ATG +1): ATCAA mutated to ATaAA (-1124), CTGAT mutated to CTtAT (-969), CTGAT mutated to tTaAT (-764), ATCAG mutated to ATaAG (-591), ATCAA mutated to ATaAA (-546), TTGAT mutated to TTtAT (-350), CTGAT mutated to CTtAT (-23), TTGAT mutated to TTtAT (-18).

Name	Genotype	Source
MMY116-2C	MATα ADE2	Mary Miller
SD06-A-4A	MATa *ACT1pr-DSRED::TRP1 MYO1-GFP::KanMX ADE2*	This study
SD06-B-5D	MATα *ACT1pr-DSRED::TRP1 MYO1-GFP::KanMX ADE2*	This study
SD08-C-12A	MATα *cln3::URA3ACT1pr-DSRED::TRP1 MYO1-GFP::KanMX ADE2*	This study
SD08-D-5D	MATa *cln3::URA3 ACT1pr-DSRED::TRP1 MYO1-GFP::KanMX ADE2*	This study
SD09	Diploid MATa/MATα *ACT1pr-DSRED::TRP1 MYO1-GFP::KanMX ADE2*	This study
SD-tet	Tetraploid MATa/MATa/MATα/MATα *ACT1pr-DSRED::TRP1 MYO1-GFP::KanMX ADE2*	This study
SD15-6C	MATa *ACT1pr-DSRED::TRP1 WHI5-GFP::KanMX ADE2*	This study
SD15-8A	MATα *ACT1pr-DSRED::TRP1 WHI5-GFP::KanMX ADE2*	This study
SD20-1A	MATα *2xACT1pr-DSRED::URA3 MYO1-GFP::KanMX 5xCLN3::TRP1 ADE2*	This study
SD21-1-5C	MATα *2xACT1pr-DSRED::URA3 WHI5-GFP::KanMX 5xCLN3::TRP1 ADE2*	This study
SD24-1-5A	MATα *2xACT1pr-DSRED::URA3MYO1-GFP::KanMX ADE2*	This study
SD24-3-6A	MATa *2xACT1pr-DSRED::URA3 MYO1-GFP::KanMX ADE2*	This study
SD27-1-1A	MATα *2xACT1pr-DSRED::URA3 MYO1-GFP::KanMX 5xCLN2::HIS3 ADE2*	This study
SD27-1-2B	MATα *2xACT1pr-DSRED::URA3 MYO1-GFP::KanMX 5xCLN3::TRP1 5xCLN2::HIS3 ADE2*	This study
SD28-3C	MATa *ACT1pr-DSRED::TRP1WHI5-GFP::KanMX cln3::URA3 ADE2*	This study
SD28-5A	MATα *ACT1pr-DSRED::TRP1 WHI5-GFP::KanMX cln3::URA3 ADE2*	This study
SD29-1-2A	MATα *2xACT1pr-DSRED::URA3 WHI5-GFP::KanMX 5xCLN2::HIS3 ADE2*	This study
JS19	MATα *2xACT1pr-DSRED::URA3 MYO1-GFP::KanMX MET3pr-CLN2::TRP1CLN2pr-GFP$_{PEST}$::HIS3 ADE2*	Jan Skotheim
SD57-2D	MATa *ACT1pr-DSRED::TRP1 WHI5-GFP::KanMX ADE2 ace2::URA3*	This study
SD57-3B	MATa *ACT1pr-DSRED::TRP1 WHI5-GFP::KanMX ADE2 ace2::URA3*	This study
SD57-9B	MATα *ACT1pr-DSRED::TRP1 WHI5-GFP::KanMX ADE2 ace2::URA3*	This study
SD76-1-1C	MATα *ACT1pr-DSRED::TRP1 WHI5-GFP::KanMX ADE2 ash1:: KanMX*	This study
SD76-1-5A	MATa *ACT1pr-DSRED::TRP1 WHI5-GFP::KanMX ADE2 ash1:: KanMX*	This study
SD76-3-12B	MATa *ACT1pr-DSRED::TRP1 WHI5-GFP::KanMX ADE2 ash1:: KanMX*	This study
SD58-5-2A	MATa *ACT1pr-DSRED::TRP1 WHI5-GFP::KanMX ADE2 ash1:: KanMX ace2::URA3*	This study

SD33-1D	MATa *ACT1pr-DSRED::TRP1 WHI5-GFP::KanMX ADE2 ace2::HIS3::ACE2G128E::URA3*	This study
SD33-2A	MATa *ACT1pr-DSRED::TRP1 WHI5-GFP::KanMX ADE2 ace2::HIS3::ACE2G128E::URA3*	This study
SD33-5C	MATa *ACT1pr-DSRED::TRP1 WHI5-GFP::KanMX ADE2 ace2::HIS3::ACE2G128E::URA3*	This study
SD50-13C	MATα *ACT1pr-DSRED::TRP1 WHI5-GFP::KanMX ADE2 ash1:: KanMX ASH1-MUT::LEU2*	This study
SD50-11A	MATa *ACT1pr-DSRED::TRP1 WHI5-GFP::KanMX ADE2 Ace2::HIS3::ACE2G128E::URA3 ash1:: KanMX ASH1-MUT::LEU2*	This study
FC2147-7C	MATα *cdc20::LEU2 GALL-CDC20::ADE2*	Frederick Cross
SD59-6C	MATa *cdc20::LEU2 GALL-CDC20::ADE2 ACE2-YFP::URA3*	This study
SD60-4C	MATα *cdc20::LEU2 GALL-CDC20::ADE2 SWI5-GFP::KanMX*	This study
SD62-7C	MATα *cdc20::LEU2 GALL-CDC20::ADE2 ASH1-GFP::KanMX*	This study
SD42-7A	MATα *MYO1-mCherry::HIS5 ACE2-YFP::URA3 ADE2*	This study
SD73-8A	MATa *MYO1-mCherry::HIS5 SWI5-GFP::KanMX ADE2*	This study
SD74-9C	MATa *MYO1-mCherry::HIS5 ASH1-GFP::KanMX ADE2*	This study
JB55-4C	MATα *cdc20::LEU2 GALL-CDC20::ADE2 ace2::URA3*	James Bean
JB55-8A	MATa *cdc20::LEU2 GALL-CDC20::ADE2 swi5::KanMX*	James Bean
JB55-13C	MATα *cdc20::LEU2 GALL-CDC20::ADE2 swi5::KanMX ace2::URA3*	James Bean
SD49-1-1B	MATα *cdc20::LEU2 GALL-CDC20::ADE2 ace2::HIS3::ACE2G128E::URA3*	This study
SD51-10B	MATa *cdc20::LEU2 GALL-CDC20::ADE2 ash1:: KanMX HOpr-CAN1 HOpr-ADE2*	This study
SD51-12B	MATa *cdc20::LEU2 GALL-CDC20::ADE2 ash1:: KanMX ASH1-MUT::LEU2 HOpr-CAN1 HOpr-ADE2*	This study
SD52-2A	MATa *cdc20::LEU2 GALL-CDC20::ADE2 ACE2-TAP::HIS3*	This study
SD53-3B	MATα *cdc20::LEU2 GALL-CDC20::ADE2 SWI5-TAP::HIS3*	This study
SD72-9C	MATa *cdc20::LEU2 GALL-CDC20::ADE2 ASH1-TAP::HIS3*	This study
SD65-1	MATa *ACT1pr-DSRED::TRP1 WHI5-GFP::KanMX CLN3-9xMYC::HIS3 ADE2*	This study
SD65-2	MATa *ACT1pr-DSRED::TRP1 WHI5-GFP::KanMX CLN3-9xMYC::HIS3 ADE2*	This study
SD66-1	MATa *ACT1pr-DSRED::TRP1 WHI5-GFP::KanMX ACT1pr-CLN3-9xMYC::HIS3::LEU2 ADE2*	This study
SD66-2	MATa *ACT1pr-DSRED::TRP1 WHI5-GFP::KanMX ACT1pr-CLN3-9xMYC::HIS3::LEU2 ADE2*	This study
SD67-1	MATa *ACT1pr-DSRED::TRP1 WHI5-GFP::KanMX ADH1pr-CLN3-9xMYC::HIS3::LEU2 ADE2*	This study
SD67-2	MATa *ACT1pr-DSRED::TRP1 WHI5-GFP::KanMX ADH1pr-CLN3-9xMYC::HIS3::LEU2 ADE2*	This study
SD71-1	MATa *ACT1pr-DSRED::TRP1 WHI5-GFP::KanMX CDC28pr-CLN3-9xMYC::HIS3::LEU2 ADE2*	This study
SD71-2	MATa *ACT1pr-DSRED::TRP1 WHI5-GFP::KanMX CDC28pr-CLN3-9xMYC::HIS3::LEU2 ADE2*	This study
SD75-1	MATα *ACT1pr-DSRED::TRP1 WHI5-GFP::KanMX cln3::URA3 CDC28pr-CLN3::LEU2 5xCDC28pr-CLN3::HIS3 ADE2*	This study
SD75-3	MATα *ACT1pr-DSRED::TRP1 WHI5-GFP::KanMX cln3::URA3 CDC28pr-CLN3::LEU2 3xCDC28pr-CLN3::HIS3 ADE2*	This study

SD54-1	MATα *ACT1pr-DSRED::TRP1 WHI5-GFP::KanMX cln3::URA3 ADH1pr-CLN3::LEU2 ADE2*	This study
SD54-2	MATα *ACT1pr-DSRED::TRP1 WHI5-GFP::KanMX cln3::URA3 ADH1pr-CLN3::LEU2 ADE2*	This study
SD80-1	MATa *ACT1pr-DSRED::TRP1 WHI5-GFP::KanMX ADE2 Ace2/Swi5 binding sites deleted on the CLN3 promoter*	This study
SD80-2	MATα *ACT1pr-DSRED::TRP1 WHI5-GFP::KanMX ADE2 Ace2/Swi5 binding sites deleted on the CLN3 promoter*	This study
SD81-1	MATa *ACT1pr-DSRED::TRP1 WHI5-GFP::KanMX ADE2 Ash1 binding sites deleted on the CLN3 promoter*	This study
SD81-2	MATα *ACT1pr-DSRED::TRP1 WHI5-GFP::KanMX ADE2 Ash1 binding sites deleted on the CLN3 promoter*	This study
SD82-1	MATa *ACT1pr-DSRED::TRP1 WHI5-GFP::KanMX ADE2 Ace2/Swi5 and Ash1 binding sites deleted on the CLN3 promoter*	This study
SD82-2	MATα *ACT1pr-DSRED::TRP1 WHI5-GFP::KanMX ADE2 Ace2/Swi5 and Ash1 binding sites deleted on the CLN3 promoter*	This study

Table 2.1 Strain list. All strains are congenic W303 (*leu2-3,112 his3-11,15 ura3-1 trp1-1 can1-1*).

Name	Description	Construction
pJB06T	pRS404-*ACT1pr-DsRed*	see above
pTY24	DsRed source plasmid	NCRR Yeast Resource Center, University of Washington
pSD02	pRS406-*ACT1pr-DsRed*	see above
pSD03	pRS403-*CLN2*	see above
pJH132	YCp50-*GAL-HO*	kind gift from Jim Haber
p405CYC1	pRS405-*CYC1pr*	Nicolas Buchler
pSD07	pRS405-*CYC1pr-CLN3*	see above
pSD08	pRS405-*CDC28pr-CLN3*	see above
pSD09	pRS405-*ACT1pr-CLN3*	see above
p405ADH1	pRS405-*ADH1pr*	Nicolas Buchler
pSD10	pRS405-*ADH1pr-CLN3*	see above
pSD13	pRS403-*CDC28pr-CLN3*	see above
pMM99	pRS414-*CLN3-9xMYC*	Mary Miller
pSD14	pRS403-truncated *CLN3-9xMYC*	see above
FC101	YCp50 without centromere +6.5 Kb *CLN3* genomic region	Fred Cross
pSD15	FC101 with Ace2/Swi5 sites on the *CLN3* promoter mutated	see above
pSD16	FC101 with Ash1 sites on the *CLN3* promoter mutated	see above
pSD17	FC101 with Ace2/Swi5 and Ash1 sites on the *CLN3* promoter mutated	see above

Table 2.2 Plasmid list

Time-lapse microscopy. Preparation of cells and time-lapse microscopy were performed as previously described (Bean et al., 2006). Detection of GFP and DsRed fluorescence was by illumination with a 100 W short arc mercury lamp type 103 W/2. Illumination was passed through a Chroma neutral density filter ND 2.0 allowing 1% transmission and either a Chroma EGFP filter set #41001 (peak excitation wavelength at 480 nm, peak emission at 535 nm) or a Chroma TRITC filter set #41002c (peak excitation wavelength at 545 nm, peak emission at 620 nm). The frame rate was 1frame/3min for cells grown in glucose and 1frame/6min for cells grown in glycerol/ethanol. The exposure time was 1 second for GFP and 0.35 seconds for DsRed for cells grown in glucose and 0.4 seconds for GFP and 0.1 seconds for DsRed for cells grown in glycerol/ethanol (cells grown in glycerol/ethanol were more sensitive to light damage). Fluorescent images of strains grown in glycerol/ethanol were acquired by 2x2 binning of camera pixels, which allows detection of Myo1-GFP and Whi5-GFP using reduced exposure times. With these exposures the two chromophores were well separated and we did not observe any significant photo-toxicity or perturbations of cell cycle timing except for a few sporadic cells having a long budded period, perhaps due to damage from illumination. These events did not affect our quantitative or qualitative results.

Image analysis. Automated image segmentation and fluorescence quantification of yeast grown under time-lapse conditions and semi-automated assignment of microcolony pedigrees were performed as previously described. Budding and division were scored by visual inspection for the appearance and disappearance of the Myo1-GFP signal at the

bud neck. The detection of the Myo1-GFP signal was facilitated by setting pixels whose value was smaller than a suitably chosen threshold (median+1.5 standard deviations of cell fluorescence values) to zero (black color). The remaining pixels were plotted in gray scale with white color assigned to the highest pixel value. The ring disappearance was easy to score. Myo1-GFP appearance at the bud neck was usually detected for the first time 6-9 minutes before budding could be scored by visual inspection. Uncertainty in the ring appearance was confined to 1-2 frames for most cells. Occasional cells that budded upwards in the middle of the colony were hard to score. We consistently decided not to score cells for which the uncertainty on the ring appearance was bigger than 2-3 frames. The nuclear residence of Whi5-GFP was scored by visual inspection of composite phase contrast-fluorescent movies and confirmed by the method described for Myo1-GFP detection.

Data analysis. Time-lapse fluorescence microscopy and microarray data were analyzed with custom software written in MATLAB software (see Appendix for detail on the analysis of fluorescence-based measurements of cell size). For cluster analysis, the $\log_2$ of the arrays data or of the subtracted arrays data were hierarchically clustered by agglomerative algorithm (Eisen et al., 1998). Data were visually presented using JavaTreeView.

Cell cycle synchronization. YEP medium was used for all the cell cycle synchronization experiments, supplemented with the appropriate carbon source as indicated below. Cell-cycle synchronization was achieved by the *cdc20 GALL-CDC20*

block release by growing cells to early log phase in YEP + galactose (3%) and then filtering them and growing them in YEP + glucose (2%) for 3 hr to arrest cells in metaphase. Cells were released from the block by filtering back into YEP + galactose (3%). *GALL* is a truncated version of the *GAL1* promoter that shows inducible but significantly lower expression than the full-length *GAL1* promoter (Mumberg et al., 1994).

Gene arrays. Microarrays were performed at the Stony Brook Microarray facility as previously described (Oliva et al., 2005).

Chromatin immunoprecipitations. Chromatin immunoprecipitations (ChIP) were performed by Hongyin Wang (Di Talia et al., in preparation).

Chapter 3: Size control and molecular noise in Start of the budding yeast cell cycle.

Control of the G1 phase in the budding yeast cell cycle has been classically attributed to a size sensing mechanism that assures that cells progress through a commitment point in G1, called Start, after having achieved a critical size or translation rate (see Chapter 1). However, cell cycle intervals in budding yeast exhibit substantial variability even when cell size is taken into account (Wheals, 1982). In this Chapter, we present a quantitative characterization of the roles of cell size control and molecular noise in generating and controlling variability of the G1 phase of the cell cycle. We show that variability in G1 decreases with the square root of the ploidy, consistent with simple stochastic models for molecular noise and that increasing G1 cyclin gene dosage also decreases G1 variability. By using a novel single-cell reporter for cell size we determine the contribution to temporal G1 variability of deterministic size control (i.e. smaller cells extending G1) and molecular noise. Size-independent (molecular) noise is the largest quantitative contributor to G1 variability. We finally show that Start regulatory dynamics can be decomposed into two independent modules, a size sensing module and a timing module, each predominantly controlled by different G1 cyclins.

The effects of molecular noise on the variability of cell cycle timing. Molecular noise in gene expression (Samoilov et al., 2006) of critical regulatory molecules, due to small numbers of molecules (e.g. transcription factors bound or not bound to promoters, small numbers of mRNA molecules), could in principle be a significant generator of cell

cycle variability. To study if noise in gene expression generates significant cell cycle variability, we measured the variability of cell cycle timing in yeast cells of different ploidy. Doubling ploidy is known to double the average content of all cellular constituents (RNA, protein, etc.); cell volume also doubles, so that average concentrations remain constant. If stochastic variations in small numbers of molecules control noise in gene expression (Schroedinger, 1944; Spudich and Koshland, 1976), then doubling the average should reduce the noise (standard deviation divided by the mean) in gene expression by about √2. This prediction follows from the fact that for a large class of stochastic processes (such as Poisson or Bernoulli processes) the standard deviation increases as √n, where n indicates the number of molecules. As a consequence, the variability scales as 1/√n. We can therefore predict that doubling ploidy will reduce variability in gene expression by about √2 resulting in reduction of the cell cycle noise by a similar factor, if molecular noise in gene expression contributes significantly to overall cell cycle variability.

We measured times from cytokinesis to budding (G1) and from budding to cytokinesis in haploids, diploids or tetraploids (mothers and daughters), using time-lapse fluorescence microscopy of strains expressing Myo1-GFP. Myo1 forms a ring at the new bud neck (Bi et al., 1998) (concomitant with initiation of DNA replication (Johnston et al., 1977)), which disappears at cytokinesis (Bi et al., 1998) (Figure 3.1, Table 3.1). G1 variability is reduced in both mothers and daughters by about the expected factor of √2 for each ploidy doubling (Figure 3.1, Table 3.2, Figure 3.2). Thus molecular noise may

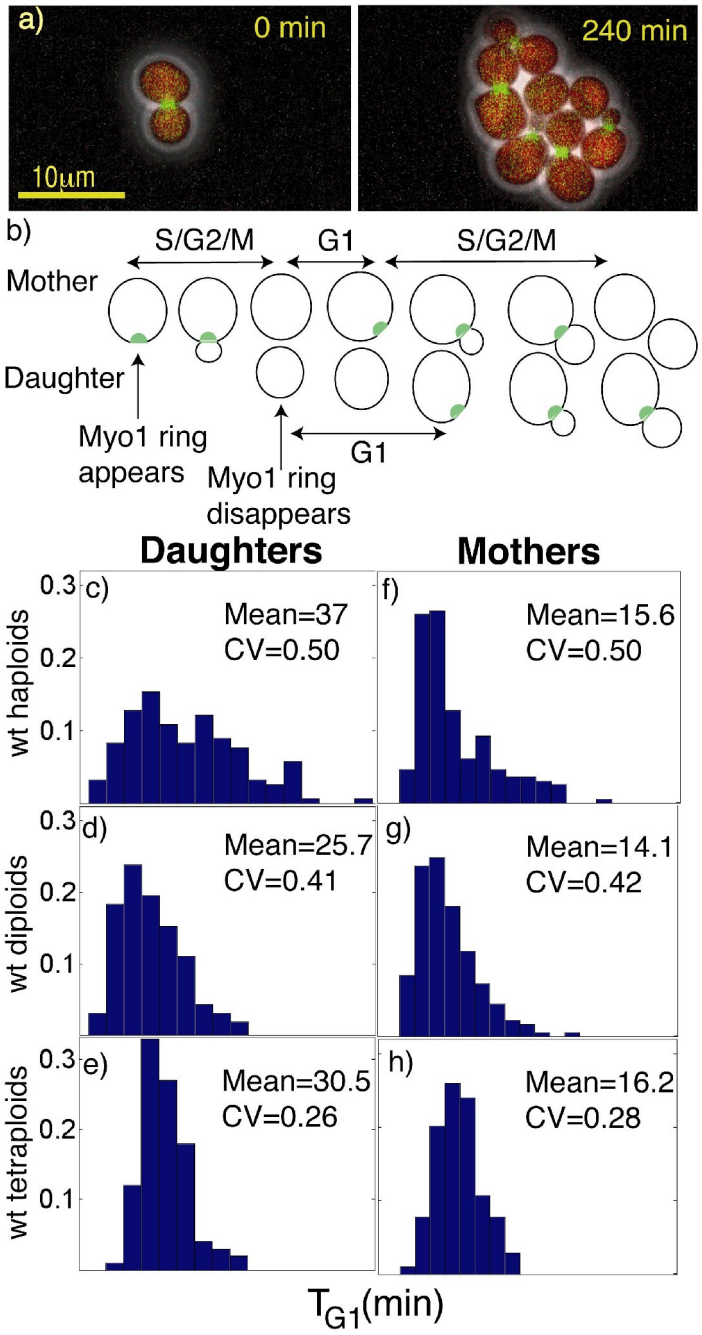

Figure 3.1 Noise in G1 duration is reduced by increased ploidy. a) Composite phase contrast, Myo1-GFP and *ACT1pr*-DsRed images for haploid cells, b) Illustration of measured intervals. (c-h): Frequency histograms (n from 87-202) of the duration of G1 for wild-type haploid (c,f), diploid (d,g) and tetraploid (e,h), daughters (c,d,e) and mothers (f,g,h). Insets: average and the coefficient of variation (CV: the standard deviation divided by the mean, a standardized noise measure).

	Haploids	**Diploids**	**Tetraploids**
G1 daughter	37±2 (158)	25.7±0.8 (164)	30.5±0.8 (100)
Budded period daughter	76±2 (97)	81±1 (95)	82±2 (52)
G1 mother	15.6±0.5 (202)	14.1±0.4 (184)	16.2±0.4 (104)
Budded period mother	72±1 (116)	71±1 (105)	74±2 (54)
Total cycle daughter	112±3(97)	106±2 (95)	113±2 (52)
Total cycle mother	87±1 (116)	85±1 (105)	90±2 (54)

Table 3.1 Average cell cycle periods for cells of different ploidy. The table shows the mean +/- standard error of the mean in minutes with the number of observations reported in parenthesis.

Coefficient of variation	**Haploids**	**Diploids**	**Tetraploids**
G1 daughter	0.50±0.05 (158)	0.41±0.04 (164)	0.26±0.03 (100)
Budded period daughter	0.20±0.06 (97)	0.17±0.05 (95)	0.15±0.04 (52)
G1 mother	0.50±0.05 (202)	0.42±0.4 (184)	0.28±0.03 (104)
Budded period mother	0.17±0.02 (116)	0.16±0.02 (105)	0.15±0.02 (54)
Total cycle daughter	0.22±0.02(97)	0.16±0.01 (95)	0.14±0.02 (52)
Total cycle mother	0.14±0.01 (116)	0.13±0.02 (105)	0.14±0.02 (54)

Table 3.2 Coefficient of variation of cell cycle periods for cells of different ploidy. The number of observations is reported in parenthesis.

be a major source of G1 variability. In marked contrast, variability in the time from budding to cytokinesis is nearly unaffected by ploidy (Table 3.2). These results suggest that molecular noise is a major contributor to the variability of the G1 phase of the cell cycle, but that other sources of noise, such as morphological transitions, may play an important role in determining the timing of the budded phase (approximately S/G2/M).

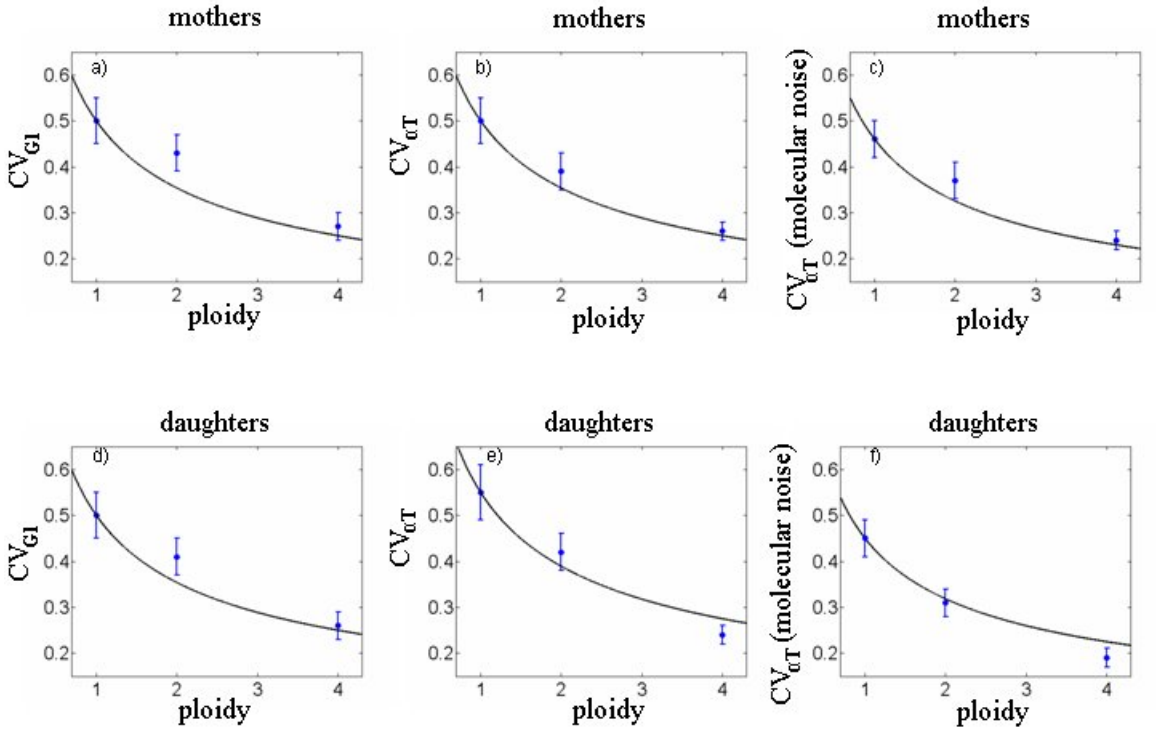

Figure 3.2 Molecular noise is responsible for most of the fluctuations of the duration of G1 period. Plot of the noise (coefficient of variation: CV) as a function of ploidy for the duration of G1 (CV_{G1}), for the duration of G1 scaled to the growth rate, $CV_{\alpha T}$ and for the portion of this noise that is size and growth rate-independent and can be attributed to molecular noise (see Table 3.7) (i.e., this is variation about the αT vs. $\ln(M_{birth})$ line for cells of varying ploidy). The black lines are curves ~1/√ploidy.

Noise in the expression of G1 cyclins contributes to the variability of G1. The magnitude and ploidy sensitivity of G1 noise suggest that the noise might be due to small variable numbers of key regulatory molecules. G1 cyclins (Cln1, Cln2 and Cln3) control average G1 duration (see Chapter 1). Cln3, in complex with the Cdc28 Cdk, is the most upstream activator of Start. Cln3/Cdc28 promotes the transcription of G1 cyclins *CLN1*

and *CLN2* as well as many other genes (Koch et al., 1996; Spellman et al., 1998; Wijnen et al., 2002). Cln1,2/Cdc28 complexes drive bud emergence, microtubule organization center duplication and activation of B type cyclins which initiate DNA replication (Cross, 1995; Dirick et al., 1995).

Since G1 cyclins are expressed at a few mRNA transcripts per cell (Holstege et al., 1998), molecular noise in their expression could account for G1 variability, and its ploidy-dependent reduction. If this is so, integration of multiple copies of G1 cyclin genes in a haploid genome should reduce the variability of G1, by reducing variability in the expression of these critical genes, even while all other genes remain at single copy.

We quantified cell cycle time variability in haploid strains containing integrated arrays of 5 copies of *CLN3*, 5 copies of *CLN2*, or both, in addition to the normal copies. A strain carrying 6 copies of *CLN3* exhibited strongly reduced G1 variability in daughter cells, but mother cell G1 variability was much less affected (Figure 3.3). In contrast, G1 variability in a strain with six copies of *CLN2* showed a very strong reduction of noise in mother cells but a smaller reduction of noise in daughter cells (Figure 3.3). Noise in a strain having six copies of both *CLN3* and *CLN2* is reduced in both mothers and daughters (Figure 3.3).

Figure 3.3 Noise in G1 duration is reduced by increasing the number of copies of G1 cyclins. a), A map of the core molecular network driving Start. Histograms of the G1 duration for daughters: wt (b), *6xCLN3* (c), *6xCLN2* (d), *6xCLN3 6xCLN2* (e). Histograms of the G1 duration for mothers: wt (f), *6xCLN3* (g), *6xCLN2* (h), *6xCLN3 6xCLN2* (i). For every histogram we report the number of measurements, the average G1 duration and the coefficient of variation (standard deviation divided by the mean).

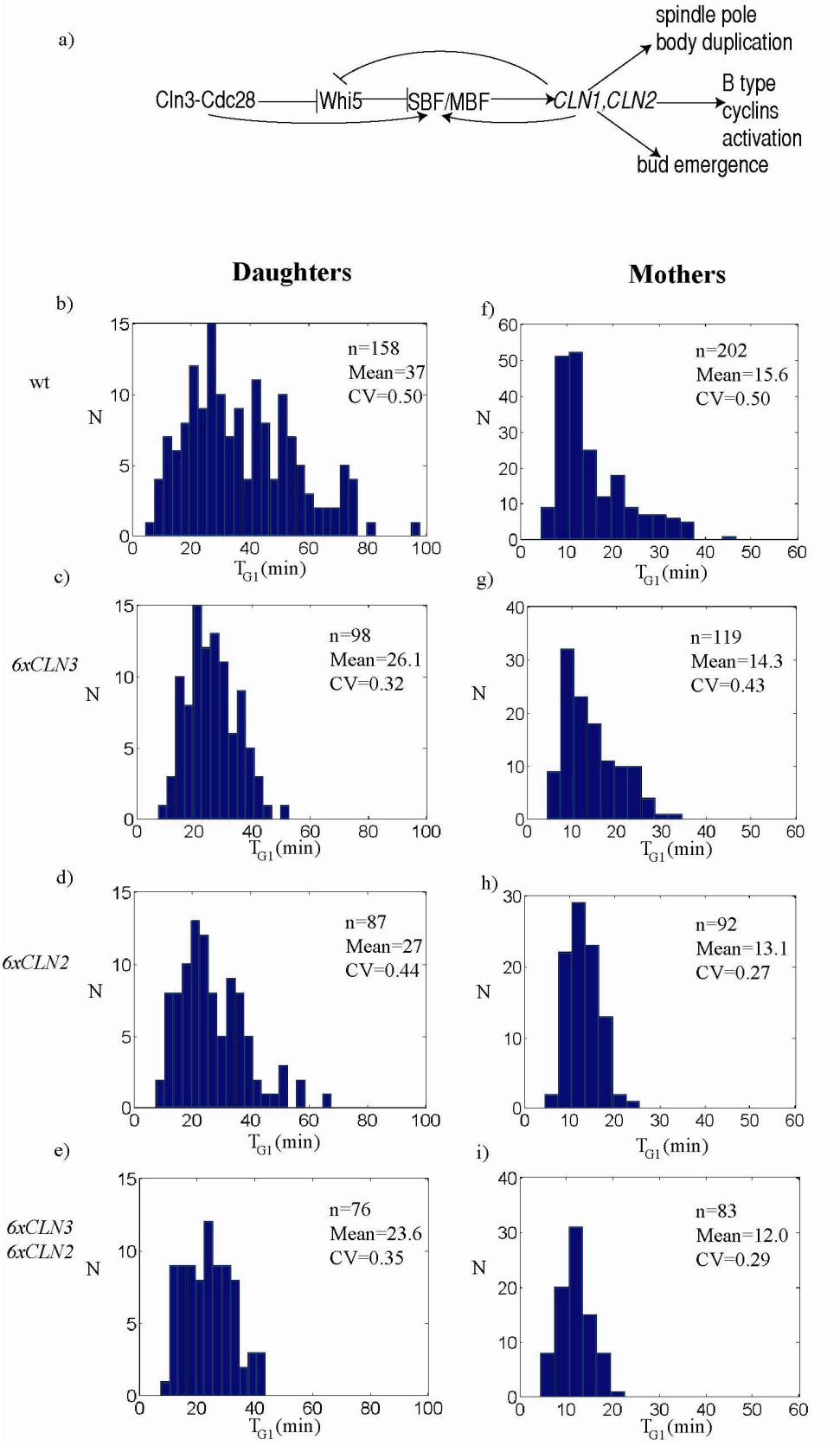
a)
Cln3-Cdc28
Whi5
SBF/MBF
CLN1,CLN2
spindle pole body duplication
B type cyclins activation
bud emergence
Daughters
Mothers
b)
wt
n=158
Mean=37
CV=0.50
f)
n=202
Mean=15.6
CV=0.50
c)
6xCLN3
n=98
Mean=26.1
CV=0.32
g)
n=119
Mean=14.3
CV=0.43
d)
6xCLN2
n=87
Mean=27
CV=0.44
h)
n=92
Mean=13.1
CV=0.27
e)
6xCLN3
6xCLN2
n=76
Mean=23.6
CV=0.35
i)
n=83
Mean=12.0
CV=0.29
N
T_G1(min)

Whi5 enters the nucleus late in mitosis, about 6 minutes before cytokinesis (Figure 3.4), and Cln3/Cdc28 initiates Whi5 nuclear exit and SBF/MBF activation in the succeeding cell cycle (Costanzo et al., 2004; de Bruin et al., 2004). We used a Whi5-GFP fusion (Bean et al., 2006; Costanzo et al., 2004) to quantify the timing of Whi5 nuclear residence in mothers and daughters (Figure 3.4). In mother cells, Whi5 exits the nucleus within few minutes after cytokinesis (Table 3.3) and as a consequence the length of G1 in mothers is mainly determined by the post-Whi5 nuclear exit period. Daughter cells, in contrast, exhibit a significant duration of Whi5 nuclear residence (20 min on average). This period was reduced to 10 min in *6X CLN3* daughters; in *6X CLN2* daughters Whi5 nuclear residence was closer to that in wild-type (16 min). Consistent with previous data (Bean et al., 2006), deletion of *cln3* significantly increased average Whi5 nuclear residence time in both mothers and daughters (average 13 and 30 min respectively). The latter result indicates that Cln3 is functioning in both mothers and daughters to drive Whi5 nuclear exit, but that the Cln3 requirement is attained almost immediately upon cell division in mothers, while requiring a significant period in daughters.

The observations on Whi5 nuclear residence in mothers and in daughters of differing G1 cyclin gene dosage can be integrated with the observations on the effects of G1 cyclin dosage on variability of G1 by the following model. We propose a decomposition of Start into two steps, a Cln3-dependent step (fast in mothers, slow in daughters), the conclusion of which is marked by Whi5 nuclear exit, and a Cln2-dependent step that may have similar duration and variability in mothers and daughters. In daughters, the durations of the pre-Whi5 exit and post-Whi5 exit periods are highly variable and

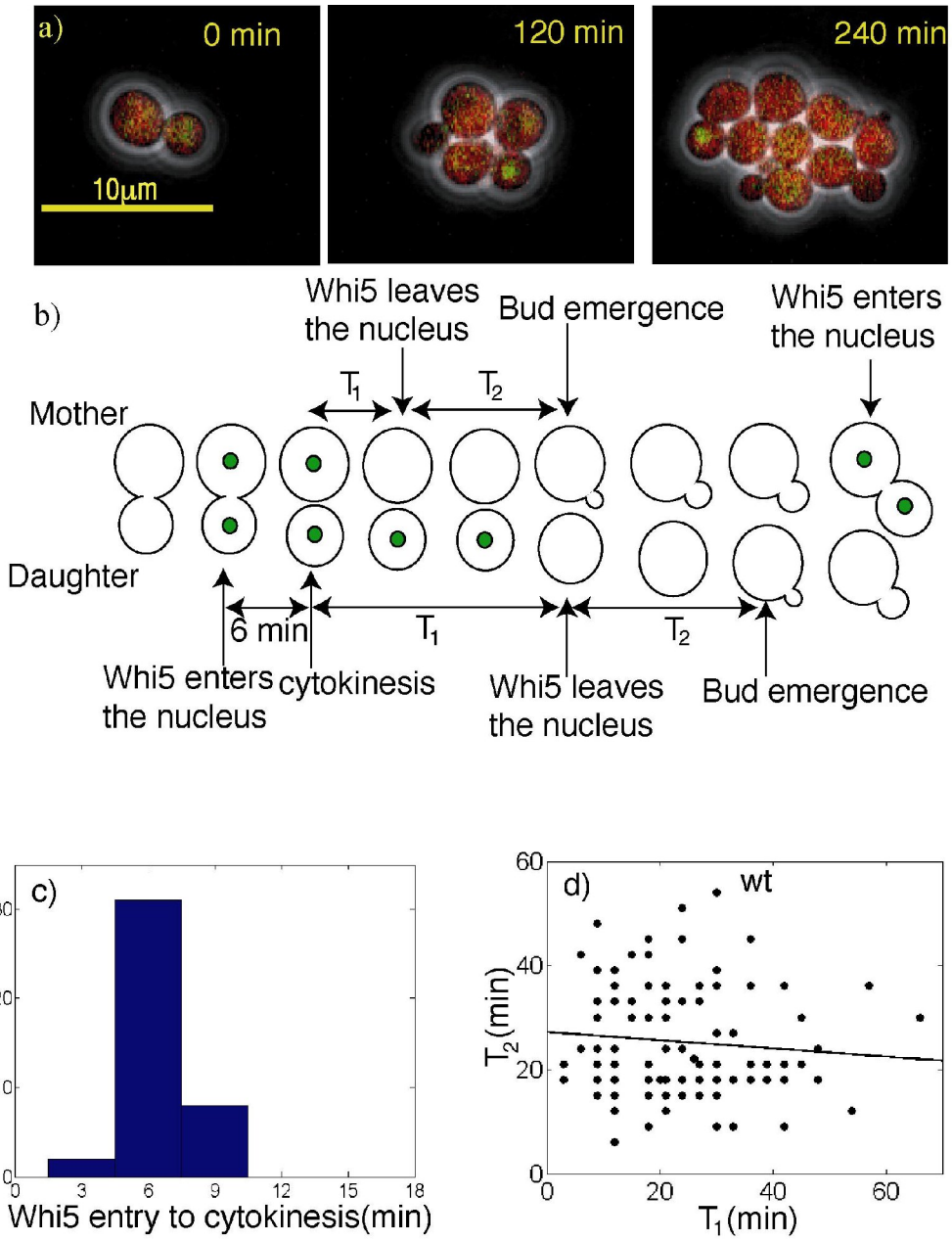

Figure 3.4 The regulation of Whi5 nuclear residence. a) Composite phase contrast, Whi5-GFP and *ACT1pr*-DsRed images for haploid cells; Whi5-GFP is mostly observed in new-born daughter cells; b) Diagram of the measured intervals; T_{G1} (Figure 3.1) is approximately $T_1 + T_2$. c) Histogram of the duration of the interval from Whi5 nuclear entry to Myo1 disappearance. d) Scatter plot of T_1 and T_2 for daughter cells, showing that they are uncorrelated.

	wt	*cln3*	*6xCLN3*	*6xCLN2*
T_1 in daughters	20±1 (157)	30±4 (47)	10±1 (53)	16±1 (80)
T_1 in mothers	0.9±0.3 (170)	13±1 (55)	0.7±0.5 (56)	1.1±0.4 (90)
T_2 in daughters	17±2 (157)	14±2 (47)	16±1 (53)	11±1 (80)
T_2 in mothers	14.7±0.6 (170)	13±1 (55)	13.6±0.8 (56)	12.0±0.6 (90)

Table 3.3 Average durations of the period from cytokinesis to Whi5 nuclear exit (T_1) and the period from Whi5 exit to bud emergence (T_2) in different strains. T_1 and T_2 are diagrammed in Figure 3.4. Mean +/- standard error of the mean in minutes (number of observations).

independent (correlation coefficient -0.1, see Figure 3.4), consistent with Whi5 exit marking the boundary between two separate steps. This model accounts for *CLN3*-dependent reduction of G1 noise preferentially in daughters, because the pre-Whi5-exit period is very short in mothers; *CLN2*-dependent reduction of G1 noise preferentially in mothers could come about because almost the entire G1 period in mothers is dependent on *CLN2*, while only a portion of G1 in daughters is affected by *CLN2*.

A new metric for the analysis of cell size control. The previous analysis was based solely on timing; however, cell size has long been proposed as a deterministic regulator of Start (Hartwell and Unger, 1977; Johnston et al., 1977; Jorgensen and Tyers, 2004). While traditional analysis of yeast cell size has been largely based on cell volume, we were concerned that cell volume does not directly reflect intra-cellular protein content; in cells with large vacuoles, this will clearly not be the case (Han et al., 2003). Therefore, to provide a protein-based single cell marker of cell size, we placed the DsRed Red Fluorescent Protein under control of the constitutive, strongly expressed *ACT1* promoter. Assuming that DsRed transcript accumulates and is translated in parallel with bulk

cellular mRNA, then total red fluorescence per cell will reflect total cell protein content (see Appendix). Quantifying total red fluorescence per cell using the semi-automated image analysis program described previously (Bean et al., 2006), we observed exponential growth in single cells (Figure 3.5a; see Appendix), as deduced previously from pulse-labeling of size-selected populations (Elliott and McLaughlin, 1978). The single-cell growth rate α is moderately variable, but its average agrees well with the bulk culture growth rate (Figure 3.5b, see Appendix). Total red fluorescence scales linearly with ploidy (Table 3.4) and with geometric estimates of cell size (see Appendix). However, using our methods, DsRed fluorescence is a more reliable indicator of cell size than geometric volume estimation (see Appendix). Total red fluorescence for a colony increases exponentially (Figure 3.5c), so changes in the microenvironment do not interfere with these measurements. These results support the use of total red fluorescence from *ACT1pr-DsRed* as a single-cell marker for cell size.

Size control at Start would require smaller cells to prolong G1 for growth, thereby linking birth-size and G1 duration. Given exponential growth, the size at budding, M_{bud}, is related to the size at birth M_{birth}, through the amount of time spent in G1 via the simple formula: $M_{bud} = M_{birth}\, e^{\alpha T\_G1}$, where α is the growth rate for exponential growth. This expression yields: $\alpha T_{G1} = \ln(M_{bud}) - \ln(M_{birth})$. Plotting correlations between αT_{G1} and $\ln(M_{birth})$ allows us to distinguish between two classical concepts for G1 control: timers and sizers (Donnan and John, 1983; Sveiczer et al., 1996). If G1 duration is under control of a timer, then αT_{G1} is independent of cell size at birth, and the slope of the linear

fit of the plot of αT_{G1} vs. $\ln(M_{birth})$ will be 0. In contrast, if G1 is controlled by a sizer, all cells

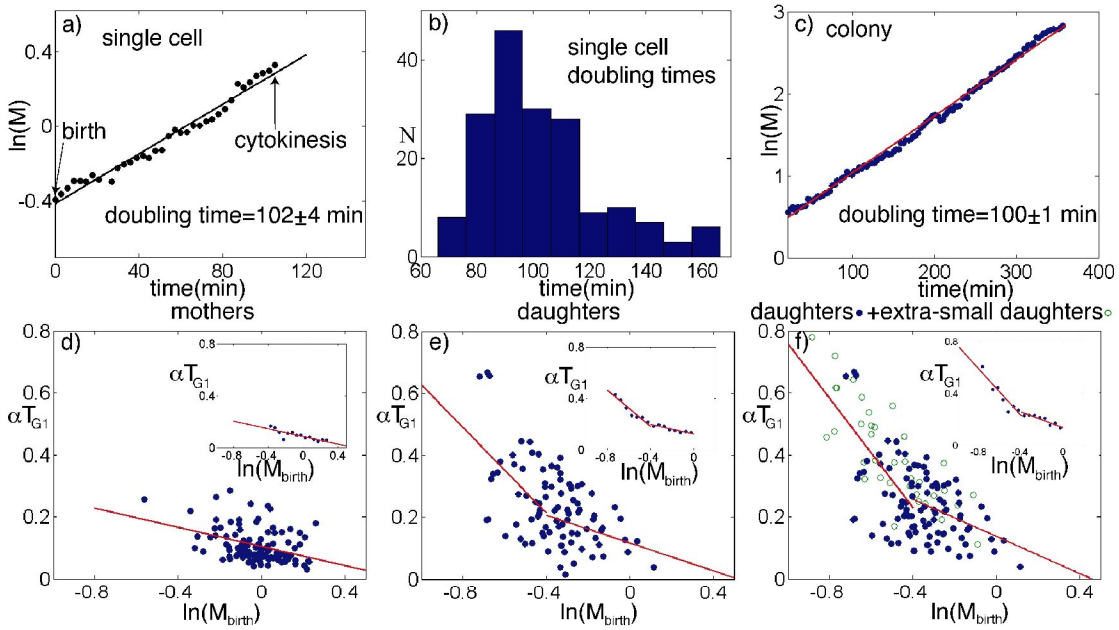

Figure 3.5 The correlation between cell size and G1 duration demonstrates a noisy size control operative in daughters. a) Logarithm of total DsRed fluorescence (M) per cell in a single representative cell from birth to cytokinesis. Doubling time is ln(2)/α; α is the slope of this line; b) haploid cell doubling time distribution. c) Total DsRed fluorescence in an entire colony over time; d, e) correlation between αT_{G1} (growth-rate-standardized time in G1) and ln(M) for haploid mothers (d) and daughters (e) at birth ('$\ln(M_{birth})$') (insets: binned data); f) the data from (e) (solid blue dots), supplemented with data from unusually small wild-type haploid daughters (open green circles), generated using essentially the method of Dirick et al. (1995). Statistical analysis and estimated slopes in Tables 3.5 and 3.6.

will bud at the same size M_{bud}, independent of their size at birth, implying that the slope of the linear fit of αT_{G1} vs. $\ln(M_{birth})$ will be -1 (Sveiczer et al., 1996).

For the following analysis, rigorous statistical testing of fits and estimated slopes are reported in Tables 3.5, 3.6. Scaled G1 duration in mother cells is essentially independent of cell size (slope ≈ -0.1), demonstrating 'timer' control of mother G1 (Figures 3.5d, 3.8). Daughters, in contrast, demonstrate significant size control (slope ≈ -0.4). Binning the daughter data (Figure 3.5e inset) suggested decomposition into two segments, one for small newborn daughters (< 67% of the average budding size), in which an efficient sizer was deduced (slope ≈ -0.7), and a second segment for larger-born daughters showing much less dependence on cell size (slope ≈ -0.3) (Figure 3.5e, 3.9). Statistical confidence in this decomposition was limited by the small number of very small daughters obtained; therefore, we employed the genetic method of Dirick et al. (1995) to make unusually small wild-type daughter cells by transient expression of conditional *MET3pr-CLN2* (Dirick et al., 1995). Inclusion of these data (Figure 3.5f) provided strong statistical support for the 2-slope model (linear fit: $P<0.05$; 2-slope fit: $P>0.7$, see also Table 3.5). These observations are robust to changes in nutrient conditions: growth of cells in glycerol/ethanol instead of glucose, resulting in slow growth and generation of very small newborn daughter cells, gave quantitatively similar results, supporting a two-slope model for daughter G1 control (Figure 3.6, Table 3.5). Remarkably, the data for glycerol-ethanol grown daughters fell on the same quantitative line as that already established for glucose-grown cells, implying a growth-rate-independent size control mechanism operating over a wide range of daughter cell sizes (Figure 3.6). This is true also for tetraploid cells, which usually do not display unusually small daughter cells, supporting the idea that a two-slope model describes well daughter G1 control also in cells of higher

ploidy (Figure 3.7). Even in glycerol-ethanol, mother cells exhibit no evidence of size control.

	Average size at bud
wt haploids	1.00±0.06
wt diploids	2.0±0.1
wt tetraploids	3.9±0.1
6xCLN2	0.94±0.06
6xCLN3	0.77±0.05
6xCLN3 6xCLN2	0.81±0.05

Table 3.4 Average sizes at budding for various strains. The data were normalized to the average size at budding of wt haploid cells. The comparison was done only for cells imaged the same day to reduce variation due to the illumination source. The table shows the mean +/- standard error of the mean.

	One-slope model	**Two-slope model**
αT_1 vs. $\ln(M_{birth})$ haploid wt dataset	P=0.05	P=0.65
αT_1 vs. $\ln(M_{birth})$ haploid wt glucose + glycerol/ethanol datasets	$P=2\cdot10^{-5}$	P=0.07
αT_{G1} vs. $\ln(M_{birth})$ haploid wt+small *MET3pr-CLN2* daughters datasets	P=0.02	P=0.72
αT_{G1} vs. $\ln(M_{birth})$ haploid wt glucose + glycerol/ethanol datasets	$P=1\cdot10^{-5}$	P=0.22
αT_{G1} vs. $\ln(M_{birth})$ tetraploid wt glucose + glycerol/ethanol datasets	$P=2\cdot10^{-7}$	P=0.06

Table 3.5 A two-slope model fits the correlation between αT_{G1} and αT_1 with the $\ln(M_{birth})$ of daughter cells better than a one-slope model. The table shows the p-values of a Pearson's χ^2 test using a one-slope or two-slope model.

	αT_{G1} vs. $\ln(M_{birth})$	αT_1 vs. $\ln(M_{birth})$
wt mothers	-0.13 (-0.20:-0.08)	-0.06 (-0.09:-0.02)
wt daughters	-0.38 (-0.49:-0.24)	-0.43 (-0.56:-0.31)
small wt daughters	-0.69 (-1.10:-0.27)	-0.66 (-1.00:-0.30)
big wt daughters	-0.32 (-0.52:-0.12)	-0.20 (-0.37:0.00)
small wt+*MET3pr-CLN2*daughters	-0.84 (-1.10:-0.58)	N/A
big wt+*MET3pr-CLN2*daughters	-0.36 (-0.56:-0.17)	N/A
small wt in D+g/e daughters	-0.84 (-1.01:-0.67)	-0.72 (-1.02:-0.46)
big wt in D+g/e daughters	-0.31 (-0.48:-0.13)	-0.25 (-0.38:-0.13)
small tetraploid daughters in D+g/e	-0.79 (-1.12:-0.47)	N/A
big tetraploid daughters in D+g/e	-0.26 (-0.37:-0.14)	N/A
6xCLN3 daughters	-0.25 (-0.34:-0.16)	-0.19 (-0.31:-0.06)
6xCLN3 small daughters	-0.34 (-0.52:-0.12)	-0.31 (-0.51:-0.11)
6xCLN3 big daughters	-0.33 (-0.54:-0.13)	-0.30 (-0.56:-0.06)
whi5 daughters	-0.23 (-0.30:-0.15)	N/A
whi5 small daughters	-0.22 (-0.43:-0.02)	N/A
whi5 big daughters	-0.22 (-0.39:-0.05)	N/A

Table 3.6 Values of the estimated slopes for the correlation of αT_{G1} and αT_1 with the $\ln(M_{birth})$. The table shows the values of the slopes and their 95% confidence bounds. The figures with the raw and binned data are referenced in parenthesis. All the strains are haploid except when indicated. (D = glucose, g/e = glycerol/ethanol).

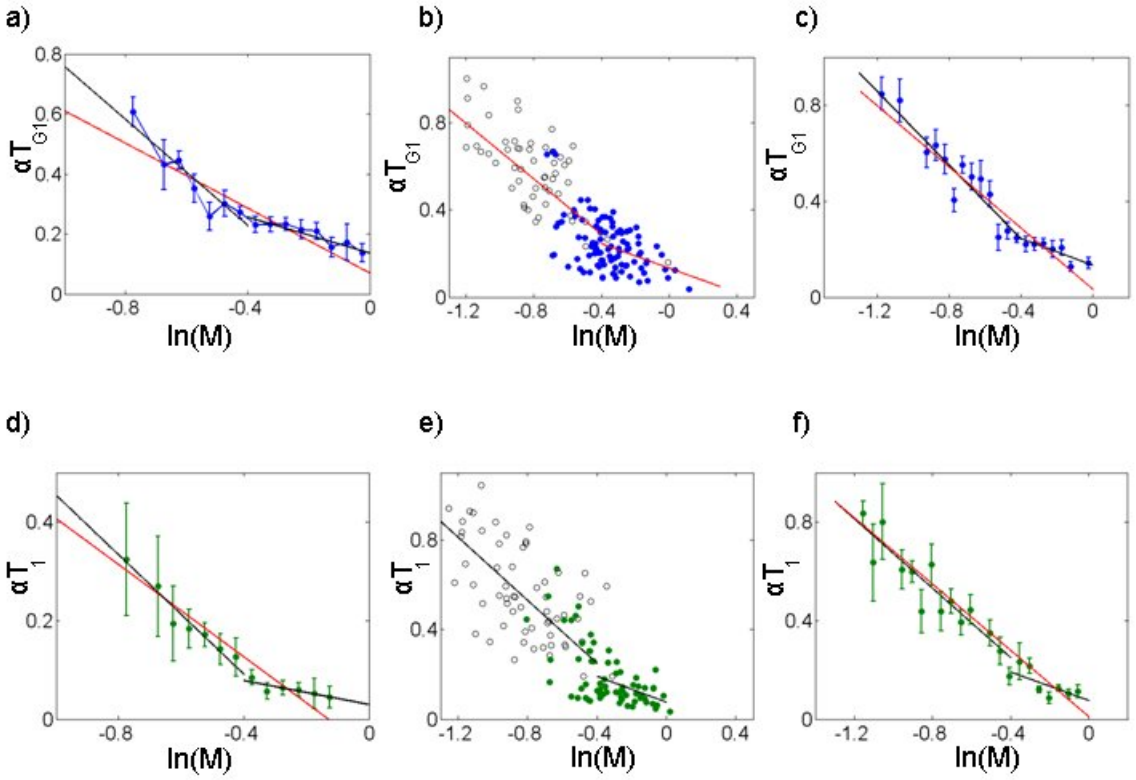

Figure 3.6 A two-slope model describes the correlation of αT_1 or αT_{G1} with $\ln(M_{birth})$ better than a one-slope model. a) Two-slope model fit or one-slope model fit of binned data of αT_{G1} vs. $\ln(M_{birth})$ combining the data obtained with the *MET3pr-CLN2* strain and with the wt strain, b) combination of data sets of wt cells grown in glucose (blue closed circles) and in glycerol/ethanol (black open circles) for αT_{G1} vs. $\ln(M_{birth})$, c) two-slope model fit or one-slope model fit of binned data of αT_{G1} vs. $\ln(M_{birth})$ combining the wt data obtained for cells grown in glucose and in glycerol/ethanol (data from b)), d) two-slope model fit or one-slope model fit of binned data of αT_1 vs. $\ln(M_{birth})$ for glucose grown cells, e) combination of data sets of wt cells grown in glucose (green closed circles) and in glycerol/ethanol (black open circles) for αT_1 vs. $\ln(M_{birth})$, f) two-slope model fit or one-slope model fit of binned data of αT_1 vs. $\ln(M_{birth})$ combining the wt data obtained for cells grown in glucose and in glycerol/ethanol (data from e)).

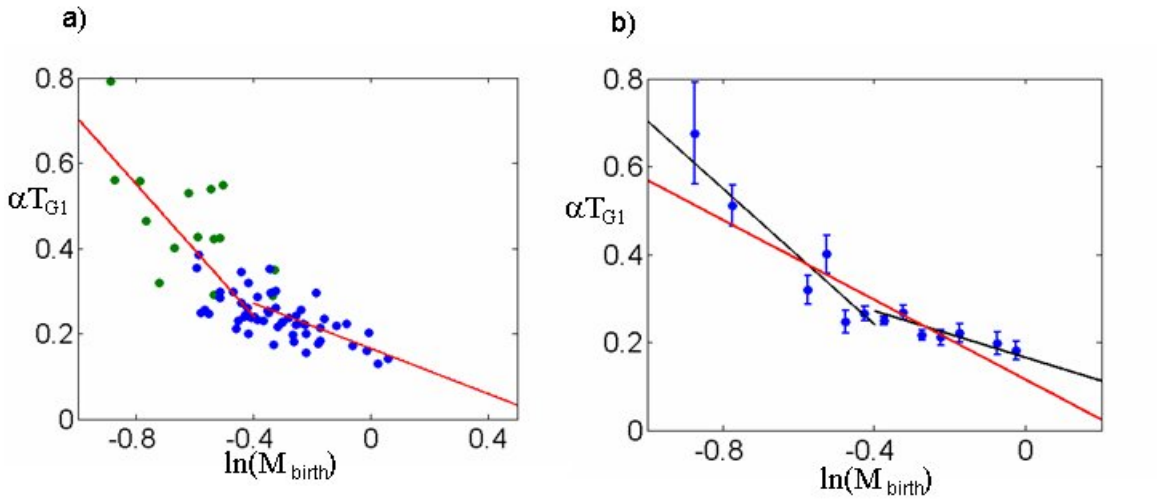

Figure 3.7 A two-slope model describes the correlation of αT_{G1} with the $\ln(M_{birth})$ for tetraploid cells better than a one-slope model. a) Combination of data sets of wt tetraploid cells grown in glucose (blue circles) and in glycerol/ethanol (green circles) for αT_{G1} vs. $\ln(M_{birth})$, b) two-slope model fit or one-slope model fit of binned data of αT_{G1} vs. $\ln(M_{birth})$ combining the data obtained for cells grown in glucose and in glycerol/ethanol (data from a)).

Decomposition of G1 variability in size-dependent and size-independent noise.

Efficient size control ensures that all cells bud at the same size. Since there is variability in cell size at birth, an efficient sizer would ensure that smaller cells spend longer in G1, generating cell-to-cell variability in G1 duration. Measuring individual growth rates and cell sizes allows decomposition of G1 variability into variability due to size control and a size-independent residual attributable to molecular noise. Assuming G1 duration for an individual cell is the sum of a deterministic function of cell size at birth, $f(M_{birth})$, and stochastic variable, η, then: $\alpha T_{G1}=f(M_{birth})+\eta$, where $f(M_{birth})$ is obtained empirically by binning data. For a measured distribution of sizes at birth, the variance of $f(M_{birth})$ yields

the amount of G1 variability produced by size control. Size-independent variability is the average distance between a data point and the deterministic $f(M_{birth})$.

This decomposition shows that size-independent (presumably molecular) noise is the leading source of variability in the duration of G1 in both mothers and daughters (Table 3.7). However, size control accounts for about 30-40% of overall G1 variability in daughters. Consistent with our previous timing analysis, size-independent noise decreases by approximately a factor of $\sqrt{2}$ for each ploidy doubling (Table 3.7; Figures 3.2,3.8,3.9); thus, ploidy-dependent noise reduction is robust to statistical removal of all detectable size and growth rate effects, strongly suggesting that molecular noise explains size-independent variability. G1 cyclin gene dosage also decreases size-independent variability; therefore, some of this variability may be attributable to stochastic variation in the expression of G1 cyclins themselves, although other targets cannot be excluded.

	G1 noise, birth to budding (coefficient of variation of αT_{G1})	Noise due to size control (percentage of the total variance of αT_{G1})	Size and growth rate-independent noise (percentage of the total variance of αT_{G1})
DAUGHTERS			
wt haploids	0.55±0.06	0.31±0.04 (32)	0.45±0.04 (68)
wt diploids	0.42±0.04	0.28±0.03 (45)	0.31±0.03 (55)
wt tetraploids	0.24±0.02	0.15±0.01 (39)	0.19±0.02 (61)
haploid *6xCLN2*	0.48±0.04	0.30±0.03 (39)	0.37±0.03 (61)
haploid *6xCLN3*	0.44±0.04	0.25±0.02 (32)	0.36±0.03 (68)
haploid *6xCLN3 6xCLN2*	0.37±0.03	0.18±0.02 (24)	0.32±0.03 (76)
MOTHERS			
wt haploids	0.50±0.05	0.20±0.02 (16)	0.46±0.04 (84)
wt diploids	0.39±0.04	0.13±0.01 (11)	0.37±0.04 (89)
wt tetraploids	0.26±0.02	0.09±0.01 (12)	0.24±0.02 (88)
haploid *6xCLN2*	0.33±0.03	0.13±0.01 (16)	0.30±0.03 (84)
haploid *6xCLN3*	0.48±0.05	0.16±0.02 (11)	0.45±0.04 (89)
haploid *6xCLN3 6xCLN2*	0.34±0.03	0.17±0.02 (25)	0.29±0.02 (75)

Table 3.7 Decomposition of G1 variability into a deterministic size control term and a residual attributable to molecular noise. G1 noise (column 1): coefficient of variation in αT_{G1}, (α: growth rate; T_{G1} G1 duration). G1 noise is decomposed into size-dependent and size-independent components (columns 2,3); in parentheses, the percentage of the variance of αT_{G1} accounted for in each column. (Noise in αT_{G1} is the square root of the sum of the squares of the two independent noise contributions.

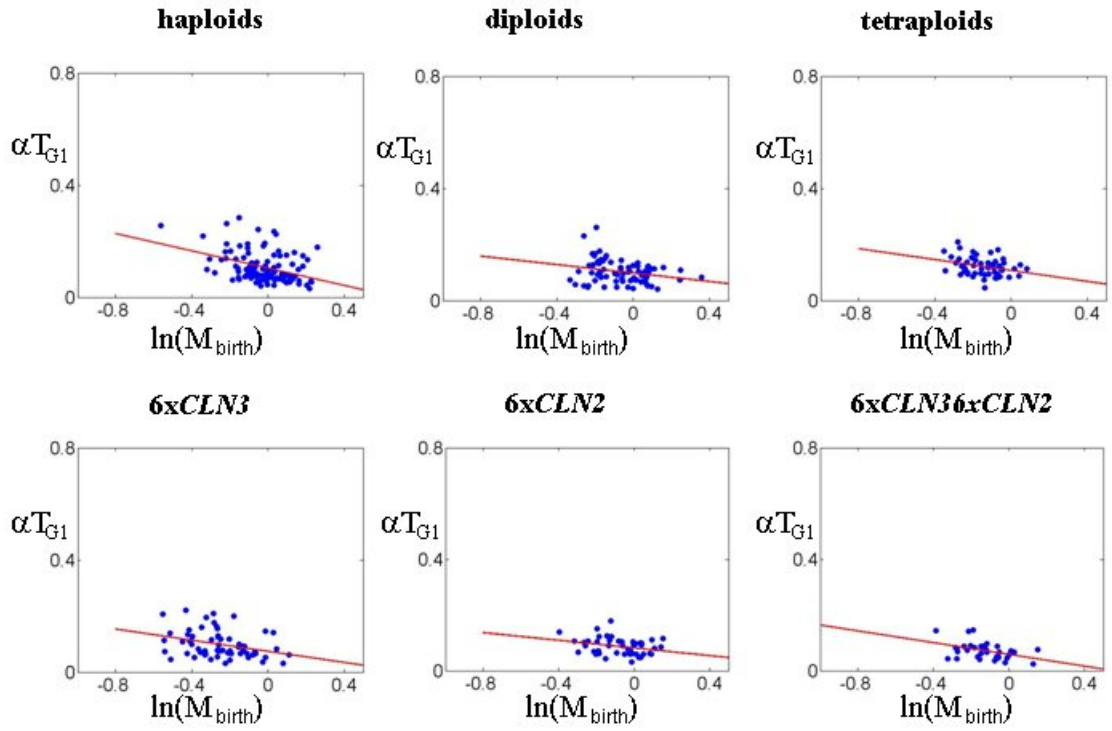

Figure 3.8 Size independent noise is reduced by ploidy and by increasing the number of copies of G1 cyclins in mother cells. Correlation between the duration of G1, T_{G1}, scaled to the growth rate, α, and the logarithm of cell size at birth shows the lack of size control in mother G1 and that cell size independent noise (Table 3.7) is reduced by ploidy and by increasing the number of copies of G1 cyclins. The size of all haploid strains was normalized to the average size at budding of wt cells. The size of diploid and tetraploid cells was normalized to the average size at budding of diploid and tetraploid cells respectively.

Figure 3.9 Size independent noise is reduced by ploidy and by increasing the number of copies of G1 cyclins in daughter cells. Correlation between the duration of G1, T_{G1}, scaled to the growth rate, α, and the logarithm of cell size at birth shows that cell size independent noise (Table 3.7) is reduced by ploidy and by increasing the number of copies of G1 cyclins. An inverse correlation (significantly different from both 0 and -1) is observed for all the strains and is indicative of a 'sloppy' size control. The size of all haploid strains was normalized to the average size at budding of wt cells. Small wt daughter cells exhibit an efficient size control (slope= - 0.7). Cells with more copies of *CLN3* no longer show efficient size control (slope= - 0.3), indicating that *CLN3* gene dosage alters the properties of size control. In contrast, increasing *CLN2* gene dosage does not alter size control (see also Figure 3.11). The size of diploid and tetraploid cells was normalized to the average size at budding of diploid and tetraploid cells respectively. The lack of a clear component of high negative slope for smaller daughter cells in diploids and tetraploids is not fully understood, but may be largely due to the lack of unusually small daughter cells generated by these higher-ploidy cells, due to a slightly longer budded period during which the bud grows, combined with a reduction in variability of growth rate of individual cells (see Table 3.1 and Appendix). These explanations do not account for the lack of this slope in *6X CLN3* and *6X CLN3 6X CLN2* cells. We have tested this explanation by growth of tetraploids in glycerol/ethanol (Figure 3.7) where we find that combining the small daughters obtained from glycerol/ethanol growth with the larger daughters obtained from glucose growth gives a continuous data set well fit with two slopes.

Daughters:

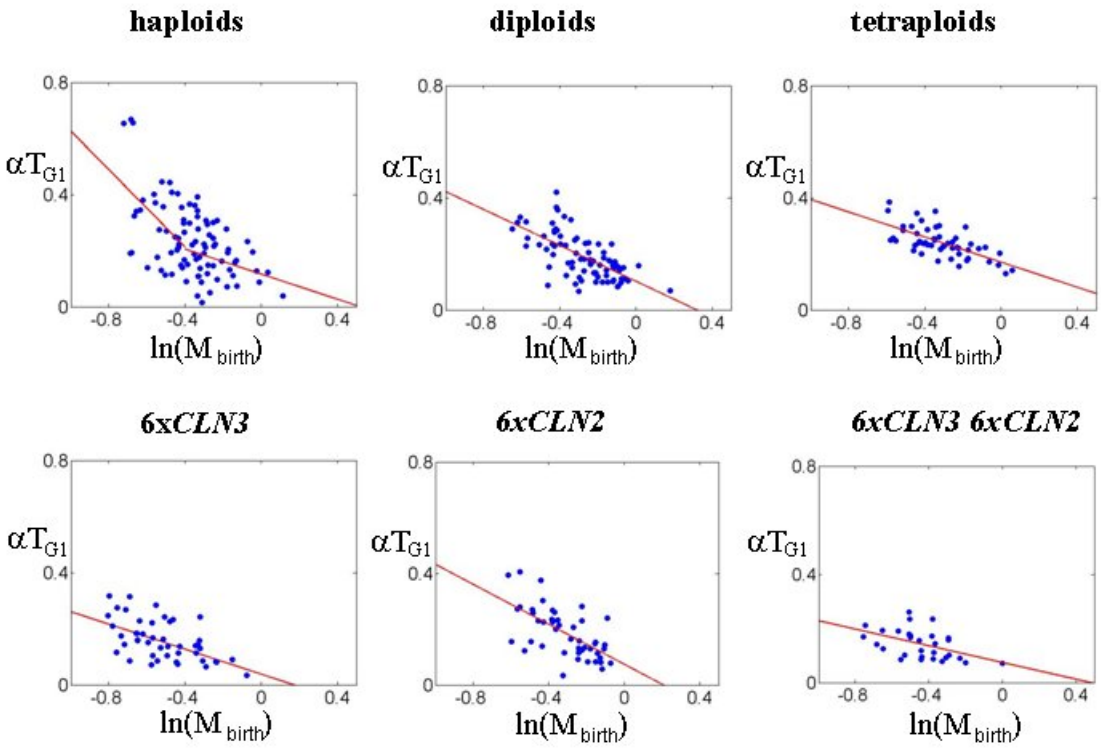
haploids
diploids
tetraploids
6x*CLN3*
6xCLN2
6xCLN3 6xCLN2
αT_G1
ln(M_birth)
0.8
0.4
0
-0.8
-0.4
0
0.4

G1 dynamics is composed of two modules: a size-sensing and a timing module. We can divide G1 into two steps, T_1 and T_2, based on nuclear residence of Whi5 (Bean et al., 2006; Costanzo et al., 2004), which enters the nucleus late in mitosis and exits during G1 (Costanzo et al., 2004) (Figure 3.4). Since T_1 and T_2 are uncorrelated, Whi5 exit marks the boundary between two independent steps in daughters (Figure 3.4d). For daughters, plotting αT_1, the time from birth to Whi5 nuclear exit scaled with the growth rate α, vs. the logarithm of the size at birth, yields a nearly identical relationship to that for overall G1 duration αT_{G1} (Figure 3.10 a-c), shifted down due to growth during T_2. The indicated two-slope model fits these data significantly better than a one-slope model, and the deduced slopes for the Whi5 data and for the total G1 data are similar (Figure 3.6). Thus G1 size control is restricted to T_1, the period of Whi5 nuclear residence. T_2, the part of G1 after Whi5 exit, is independent of cell size, and similar in mothers and daughters (Bean et al., 2006) (Table 3.3).

These observations are robust to changes in nutrient conditions: growth of cells in glycerol/ethanol instead of glucose, resulting in slow growth and generation of very small newborn daughter cells, gave quantitatively similar results (Figures 3.6, 3.10 d). As for G1 duration, also for Whi5 nuclear residence times the data for glycerol-ethanol-grown daughters fell on the same quantitative line as that already established for glucose-grown cells. This implies a growth-rate-independent size control mechanism operating over a wide range of daughter cell sizes (Figure 3.6). The combined data sets for glycerol/ethanol and glucose strongly supported a two-slope model Whi5 nuclear residence times (see Figure 3.6 and Table 3.5).

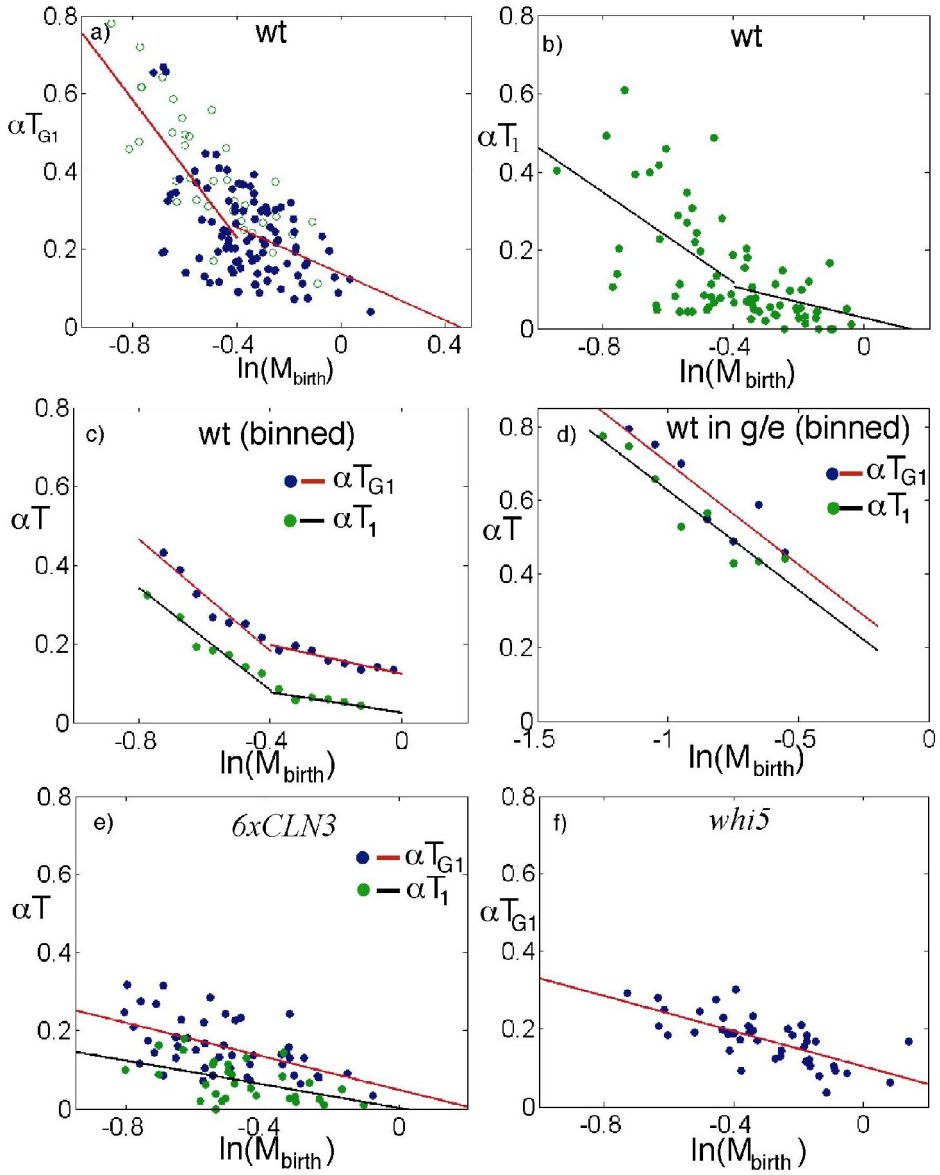

Figure 3.10 The correlation between cell size and the regulation of Whi5 nuclear residence supports decomposition of Start into a size control module and an independent timing module. a) αT_{G1} vs. $\ln(M_{birth})$ as in Figure 3.5f; wt data (solid blue dots) were supplemented with data from unusually small wild-type haploid daughters (open green circles); b) αT_1 vs. $\ln(M_{birth})$; c) binned data from Figure 3.10b (green points, black line) and Figure 3.5e (blue points, red line); d) Binned data for αT_1 (green points, black line) and αT_{G1} (blue points, red line) vs. $\ln(M_{birth})$ for cells grown in glycerol/ethanol (see also Figure 3.6); e) αT_1 and αT_{G1} vs. $\ln(M_{birth})$ for *6xCLN3* cells; f) αT_{G1} vs. $\ln(M_{birth})$ for *whi5* cells.

Even in glycerol-ethanol, mother cells exhibit no evidence of size control over Whi5 nuclear exit.

Efficient size control, indicated by the steep slope for small wild-type daughters, is essentially eliminated by increase in *CLN3* gene dosage or deletion of *WHI5* (Figures 3.10 e, f). In contrast, increasing *CLN2* gene dosage does not alter size control and the regulation of T_1 (see Figure 3.11)

CLN3 and *CLN2* copy number had differential effects on G1 variability in mothers and daughters (Figure 3.3). The two-step model explains this, since increase in *CLN3* copy number should only affect the first step, which is slow in daughters but extremely rapid in mothers. Since in mothers, G1 is temporally dominated by the second step, mother cell G1 variability is more sensitive to changes in *CLN2* copy number (Figure 3.3). Consistent with this idea and with independence of the two steps, combining *6X CLN3* together with
6X CLN2 in one haploid genome resulted in low G1 variability in both mothers and daughters (Table 3.7, Figure 3.3).

Thus we decompose G1 into two independent steps separated by Whi5 nuclear exit: a size sensing module and a size-independent timing module. The first step is dependent on both Cln3 and cell size, and the second step is dependent on Cln2, but independent of cell size and Cln3 (Figure 3.12). Temporal variability in the first step is due to the natural

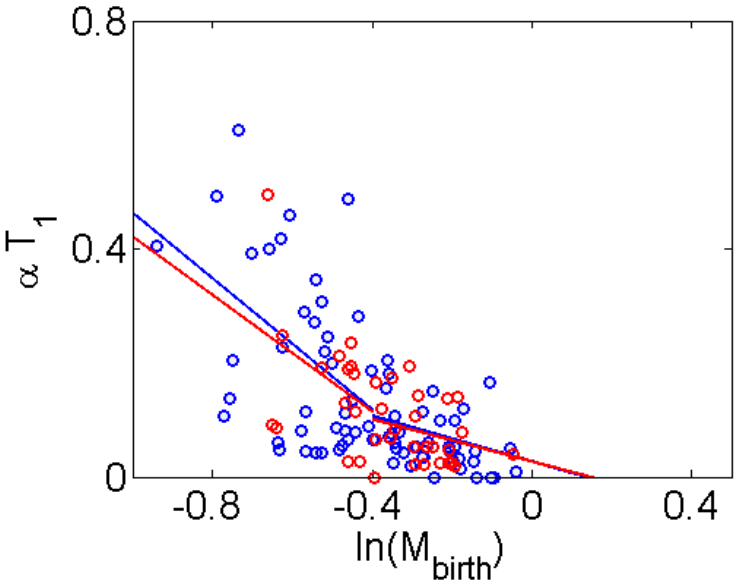

Figure 3.11 *CLN2* gene dosage does not affect the duration of the period from cytokinesis to Whi5 nuclear exit. Correlation between the duration of the period from cytokinesis to Whi5 nuclear exit, T_1, scaled with growth rate, α, and the logarithm of cell size at birth for wt (blue points and lines) and *6xCLN2* strains (red points and lines). The same break-point deduced for wt cells was used for the two-slope model of *6xCLN2* cells.

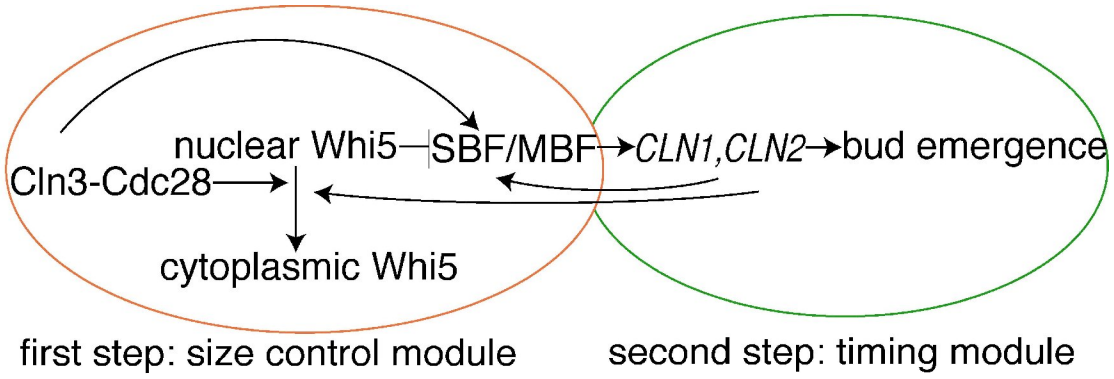

Figure 3.12 Start regulatory dynamics is composed of two independent modules. A model decomposing Start into a size control module and an independent timing module unaffected by cell size.

variability in cell size at birth coupled to size control, as well as molecular noise, possibly due to variability in *CLN3* expression. The duration of the second step is cell-size independent; its variability is affected by the expression of the G1 cyclin *CLN2*, one of the primary final effectors of Start (Cross, 1995; Dirick et al., 1995; Tyers et al., 1993).

Positive feedback sharpens the transition between the two modules of Start and ensures coherent cell cycle entry. The modular dynamics of Start suggest that the transition between the two modules could be controlled by a switch-like molecular network. In recent work led by Jan Skotheim, in which I collaborated, we have shown that the switch-like properties of Start are the result of positive feedback of Cln1 and Cln2 on their own transcription (Skotheim et al., 2008).

In order to investigate if Cln1- and Cln2-dependent positive feedback operated through Whi5, we developed a quantitative assay for nuclear levels of Whi5–GFP by marking the nucleus with HTB2-mCherry (histone H2B) and measuring the difference between nuclear and cytoplasmic GFP fluorescence intensity (Figure 3.13a-c) (Skotheim et al., 2008). Whi5 entered the nucleus rapidly in both wild-type and *cln1 cln2* cells. In wild-type cells, Whi5 also exited very rapidly; in *cln1 cln2* cells, Whi5 exited much more slowly (Figure 3.13d-g, i) consistent with biochemical data showing that Whi5 remains on the *CLN2* promoter longer in *cln1 cln2* than in wild-type cells (de Bruin et al., 2004). Because Whi5–GFP remained nuclear in *cln1 cln2 cln3* cells (Figure 3.13h), the slow Whi5 exit in *cln1 cln2* cells is Cln3-dependent (this also excludes photobleaching artifacts). Thus, Cln3 initiates the slow exit of Whi5 from the nucleus, whereas Cln1 and Cln2 rapidly remove the remainder. It can also be shown that rapid Whi5 exit coincided

with the time of activation of *CLN1* and *CLN2* transcription and initiation of Cln1- and Cln2-dependent positive feedback (Skotheim et al 2008). Once feedback is initiated, the rapidly accumulating Cln1 and Cln2 probably dominate cellular Cln-kinase activity, and Cln3, the rate-limiting upstream activator, is probably rendered unimportant after this point. Thus, positive feedback sharpens the transition between the size control module and the timing module, with the transition marked by Whi5 nuclear exit.

Figure 3.13 Cln1 and Cln2 are required for rapid phosphorylation and inactivation of the rate-limiting inhibitor Whi5. a)–c), Combined phase and fluorescence images showing Whi5–GFP and Htb2–mCherry (to mark the nucleus) fusion proteins for wild-type (a), *cln1 cln2* (b) and *cln1 cln2 cln3* (c) cells. The difference between nuclear and non-nuclear fluorescence intensity was used to quantify nuclear Whi5 by automated image analysis. d)–h), Nuclear Whi5–GFP fluorescence. In comparison to wild-type cells (d, e), *cln1 cln2* cells display delayed and less sharp Whi5 nuclear exit (f, g). Whi5 remains nuclear in *cln1 cln2 cln3* cells (h). i) The percentage of cells in which Whi5 has left the nucleus (defined as attaining half the maximum amount) versus the time from Whi5 nuclear entry. (Figure courtesy of Jan Skotheim).

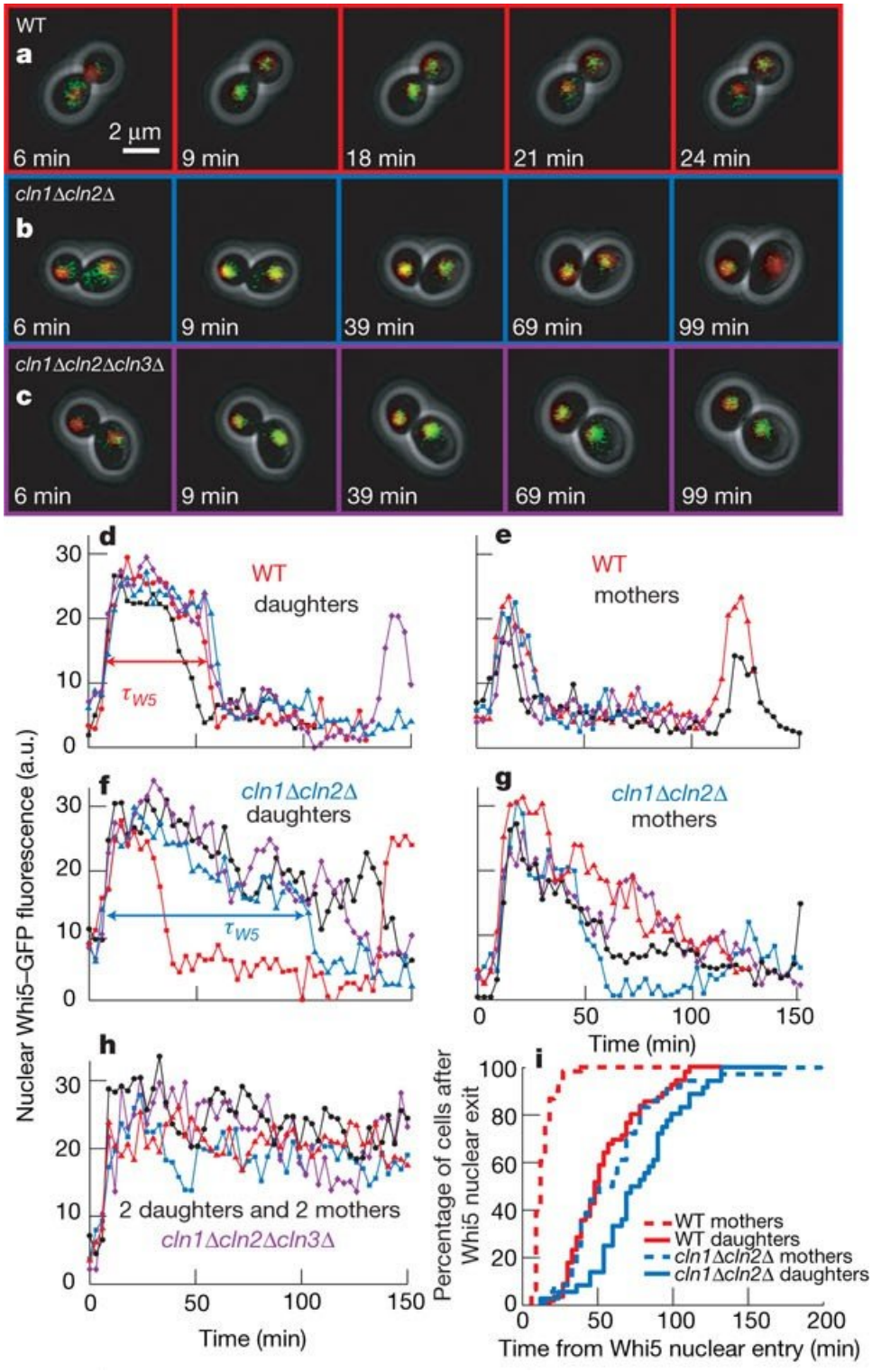
WT
a
2 µm
6 min
9 min
18 min
21 min
24 min
cln1Δcln2Δ
b
6 min
9 min
39 min
69 min
99 min
cln1Δcln2Δcln3Δ
c
6 min
9 min
39 min
69 min
99 min
d
WT
daughters
τW5
e
WT
mothers
f
cln1Δcln2Δ
daughters
τW5
g
cln1Δcln2Δ
mothers
h
2 daughters and 2 mothers
cln1Δcln2Δcln3Δ
Nuclear Whi5–GFP fluorescence (a.u.)
Time (min)
i
Percentage of cells after Whi5 nuclear exit
WT mothers
WT daughters
cln1Δcln2Δ mothers
cln1Δcln2Δ daughters
Time from Whi5 nuclear entry (min)

Chapter 4: Asymmetric cell fates and regulation of Start.

Cell division in budding yeast is asymmetric yielding a bigger mother cell and a smaller daughter cell (Hartwell and Unger, 1977). Regulation of gene expression is also asymmetric in mother and daughter cells as result of the daughter-specific localization of transcription factors Ace2 and Ash1 (see Chapter1). We have shown in the previous Chapter that cell size plays a crucial role in the regulation of Start with small daughter cells delaying cell cycle commitment and mother cells progressing quickly through Start. In this Chapter, we analyze the interaction between daughter-specific transcriptional programs, G1 cell size control, and irreversible commitment to the cell cycle at Start.

Differential regulation of Start in mothers and daughters is dependent on Ace2 and Ash1. We have shown in Chapter 3 how size control is restricted to T_1, the period of nuclear residence of transcriptional repressor Whi5, and that this interval accounts for the longer duration of G1 in daughter cells. The different duration of the period T_1 in mothers and daughters could in principle be solely a consequence of size control imposing a delay in the smaller daughter cells (Hartwell and Unger, 1977). To investigate if cell size is solely responsible for the longer T_1 of daughter cells, we analyzed the correlation between αT_1 and $\ln(M_{birth})$ specifically for the sub-population of mothers and daughters with similar sizes at birth. This comparison demonstrates an increase in αT_1 in daughters compared to mothers of similar size (Figure 4.1b, 4.1c; Table 4.1). This delay is most readily detectable in glycerol-ethanol medium, in which cell growth is much slower than in glucose medium; slower growth results in smaller daughter size at the time of cell

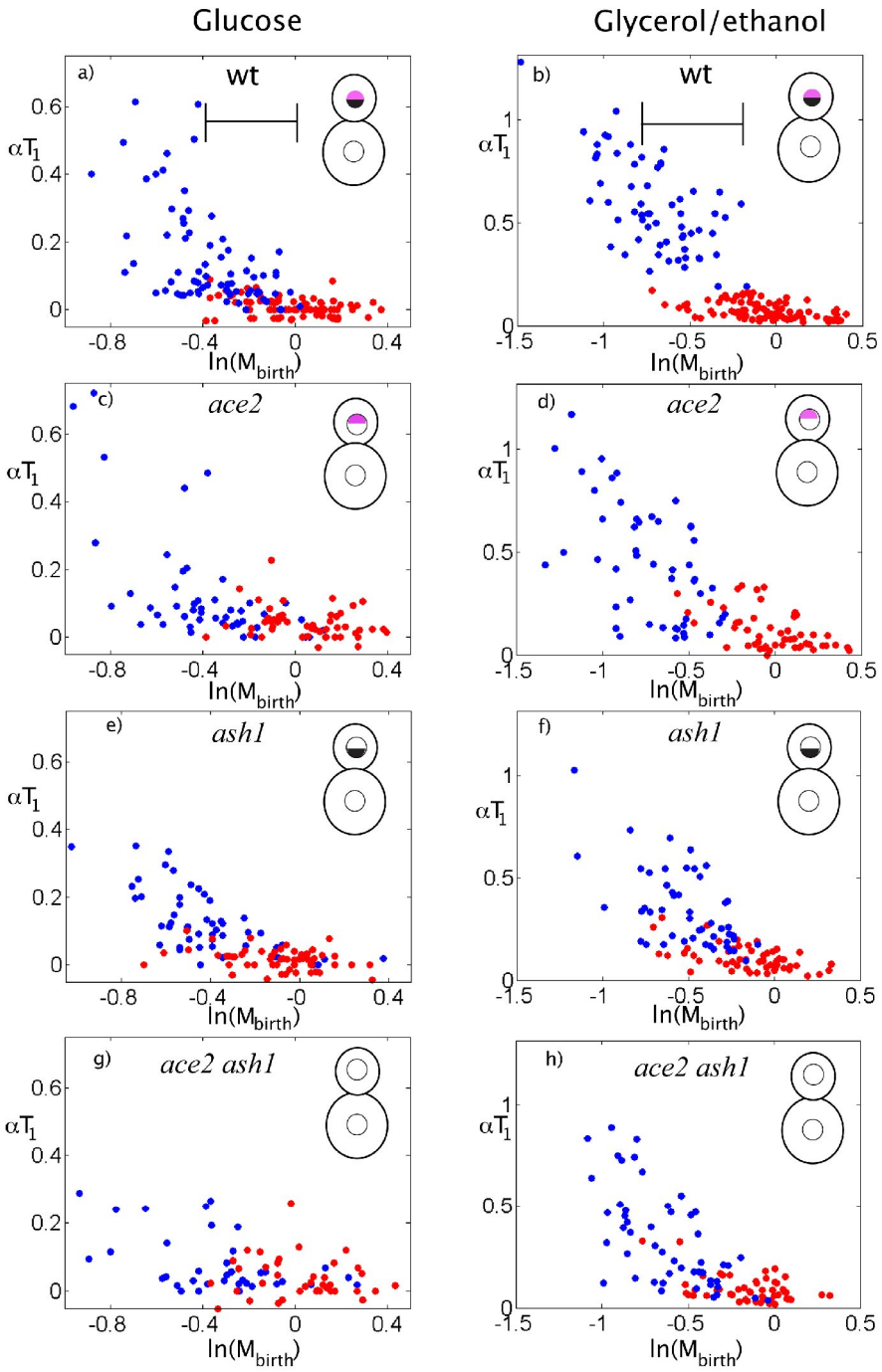

Figure 4.1 Differential regulation of Start is dependent on Ace2 and Ash1. a)-h) Correlation between αT_1 and ln (M_{birth}) for cells grown in glucose or glycerol/ethanol. (a, b) wt, (c, d) *ace2*, (e, f) *ash1*, (g, h) *ace2 ash1*. Bars in a) and b) illustrate the region of size overlap in the case of wt cells. Red dots: mothers, blue dots: daughters. Black semicircles: Ace2, yellow semicircles: Ash1.

division (Hartwell and Unger, 1977) (Figure 4.1c). In glycerol-ethanol, in the region of size overlap daughters exhibit clear size control (slope ~-0.8) while mothers exhibit essentially none (slope ~0). A daughter delay independent of cell size in G1 was previously observed in cells grown in low concentration of hydroxyurea that results in mother and daughter cell size at birth significantly larger than that of wt cells (Lord and Wheals, 1983). Our observations confirm and extend this result in unperturbed cycling cells, relying solely on natural variation in cell size at birth.

Because Ace2 and Ash1 are specifically inherited by daughters, and because previous results implicated Ace2 in a daughter delay (Laabs et al., 2003), we analyzed the correlation between αT_1 and $\ln(M_{birth})$ in *ace2* and *ash1* single and double mutants. Deletion of these transcription factors greatly reduces the daughter-specific delay compared to mothers of similar size, and results in altered size control properties of daughter cells (Figures 4.1h, 4.1i and Table 4.1). Only very small *ace2 ash1* daughters present in cultures grown in glycerol/ethanol display efficient size control (Figure 4.1i). According to this analysis, the effect of deleting *ACE2* and *ASH1* is to shift efficient size control to smaller cell size.

Single mutants (*ace2 ASH1* and *ACE2 ash1*) display a phenotype similar to but less extreme than *ace2 ash1* double mutants (Figures 4.1d-4.1g, Table 4.1). Ace2 contributes to transcriptional activation of *ASH1* (McBride et al., 1999), so some but not all of the effects of *ACE2* deletion may be a consequence of reduced *ASH1* expression.

	wt	***ash1***	***ace2***	***ace2 ash1***
Daughter-mother delay in glucose	8 ± 1 min	5 ± 1 min (0.03)	2 ± 3 min (0.06)	2 ± 3 min (0.06)
Daughter-mother delay in gly/eth	87 ± 9 min	47 ± 8 min ($<10^{-3}$)	16 ± 13 min ($<10^{-5}$)	18 ± 9 min ($<10^{-7}$)
	wt	***ASH1****	***ACE2****	***ASH1* ACE2****
Daughter-mother delay in glucose	8 ± 1 min	5 ± 1 min (0.03)	1.3 ± 0.9 min ($<10^{-5}$)	1.3 ± 0.9 min ($<10^{-5}$)
Daughter-mother delay in gly/eth	87 ± 9 min	19 ± 7 min ($<10^{-8}$)	46 ± 12 min (0.006)	5± 7 min ($<10^{-12}$)
	wt	***cln3***	***ADH1p-CLN3***	***nxCDC28p-CLN3***
Daughter-mother delay in glucose	8 ± 1 min	2 ± 1 min ($<10^{-4}$)	N/A	3 ± 1 min ($<10^{-3}$)
Daughter-mother delay in gly/eth	87 ± 9 min	9 ± 13 min ($<10^{-6}$)	22 ± 13 min ($<10^{-4}$)	36 ± 14 min (0.003)

Table 4.1 Average daughter delay in new-born cells of the same size. Data from the correlation of αT_1 and $\ln(M_{birth})$ were divided in small bins and the daughter delays computed for every bin were averaged. In parenthesis is the p-value computed by t-test for the null hypothesis that the delay of daughters compared to mothers is the same for the mutants as for wild-type.

In strains with *ACE2* and/or *ASH1* deleted, little effect on mother cell size control is expected or observed, since mother cells naturally lack Ace2 and Ash1 due to differential segregation of the factors at cell division (see Chapter 1). *ace2 ash1* daughters exhibit efficient size control only when born at a size that mothers almost always exceed due to the budding mode of growth (Hartwell and Unger, 1977) (Figures 4.1b, 4.1c).

To test whether Ace2 or Ash1 have the capacity to affect size control in mothers, we employed mutations resulting in symmetrical inheritance of the factors to mothers and daughters. We used an Ace2 mutant, *ACE2G128E* (indicated as '*ACE2**' from here on), which accumulates in both mother and daughter nuclei, activating Ace2-dependent transcription in both (Colman-Lerner et al., 2001; Racki et al., 2000), and an *ASH1* mutant, *ASH1-MUT* ('*ASH1**') in which mutation of localization elements in *ASH1* mRNA results in accumulation of Ash1 in both mother and daughter nuclei (Chartrand et al., 2002). Symmetric localization of both factors greatly reduces the difference in T_1 length in mothers and daughters born at similar sizes (Figures 4.2g, 4.2h, Table 4.1). Strikingly, *ACE2* ASH1** mothers exhibit efficient size control when born small (such mother cells are observed in significant numbers in glycerol-ethanol culture) (Figure 4.2h). Strains in which only Ash1 or Ace2 is symmetrically localized show intermediate phenotypes (Figures 4.2c-4.2f, Table 4.1), suggesting again that both transcription factors contribute to the daughter-specific delay in partially independent ways. Interestingly, symmetric localization of Ace2 but not Ash1 drives almost completely symmetric control of Start in glucose medium, while the opposite is true in glycerol/ethanol (Table 4.1).

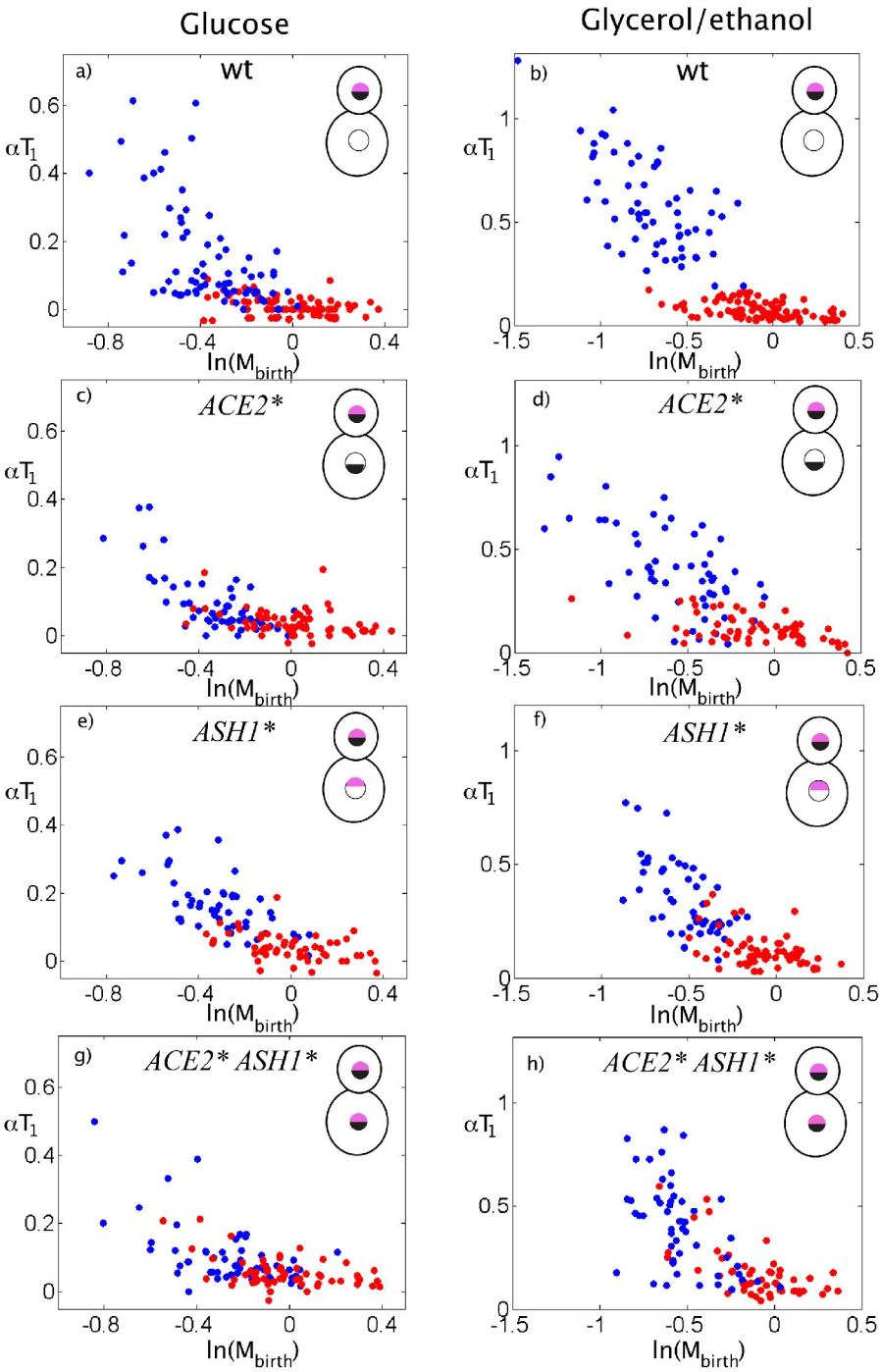

Figure 4.2 Symmetric localization of Ace2 and Ash1 result in symmetric control of Start in mothers and daughters. a)-h) Correlation between αT_1 and ln (M_{birth}) for cells grown in glucose or glycerol/ethanol. (a, b) wt, (c, d) *ACE2**, (e, f) *ASH1**, (g, h) *ACE2* ASH1**. Red dots: mothers, blue dots: daughters. Black semicircles: Ace2, yellow semicircles: Ash1.

*ACE2** and *ASH1** had little effect on size control properties of daughter cells, as expected since these factors are already present in wild-type daughters.

Altogether, these results show that Ace2 and Ash1 define daughter-specific programs that set the size range at which daughters display efficient size control to a higher value than that of mothers. Ace2 and Ash1 appear to be necessary and sufficient for this resetting.

This idea leads to the prediction that *ACE2* ASH1** mothers and daughters should be 'pseudo-daughters' with respect to size control, while *ace2 ash1* mothers and daughters should be 'pseudo-mothers'. To test this, we combined data for mothers and pseudo-mothers, and daughters and pseudo-daughters, in rich and poor medium. Remarkably, these combined data sets collapsed onto one plot for all mother-like cells and a different plot for all daughter-like cells (Figures 4.3a, 4.3b, 4.4, 4.5). The noise about the lines in these plots (size-independent variation) is of a magnitude consistent with previous results (see Chapter 3). Further analysis showed that the daughter-like plot could be transformed to the mother-like plot simply by shifting the curve 0.2 units of $\ln(M_{birth})$ (Figures 4.3c, 4.3d). This implies that cells containing Ace2 and Ash1 interpret a given cell size as being effectively ~20% larger than the same size in cells lacking Ace2 and Ash1, with respect to commitment to Start. This size interpretation is independent of actual mother/daughter status.

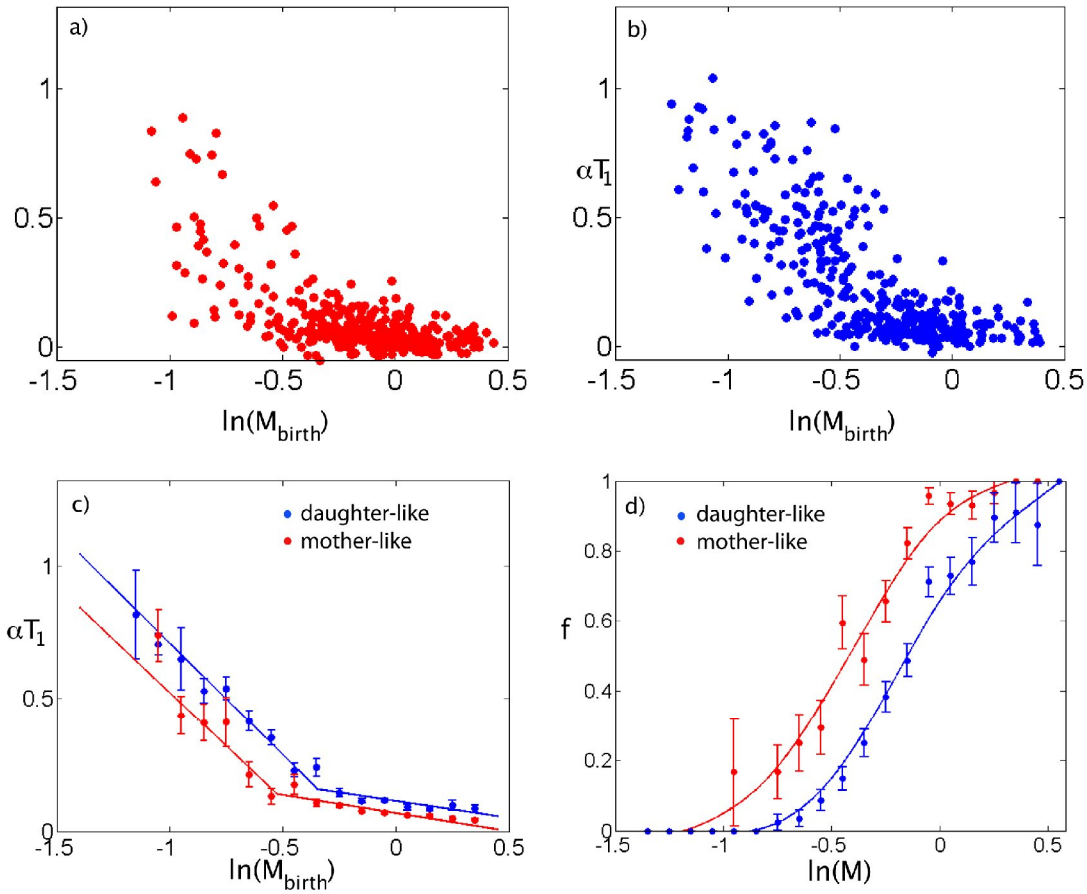

Figure 4.3 Daughter-specific localization of Ace2 and Ash1 result in asymmetric control of Start. a) Correlation between αT_1 and ln (M_{birth}) for mothers and "pseudo-mothers" grown in glucose or glycerol/ethanol. b) Correlation between αT_1 and ln (M_{birth}) for daughters and "pseudo-daughters" grown in glucose or glycerol/ethanol. c) Correlation between αT_1 and ln (M_{birth}) mother-like and daughter-like cells. The graphs are obtained by binning the data shown in a) and b). Error bars are standard errors of the mean. d) Probability of Whi5 nuclear exit as a function of ln(M) from data in c).

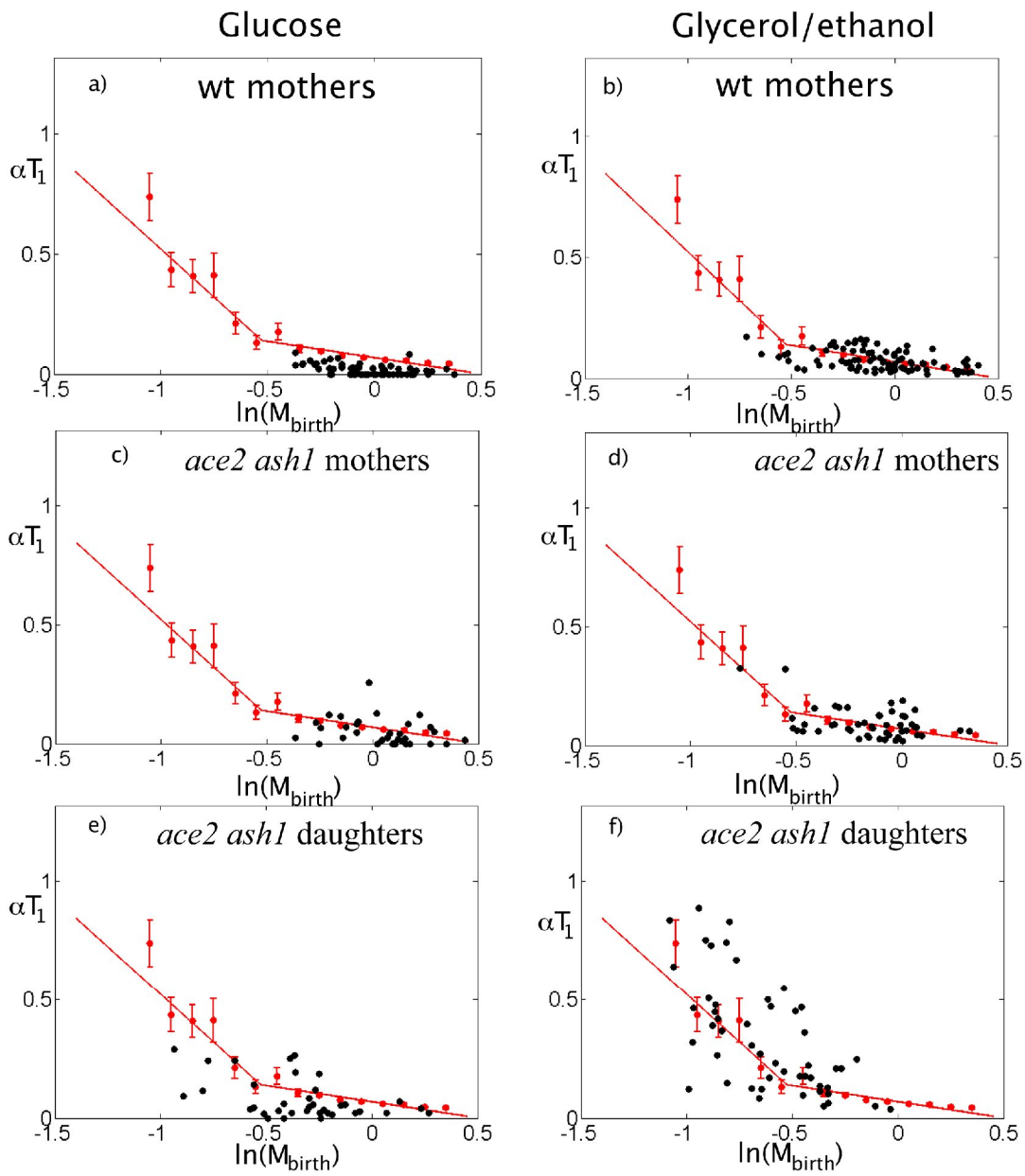

Figure 4.4 Start control is similar in mothers and "pseudo-mothers". Plot of αT_1 vs. $\ln(M_{birth})$ for the average 'mother-like' (red dots and error-bars, see Figure 4.3) compared to mothers and "pseudo-mothers" (black dots).

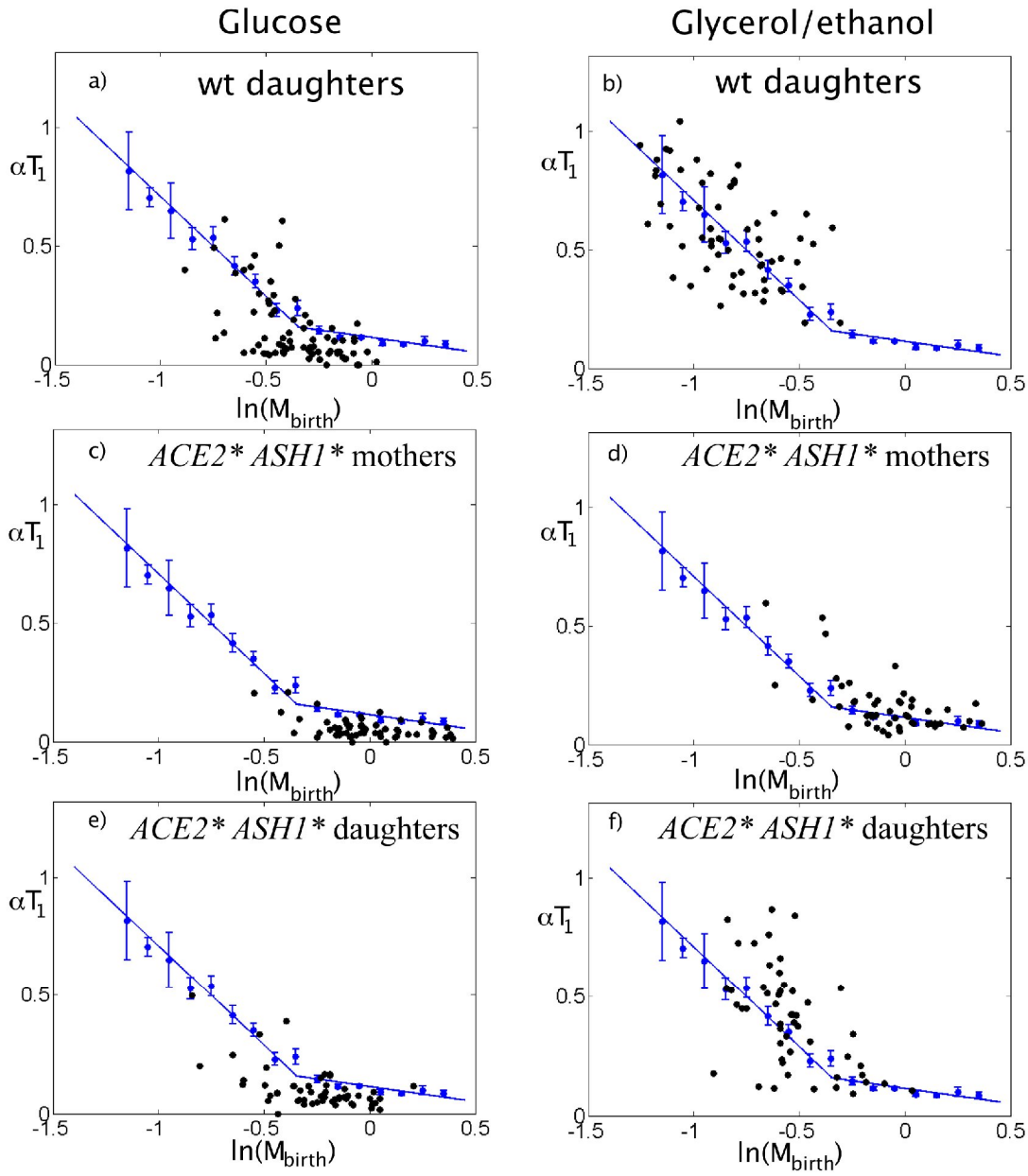

Figure 4.5 Start control is similar in daughters and "pseudo-daughters". Plot of αT_1 vs. $\ln(M_{birth})$ for the average 'daughter-like' (blue dots and error-bars, see Figure 4.3) compared to daughters and "pseudo-daughters" (black dots).

Laabs et al. (2003) claimed symmetrical G1 durations for *ace2* mothers and daughters, and for *ACE2** mothers and daughters, independent of cell size. It is important to note a critical distinction between their results and ours. We find that *ace2 ash1* mothers and daughters, and *ACE2* ASH1** mothers and daughters, are symmetrical with respect to T_1 duration in cells *of a given size*. This is independent of whether a given individual mother-daughter pair will exhibit equal T_1 durations, as claimed for time to budding by Laabs et al. (2003). Indeed, in many individual mother-daughter pairs of these mutant genotypes (especially in glycerol/ethanol medium), the daughter does exhibit a longer T_1 than the mother; we attribute this to the fact that most mothers are bigger than the daughters they produce (Hartwell and Unger, 1977) (Figures 4.1b, 4.1c). Laabs et al. (2003) compared times of second budding in mother-daughter pairs with 10 min resolution, following only the first bud emergence after plating. We time the duration of Whi5 nuclear residence, that accounts for the mother-daughter differences in G1 duration (Bean et al., 2006) rather than budding, eliminating significant variability in timing of this later step. We also have a precise time of origin for cell birth (cytokinesis occurs 6 min after Whi5-GFP nuclear entry (Figure 3.4) (Di Talia et al., 2007)allowing comparison of T_1 durations in unrelated mothers and daughters. We use 3-minute resolution rather than 10-minute resolution. Finally, we follow multiple cell cycles in unperturbed exponentially growing microcolonies rather than just the first bud emergence after plating, which avoids artifacts specifically due to the physical manipulations involved in preparing and plating the cells for time-lapse microscopy.

Genome-wide analysis of Ace2 and Ash1 targets. To determine the transcriptional target(s) through which Ace2 and Ash1 modulate size control in daughters, we performed microarray analysis of synchronized cell populations, comparing cells in which Ace2 and Ash1 are deleted to cells in which they localize symmetrically to both mother and daughter nuclei. Doing the comparisons in this way, rather than simply comparing wild-type to mutants, increases sensitivity of the analysis, since wild-type cultures always contain a mixture of mothers and daughters, reducing the detectable effects of manipulation of daughter-specific transcription factors. Our approach thus relies on three comparisons: *ace2 ash1* vs. *ACE2* ASH1**, *ace2* vs. *ACE2**, and *ash1* vs. *ASH1** cells.

We also compared *swi5*, *ace2* and *swi5 ace2* and wild-type in order to obtain insight into the set of genes regulated by one or both of these factors. Swi5 and Ace2 are closely related transcription factors that recognize the same DNA sequence and share many target genes and (Dohrmann et al., 1992; Voth et al., 2007). The best-characterized Ash1 target, *HO*, is also a Swi5 target and its regulation by Swi5 and Ash1 is required for mother-daughter asymmetry in mating type switching (Bobola et al., 1996; Sil and Herskowitz, 1996).

To synchronize cells during the critical M/G1 interval, we used strains expressing Cdc20 under the control of an inducible promoter (the truncated *GAL1* promoter, *GALL* (Mumberg et al., 1994)). Cells were arrested in metaphase by depletion of Cdc20 in glucose medium, and released from the arrest by transfer to galactose medium to reinduce Cdc20. mRNA was extracted every 5 minutes, and hybridized to microarrays. This

synchronization procedure provides excellent synchrony in the M/G1 interval (anaphase, cell division, and early G1) immediately following release, which is the time of nuclear localization and transcriptional activity of Ace2, Swi5 and Ash1 (Figure 4.6a, (Spellman et al., 1998; Voth et al., 2007)).

About 15 minutes after release, cells of all genotypes complete anaphase and degrade the mitotic cyclin Clb2 (see Figure 4.6a). Subsequently, cells separate and rebud (Figure 4.6a). Both Swi5 and Ace2 enter the nucleus at about the time of anaphase (Figure 4.6a). On average, Swi5 nuclear entry precedes Ace2 nuclear entry by 2-3 minutes (Swi5 nuclear entry: 11.4±0.4 min before cytokinesis, Ace2 nuclear entry: 8.4±0.2 min before cytokinesis). A slightly longer (10 min) Ace2 delay relative to Swi5 entry was recently reported (Sbia et al., 2008). Swi5 is rapidly degraded and disappears 4 minutes before cytokinesis (Tebb et al., 1993), (Figure 4.6a). Ace2 remains in the nucleus for a longer period and is present in the daughter nucleus during G1 (for about 15 minutes) but quickly excluded from the mother nucleus (Colman-Lerner et al., 2001) (Figure 4.6a). Ash1 protein begins to accumulate a few minutes after Swi5 and Ace2 nuclear entry, and localizes to the nucleus slightly before cytokinesis, remaining until about the time of budding (Bobola et al., 1996), (Figure 4.6a).

The microarrays for wild-type cells show well defined M/G1 and G1/S clusters consistent with previous results (Spellman et al., 1998) (Figure 4.6b). Furthermore, well-characterized Ace2 and Ash1 targets, such as *CTS1* and *HO*, behave as expected upon transcription factor deletion or mislocalization (see Figure 4.6c). Cell-cycle-regulated

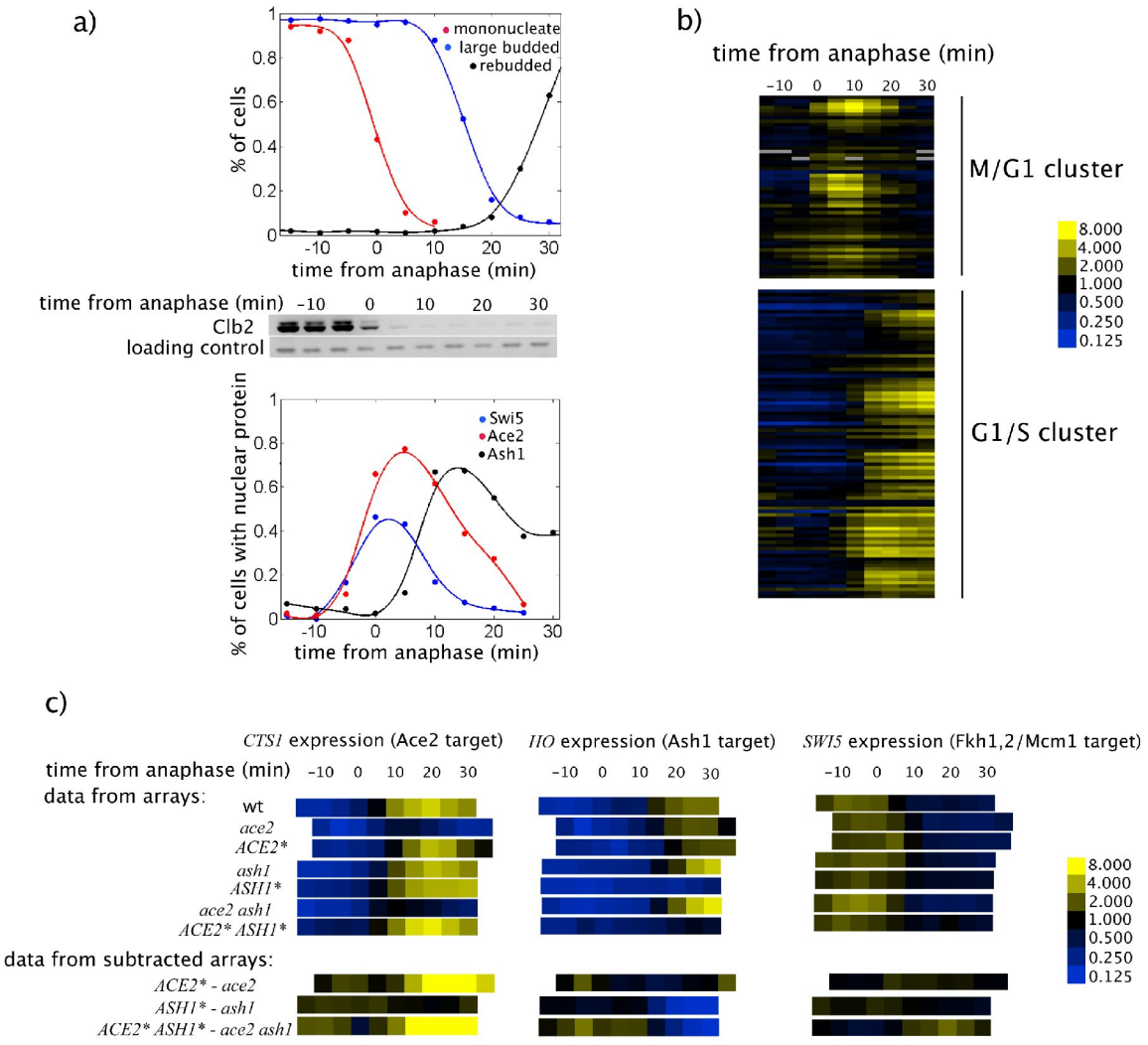

Figure 4.6 Genome-wide analyses of Ace2 and Ash1 targets. a) Analysis of cell cycle synchronization and nuclear localization of Ace2, Swi5 and Ash1 in a *cdc20* block-release experiment. Top panel shows the percentage of mononucleate cells, large budded cells and cells that have rebudded. The middle panel shows the levels of mitotic cyclin Clb2. The lower panel shows the dynamics of nuclear localization of fluorescently tagged Ace2, Swi5 and Ash1. b) Expression data from the M/G1 and G1/S cell cycle regulated cluster of genes. c) The regulation of *CTS1* (Ace2 target), *HO* (Ash1 target) and *SWI5* (Fkh1,2 Mcm1 target) expression from the microarray series, as well as data obtained by point-by-point subtraction of the arrays (*ACE2* - ace2*, *ASH1* - ash1*, *ACE2* ASH1* - ace2 ash1*) .

genes that are unaffected by the two transcription factors behave very similarly in all arrays (Figure 4.6c). Notice that the time of anaphase, which varies slightly between experiments, was used as the zero time to make the comparisons more accurate.

The high reproducibility of these microarray data allows us to do a time-point by time-point subtraction of the deletion mutant data from the mislocalization mutant data. This subtraction cancels out most of the cell-cycle-regulated changes in gene expression that are independent of Ace2 and/or Ash1, allowing the hierarchical clustering algorithm (Eisen et al., 1998) to efficiently detect changes that are specifically due to these transcription factors (see Figure 4.6c).

Clustering analysis of the subtracted data reveals a clear Ace2-dependent cluster composed of 12 genes: *PSA1*, *FAA3*, *EGT2 (EGT2* and *FAA3* expression is slightly dependent on Swi5), *DSE4*, *AMN1*, *PRY3*, *BUD9*, *SCW11*, *DSE1*, *DSE2*, *CTS1* and *SUN4*. Only two genes, *HO* and *PST1*, displayed strong changes in expression upon deletion or mislocalization of Ash1.

None of the genes whose expression is strongly Ace2- or Ash1-dependent is a known cell cycle regulator, suggesting that their misregulation is not likely to be responsible for cell-type-specific regulation of Start. We therefore performed a statistical analysis to obtain a list of genes regulated by both Ace2 and Ash1. We imposed an 'AND' logical condition that co-regulated targets should be detected as a differential signals in the subtracted *ace2* vs. *ACE2**, *ash1* vs. *ASH1** and *ace2 ash1* vs. *ACE2* ASH1**

comparisons. Additionally, we imposed a temporal requirement that the observed Ace2/Ash1-dependent changes in expression be observed only at times when these factors have accumulated in wild-type nuclei (Figure 4.6a). This criterion excludes genes whose changes in expression are long-term, indirect consequences of mutation of Ace2 or Ash1. Using a p-value cutoff sufficient for an expected false positive rate of less than one gene over the whole genome, we identified only 5 Ace2/Ash1 shared targets: *CLN3*, *HSP150*, *MET6*, *YRF1-1*, and *YRF1-5* (see Table 4.2 for details).

A direct interaction between Ace2 or Ash1 and the promoter of 3 of these genes (Ace2: *CLN3* and *HSP150*, Ash1: *YRF1-1*) has been previously observed in ChIP-chip experiments (Harbison et al., 2004; Simon et al., 2001), supporting the validity of our analysis. *YRF1* is a gene repeated 7 times in the yeast genome. While not perfectly conserved, the promoter regions of these 7 genes are very similar. The promoter region of *YRF1-5* is basically identical to that of *YRF1-1* (identical from -854 to +1), supporting its presence in our list. Ace2 has also been shown to bind to the *YRF1-2* promoter (Harbison et al., 2004).

Prominent in the list of genes affected by both Ace2 and Ash1 is the G1 cyclin, *CLN3*, a rate-limiting activator of the Start transition. This suggested the hypothesis that differential regulation of Start may be a consequence of differential regulation of *CLN3*.

Gene name	p-value in *ACE2**-*ace2* dataset	p-value in *ASH1**-*ash1* dataset	p-value in *ASH1* ACE2**-*ash1 ace2* dataset (see below)
CLN3	0.02	$4*10^{-4}$	0.04
HSP150	0.001	0.01	0.03
MET6	$4*10^{-6}$	0.01	0.04
YRF1-1	0.02	$2*10^{-4}$	0.04
YRF1-5	0.0068	$3*10^{-5}$	0.03

Table 4.2 Analysis of Ace2 and Ash1 shared targets. We report the p-values that the expression of listed genes is not affected by Ace2 and Ash1. For unknown experimental reasons the error bars on the *ASH1* ACE2*-ash1 ace2* dataset were on average two times bigger than the error bars on the *ACE2*-ace2* and *ASH1*-ash1* datasets.

Ace2 and Ash1 regulate the expression of G1 cyclin *CLN3*. *CLN3* expression in M/G1 is from 1.5 to 2.5 fold higher in *ash1 ace2* cells (pseudo-mothers) than in *ASH1* ACE2** cells (pseudo-daughters) (Figure 4.7a). While this change is small, *CLN3* is a highly dosage-sensitive activator of Start, with effects on cell size control detectable upon 2-fold changes up or down in gene dosage (McInerny et al., 1997; Nash et al., 1988). Therefore, this differential regulation could explain different T_1 times in wild-type mothers and daughters of similar size, as Cln3 controls T_1 (see Chapter 3). Differential regulation of *CLN3* was also observed in experiments with synchronized population of cells (MacKay et al., 2001; McInerny et al., 1997). In populations of cells containing both mothers and daughters, *CLN3* expression peaks at the M/G1 boundary (McInerny et al., 1997), while in populations of size-selected daughters *CLN3* expression peaks later in G1 (MacKay et al., 2001), consistent with our conclusion that *CLN*3 expression in M/G1 is higher in mothers than in daughters. M/G1 expression of *CLN*3 is driven by Mcm1

through early cell-cycle box (ECB) elements (McInerny et al., 1997); our results suggest that Ace2 and Ash1 antagonize this activation.

Analysis of *ace2* vs. *ACE2** arrays (Figure 4.7b) shows that *CLN3* behaves similarly to a cluster of nine strongly Swi5/Ace2-dependent genes (*YPL158C*, *PCL9*, *CYK3*, *NIS1*, *DSE3*, *SIC1*, *ASH1*, *PIR1*, *EXG1*). Expression of these genes in *ACE2** cells is lower than expression in *ace2* at 5 minutes after anaphase but similar at 10 minutes and higher from 15 minutes to 25 minutes (Figure 4.7e). This rather specific pattern is significantly different from a pattern assuming no regulation by Ace2 ($p<10^{-16}$). *CLN3* expression depends on Ace2 similarly to these other Swi5/Ace2 targets ($p=0.3$, Figure 4.7e); a model assuming that *CLN3* is not affected by Ace2 can be excluded ($p<0.03$, Figure 4.7f).

Ace2-dependent repression of *CLN3* was suggested previously based on analysis of a *CLN3pr-GFP* fusion (Laabs et al., 2003). Our data agree with this, and further suggest that the repression may be limited to a brief period after anaphase.

Microarrays of *swi5* vs. wild-type cells indicate that Swi5 activates *CLN3* expression, which is reduced by two fold in *swi5* cells (Figure 4.7d). Thus *CLN3* and a class of Ace2/Swi5 dependent genes follow a pattern consistent with early repression and late activation by Ace2, and with early activation by Swi5, likely acting in concert with ECB regulation (McInerny et al., 1997). We do not know the reason for this complex pattern; we speculate that Ace2 may be an intrinsically poorer activator than Swi5, but activates for a longer period due to its longer lifetime and nuclear residence. Swi5 disappears from

Figure 4.7 Ace2, Swi5 and Ash1 regulate the expression of the G1 cyclin *CLN3*. *CLN3* expression in *ACE2* ASH1** vs. *ace2 ash1* (a), *ACE2** vs. *ace2* (b), *ASH1** vs. *ash1* (c). d) Expression of Ace2 and Swi5-dependent cluster of genes. e) *CLN3* expression compared with the average expression of 9 strong Ace2 and Swi5-dependent genes from the dataset obtained by subtracting the *ACE2** data from the *ace2* data. f) *CLN3* expression compared with the average expression of the whole genome from the same dataset (i.e. *ace2* - *ACE2**). Chromatin immunoprecipitation (ChIP) analysis of the interaction between Swi5 (g), Ace2 (h) and the *CLN3* promoter. Following cross-linking and immunoprecipitation, DNA was amplified by PCR. Amplification of a region of the ORF of *DYN1* was used as negative control, while regions of the *SIC1* and *CTS1* promoters were used as positive controls for Swi5, Ace2 respectively. All the strains were TAP-tagged (NC=negative control from an untagged strain, WCE= whole cell extract). i) Representation of the Ace2/Swi5 and Ash1 putative binding sites on the *CLN3* promoter.

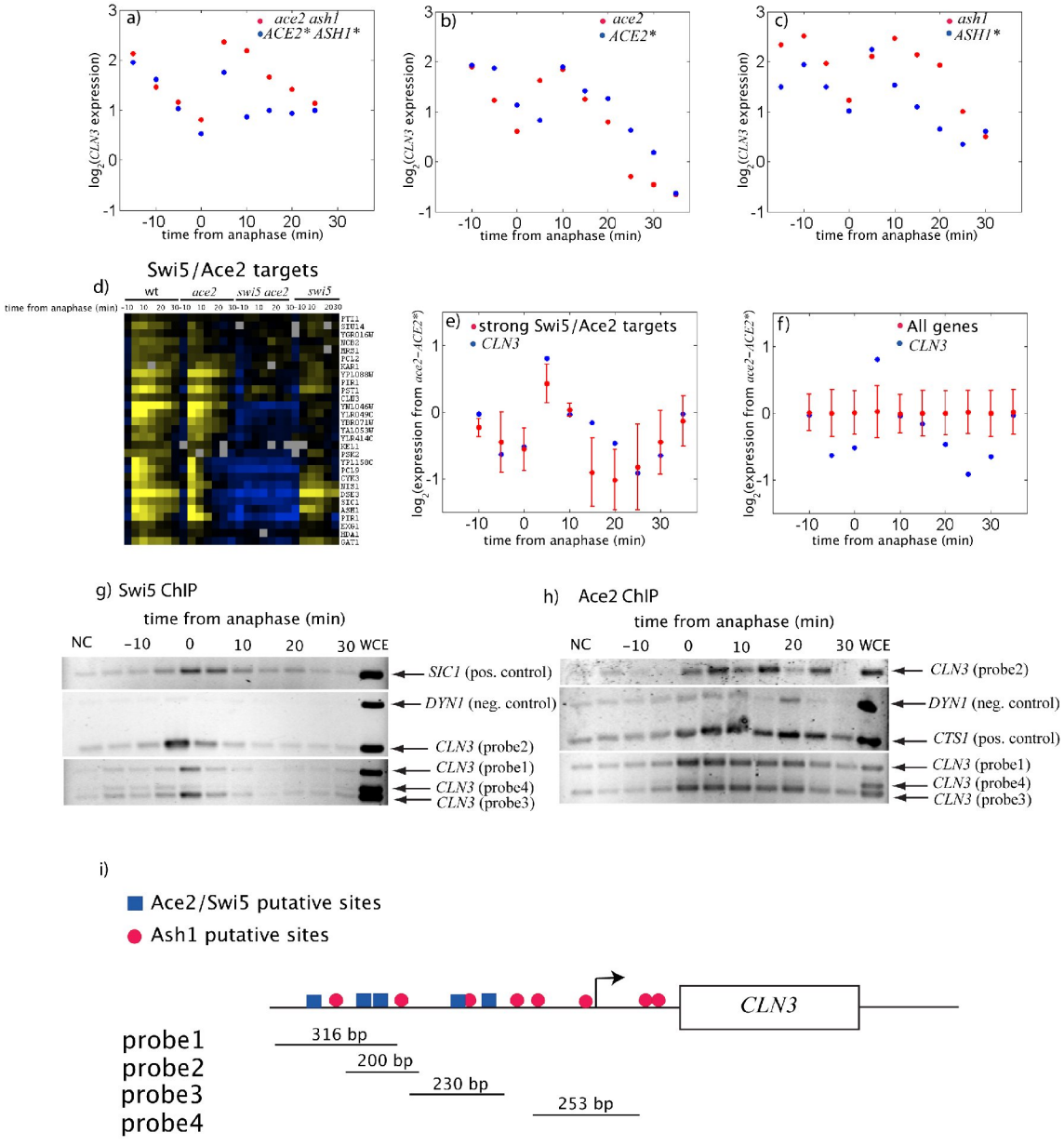
a)
ace2 ash1
ACE2* ASH1*
b)
ace2
ACE2*
c)
ash1
ASH1*
log2(CLN3 expression)
time from anaphase (min)
d)
Swi5/Ace2 targets
wt
ace2
swi5 ace2
swi5
time from anaphase (min)
e)
strong Swi5/Ace2 targets
CLN3
log2(expression from ace2-ACE2*)
f)
All genes
CLN3
g) Swi5 ChIP
time from anaphase (min)
NC
-10
0
10
20
30 WCE
SIC1 (pos. control)
DYN1 (neg. control)
CLN3 (probe2)
CLN3 (probe1)
CLN3 (probe4)
CLN3 (probe3)
h) Ace2 ChIP
time from anaphase (min)
NC
-10
0
10
20
30 WCE
CLN3 (probe2)
DYN1 (neg. control)
CTS1 (pos. control)
CLN3 (probe1)
CLN3 (probe4)
CLN3 (probe3)
i)
Ace2/Swi5 putative sites
Ash1 putative sites
CLN3
probe1
probe2
probe3
probe4
316 bp
200 bp
230 bp
253 bp

both mother and daughter nuclei a few minutes after anaphase, while Ace2 persists in daughter nuclei for about 20 min longer (Figure 4.6a). Competition between Ace2 and Swi5 for the same binding site (Dohrmann et al., 1992) could then contribute to the differential expression observed in these arrays.

Microarray analysis for *ash1* and *ASH1** shows that *CLN3* expression is repressed about two fold by Ash1 during the period from 10 minutes to 25 minutes after anaphase (Figure 4.7c). During this interval Ash1 is present in the nucleus (Figure 4.6a), suggesting that it could be a direct repressor of *CLN3* expression.

A substantial class of Swi5 and Ace2/Swi5 targets have higher expression in the absence of Ash1 (3 Swi5-specific genes: *CDC6*, *CHS1* and *YLR194C* and 29 genes co-activated by Ace2 and Swi5: *PTI1*, *SIW14*, *YGR016W*, *NCB2*, *MRS1*, *PCL2*, *KAR1*, *YPL088W*, *PIR1*, *PST1*, *CLN3*, *YNL046W*, *YLR049C*, *YBR071W*, *YAL053W*, *YLR414C*, *KEL1*, *PSK2*, *YPL158C*, *PCL9*, *CYK3*, *NIS1*, *DSE3*, *SIC1*, *ASH1*, *PIR1*, *EXG1*, *HDA1* and *GAT1*). The absolute repression of Swi5-dependent *HO* expression by Ash1 in daughter cells may thus be an enhancement of a common pattern of co-regulation.

Our data suggest that Ace2 and Ash1 may cooperate to repress *CLN3* expression in daughters. Consistently, activation of the G1/S regulon controlled by Cln3 is delayed and/or happens at larger cell size in *cdc20*-synchronized cells containing these factors (see Figure 4.9).

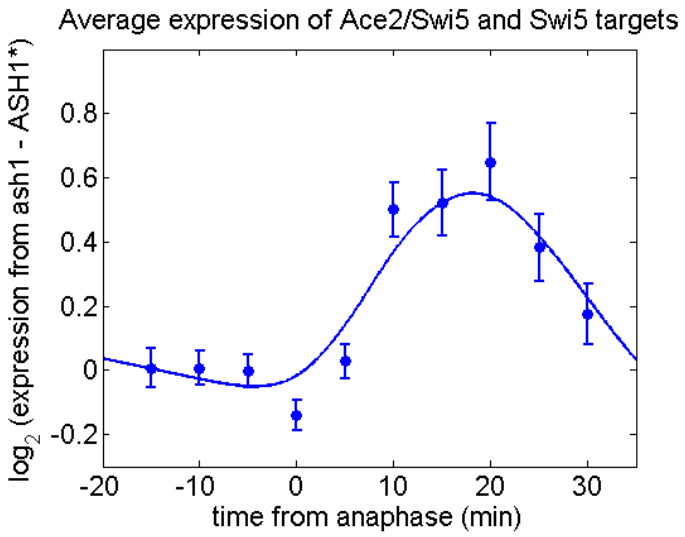

Figure 4.8 Ash1 is a modulator of Swi5-dependent expression. Average expression for Ace2/Swi5 and Swi5 targets (32 genes) in response to Ash1 (data were obtained by subtracting the *ASH1** dataset from *ash1* dataset). This graph shows that Ash1 weakly represses the expression of many Ace2/Swi5 and Swi5 targets in daughter cells.

Ace2 and Swi5 may be direct transcriptional regulators of *CLN3*. We performed chromatin immunoprecipitation (ChIP) experiments in synchronized cell populations, to test if Ace2, Swi5 and Ash1 bind to the *CLN3* promoter. Genome-wide localization data in asynchronous cell populations suggested binding of these factors to the *CLN3* promoter, but are statistically insufficient to definitively prove the association (Harbison et al., 2004; Simon et al., 2001). We used synchronized cell populations to provide dynamical information on the possible binding of Ace2, Swi5 and Ash1 to the *CLN3* promoter, providing a higher signal-to-noise ratio than can be obtained from asynchronous cells.

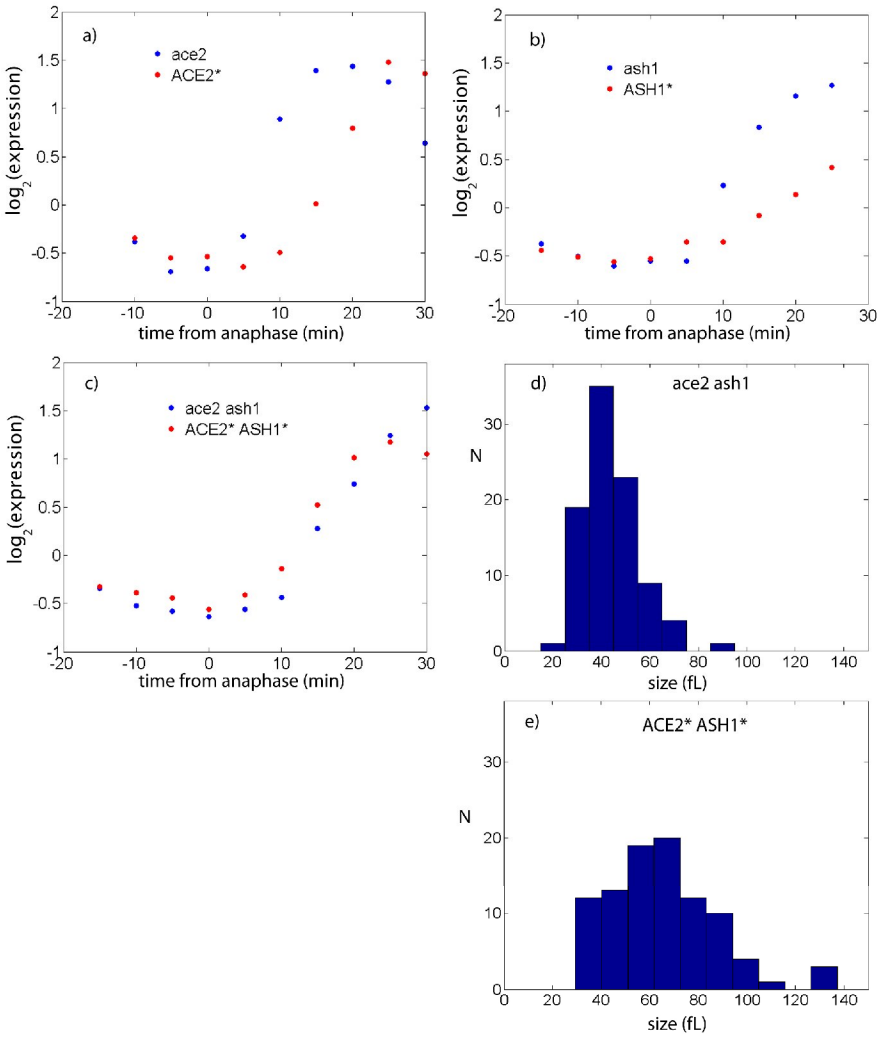

Figure 4.9 Activation of SBF and MBF is delayed by Ace2 and Ash1. Average expression of 20 SBF/MBF targets in a) *ace2* and *ACE2**, b) *ash1* and *ASH1**, c) *ace2 ash1* and *ACE2* ASH1** cells. Distribution of cell size at birth after release from the *cdc20* arrest for d) *ace2 ash1* and e) *ACE2* ASH1** cells.

Swi5 and Ace2 bound to regions in the *CLN3* promoter around the time of anaphase, coincident with their nuclear entry (Figures 4.7g, 4.7h). Swi5 is on the *CLN3* promoter for only a few minutes (Figure 4.7g), while Ace2 is on the *CLN3* promoter for about

20 minutes (Figure 4.7h), also consistent with the time of Swi5 and Ace2 nuclear localization (Figure 4.6a). Thus, Ace2 and Swi5 might regulate *CLN3* transcription by directly binding to multiple Ace2/Swi5 sites in the *CLN3* promoter (Figures 4.7g-4.7i).

We were unable to obtain reliable data on cell-cycle-specific Ash1 binding to either the *CLN3* promoter or the positive control *HO* promoter; therefore, we cannot assess if Ash1 binds directly to the *CLN3* promoter by this method.

Mutations of Ace2/Swi5 and Ash1 binding sites on the *CLN3* promoter reduce the asymmetry of Start regulation. We identified three candidate Ace2/Swi5 sites (GCTGG) (Harbison et al., 2004) in the *CLN3* promoter. We also identified two possible variant sites (GCTGA); such sites are over-represented in Ace2 and Swi5 targets (data not shown). There are eight candidate Ash1-binding sites (YTGAT) (Maxon and Herskowitz, 2001) in the *CLN3* promoter. We mutated the Ace2/Swi5 and/or the Ash1 putative binding sites in the *CLN3* promoter by exact gene replacement (see Chapter 2). Plots of αT_1 vs. $\ln(M_{birth})$ show that these mutations significantly reduce the T_1 delay in daughters compared to similarly sized mothers (Figure 4.10). This effect is especially notable in cells grown in glycerol-ethanol. Although these promoter mutations have strong effects, they are less potent than deletion of *ACE2* and *ASH1* (compare Figure 4.1 with Figure 4.10). This could reflect the presence of additional non-consensus Ace2 or Ash1 sites in the promoter. Additionally, the comparison between mutating Ace2 sites and deleting *ACE2* is not exact because removing Ace2 sites perforce also removes Swi5 sites. Ace2 and Ash1 could also have other indirect effects on *CLN3* expression, perhaps

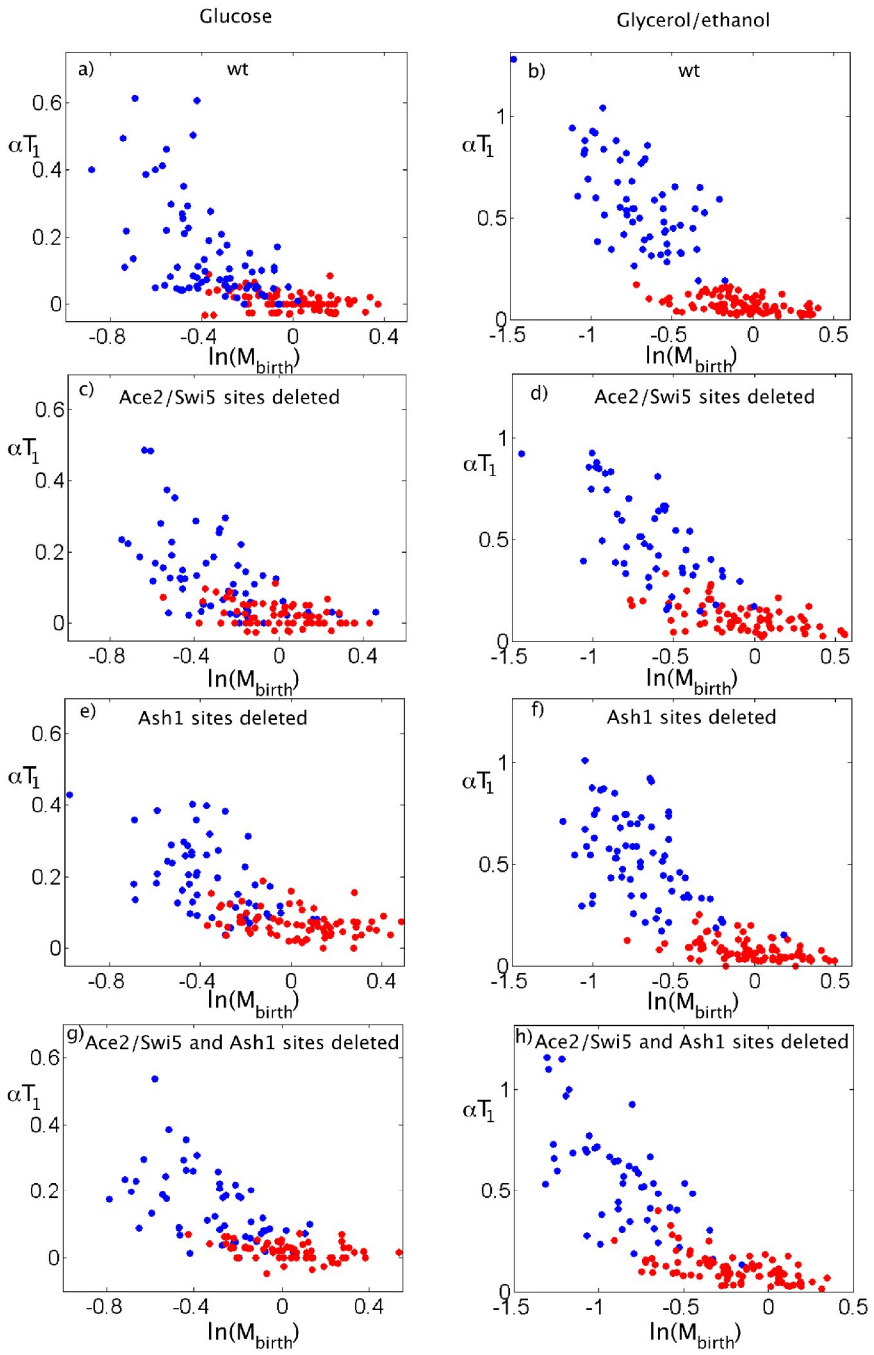

Figure 4.10 Deletion of the Ace2/Swi5 and Ash1 binding sites on the *CLN3* promoter reduces the asymmetrical regulation of Start. Correlation between αT_1 and ln (M_{birth}) for cells grown in glucose or glycerol/ethanol in mutants lacking the Ace2/Swi5 and/or Ash1 sites on the *CLN3* promoter. (a, b) wt, (c, d) Ace2/Swi5 sites deleted, (e, f) Ash1 sites deleted, (g, h) Ace2/Swi5 and Ash1 sites deleted. Red dots: mothers, blue dots: daughters.

working through the 'DDE' sites in the *CLN3* promoter, proposed by Laabs et al. (2003) as indirect Ace2 targets. Simultaneous deletion of Ace2 and Ash1 sites slightly enhanced the phenotype of deletion only of one or the other.

Still, the promoter mutants lacking Ace2/Swi5 sites and/or Ash1 sites strongly reduce asymmetry of control of Start by cell size in mothers and daughters, supporting the idea that Ace2/Ash1 directly repress *CLN3* expression in M/G1, accounting for a significant part of the regulation of G1 length by these transcription factors.

Asymmetric regulation of *CLN3* is required for asymmetric regulation of Start.

We analyzed the correlation between αT_1 and $\ln(M_{birth})$ (see above) in *cln3* cells, and in *cln3* cells expressing *CLN3* from constitutively active promoters. It is important for this analysis that the constitutive promoters provide expression levels of Cln3 similar to those in wild-type cells, and that the promoter-*CLN3* fusions complement the large-cell phenotype of *cln3* mutants, without 'overshoot' to a small-cell phenotype (Cross, 1988, 1989; Nash et al., 1988). We screened a number of different constitutive promoters of different strengths (N. Buchler, pers. comm.) for these properties, examining both cell size and Cln3 protein levels using myc-tagged Cln3, compared to wild-type (including a minor correction for cell cycle regulation of *CLN3* expression (Table 4.3) (McInerny et al., 1997)).

The *ACT1* and the *ADH1* promoters result in over-expression of Cln3 and in a small size phenotype for cells grown in glucose-containing media (Table 4.3). Expression of Cln3 from the *CDC28* promoter is weaker than expression from the *CLN3* promoter and results

in cell sizes bigger than wild-type and only slightly smaller than that of *cln3* cells (Table 4.3). Integration into the yeast genome of 6 copies of the *CDC28pr-CLN3* construct results in a cell size distribution similar to that of wt cells. We also analyzed the effects of these constructs in glycerol-ethanol medium. Four tandemly integrated copies of *CDC28pr-CLN3* results in an overall cell size distribution similar to that of wt cells in glycerol-ethanol. As a result of decreased *ADH1* expression in non-fermentable media (Denis et al., 1983), the *ADH1* promoter provides Cln3 levels similar to endogenous levels in glycerol-ethanol, resulting in a cell size distribution slightly (~ 10%) larger than wild-type (Table 4.3).

	wt	***cln3***	***CDC28pr-CLN3***	***ACT1pr-CLN3***	***ADH1pr-CLN3***
Cln3 levels in D	1	0	0.4-0.6	5-7	8-10
Cln3 levels in g/e	1	0	0.2-0.5	8-10	1.5-2.0
cell size in D (fl)	56	92	84	45	45
cell size in g/e (fl)	47	88	60	41	51

Table 4.3 Levels of Cln3 expression and average cell size for asynchronous cell populations expressing *CLN3* from various constitutive promoters. The expression of *CLN3* is cell cycle regulated with a peak in expression at M/G1 characterized by a peak to through ratio of order 3 ((McInerny et al., 1997), see Figure 4.7) . This suggests that constructs whose average expression is larger than 3 times the average expression of Cln3 are likely to be overexpressors.

Measurements of Cln3 protein levels show that Cln3 overexpressors were smaller than wt, and underexpressors larger (Table 4.3). Based on results with a single copy of

CDC28pr-CLN3-myc, 4-6 copies of *CDC28pr-CLN3* would be expected to produce approximately wt levels of Cln3 in M/G1, consistent with the observed cell size distributions (Table 4.3).

We therefore used strains containing 6*xCDC28pr-CLN3* in glucose medium, and strains containing 4*xCDC28pr-CLN3* or *ADH1pr-CLN3* in glycerol-ethanol medium to provide approximately endogenous levels of expression without mother-daughter asymmetry. In 6*xCDC28pr-CLN3* cells the daughter-specific delay is almost entirely abolished (Figures 4.11c, 4.11e and Table 4.3). Similarly, in 4*xCDC28pr-CLN3* and *ADH1pr-CLN3* cells grown in glycerol/ethanol, the daughter-specific delay is almost entirely abolished, and small mothers and daughter have similar size control properties (Figures 4.11d, 4.11f and 4.11g and Table 4.1). Thus, similarly to the results obtained by placing Ace2 and Ash1 in both mother and daughter nuclei, size control in small mother cells can be detected by eliminating differential mother-daughter control of *CLN3* expression.

Small *4xCDC28pr-CLN3* and *ADH1pr-CLN3* cells in glycerol/ethanol still exhibit strong size control (slopes of ~-0.8, compared to a theoretical expectation of -1) (Figures 4.11f, 4.11g) suggesting that while daughter-specific transcriptional regulation of *CLN3* by Ace2 and Ash1 specifies the daughter-specific set point in response to cell size, the intrinsic mechanism of size control is not dependent on *CLN3* transcription per se. We speculate that an M/G1 burst of *CLN3* expression from Mcm1 and/or Swi5 ((McInerny et al., 1997); Fig. 4.7) may be sufficient to drive cells rapidly through T_1, as is observed in

wild-type mothers of all sizes (Figures 4.1b, 4.1c; Chapter 3); in daughters, this burst may be suppressed by Ace2 and Ash1.

Remarkably, cells deleted for *cln3* still exhibit strong effects of cell size on G1 duration, although these effects are symmetrical between mothers and daughters of similar size (Figures 4.11c, 4.11d). This finding emphasizes that while cell size control set points are controlled by regulation of *CLN3*, there may be an underlying program of cell size control that is Cln3-independent.

Laabs et al. (2003) reported that *cln3* cells and cells expressing *CLN3* from ectopic promoters all had equal G1 durations for individual mother/daughter pairs. In our analysis, in almost all *cln3* mother-daughter pairs, with or without ectopic expression of *CLN3*, the daughters had a longer T_1 period. The symmetry that we observe in these mutants is only with respect to mothers and daughters of similar size (more precisely, in the mother and daughter plots of αT_1 vs $\ln(M_{birth})$, in regions where the domains of mothers and daughters overlap).

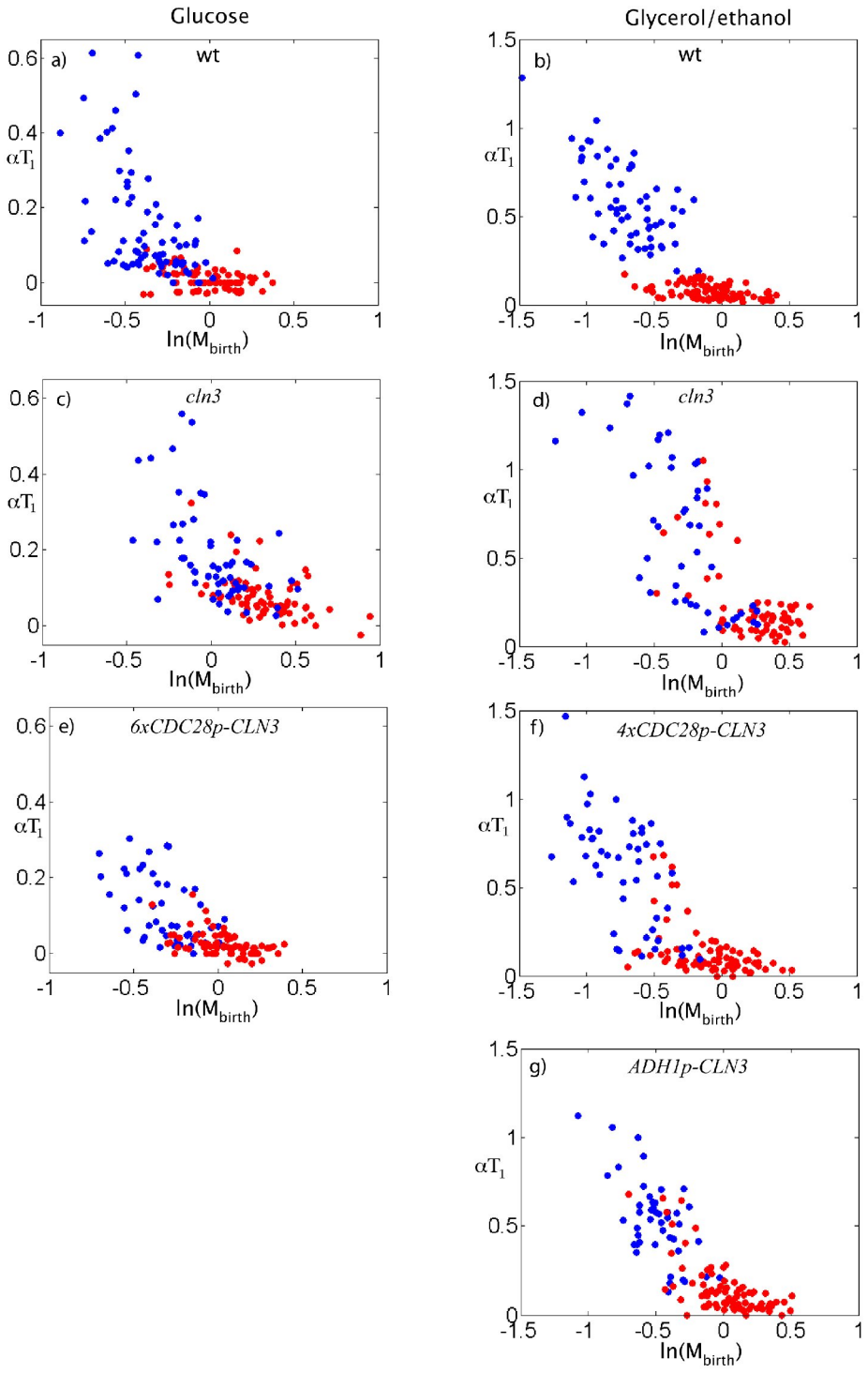

Figure 4.11 Symmetric regulation of *CLN3* expression results in symmetric control of Start in mothers and daughters. Correlation between αT_1 and ln (M_{birth}) for cells grown in glucose or glycerol/ethanol. (a, b) wt, (c, d) *cln3*, (e) *cln3 6xCDC28p-CLN3*, (f) *cln3 4xCDC28p-CLN3*, (g) *cln3 ADH1p-CLN3*. Red dots: mothers, blue dots: daughters.

Chapter 5: Discussion

The effects of molecular noise and cell size control on cell cycle variability in budding yeast. Molecular noise in gene expression can in principle be a major contributor of the variability of cellular systems (Samoilov et al., 2006). The role that this noise plays in natural eukaryotic circuits in physiological conditions remains unclear. The timing of cell cycle is variable and it is likely that both deterministic and stochastic elements contribute to this variability (Nurse, 1980). We have used single-cell imaging of fluorescently labeled budding yeast and a new metric for the analysis of size control to decompose the variability of the G1 phase into variability explained by deterministic size control and variability independent of cell size. Size-independent variability is reduced by ploidy, compatibly with the interpretation that its main source is molecular noise, and is the largest quantitative contributor to G1 variability. The observation that G1 variability is reduced by increasing the copy number of G1 cyclins, *CLN2* and *CLN3*, key rate-limiting regulators of the G1 transition, suggest that noise in their expression is one of the leading sources of variability in the timing of the G1 phase.

While molecular noise is the largest quantitative contributor of timing variability in G1, cell size control contributes significantly to the variability of daughter cells. This is due to the fact that small daughter cells display efficient size control. Cell size control seems to be independent of nutrient conditions, as cells grown in glucose and glycerol/ethanol show similar control properties.

Altogether, this analysis shows that molecular noise has a role in generating variability in a cellular transition; at the same time, we provide a precise quantitative framework demonstrating a deterministic contribution of cell size control to the same transition.

Control of the G1 phase is modular. By analyzing the nuclear localization of the transcriptional repressor Whi5, we have found that its nuclear exit marks a landmark event in the regulation of G1. Whi5 nuclear exit separates the control of G1 in two modules: a size-sensing module and a size-independent timing module. The first step depends on both Cln3 and cell size, and the second step depends on Cln2, but not on Cln3 and cell size. Temporal variability in the first step is due to the natural variability in cell size at birth coupled with size control, as well as molecular noise, possibly due to variability in *CLN3* expression. The duration of the second step is cell-size independent; its variability is affected by the expression of the G1 cyclin *CLN2*, one of the primary final effectors of Start. Thus, our analysis decompose the regulatory dynamics of G1 into two independent and functionally distinct modules, each of which is predominantly controlled by a different G1 cyclin.

Analysis of the dynamics of Whi5 nuclear exit indicates that the sharp transition between the two modules is ensured by positive feedback of Cln1 and Cln2 on their own transcription (see Chapter 3 and (Skotheim et al., 2008)). This switch-like nature of the Start transition may be important to ensure that cell cycle commitment is stable (Xiong and Ferrell, 2003).

Control of the G1 phase in mammalian cells may be characterized by a point of commitment similar to the Start event (Morgan, 2007). It would be interesting to see if the principles we have uncovered for the control of Start play an important role in the control of cell cycle initiation in mammalian cells.

Cell-type-specific Start control in the budding yeast cell cycle. Asymmetric localization of cell fate determinants during cell division is central to many developmental programs (Horvitz and Herskowitz, 1992). Asymmetric cell division often results in differential control of the cell cycle of the newborn cells (Horvitz and Herskowitz, 1992; Jensen et al., 2002; Knoblich, 2008; Roegiers and Jan, 2004).

In Chapter 4, we have shown that asymmetric localization of daughter-specific transcription factors, Ace2 and Ash1, results in differential regulation of the Start transition in the budding yeast cell cycle. In daughter cells, Ace2 and Ash1 alter the range of size over which cells display efficient size control, resulting in daughters requiring an extended period of growth compared to mothers of the same size. Mechanistically, this effect is primarily due to differential regulation of the G1 cyclin *CLN3*, whose expression is lower in daughter cells at the M/G1 boundary as a result of the presence of Ace2 and Ash1. In mothers, a 'burst' of *CLN3* activity is sufficient to drive them through Start even when they are small.

The biology of the budding process (Hartwell and Unger, 1977) ensures that mothers are almost always larger then daughters; in addition, mothers have necessarily already passed

size control, and lose little or no mass through the division process. As a consequence, wild-type mothers essentially never display size control by our metric, even though our analysis of 'pseudo-mothers' (daughter cells made mother-like by deletion of *ASH1* and *ACE2*) strongly suggests that mother cells do have potential 'cryptic' size control.

It was previously reported that asymmetric localization of Ace2 represses *CLN3* expression in daughter cells (Laabs et al., 2003). Our results differ from Laabs et al. (2003) in that we consider Ace2 regulation of *CLN3* to be direct rather than indirect; also, we incorporate interactions with Swi5 and Ash1 in *CLN3* regulation. Laabs et al. (2003) also proposed that the longer G1 of daughter cells is cell size-independent and solely a consequence of asymmetric localization of Ace2 (Laabs et al., 2003); our results show clearly that Ace2 and Ash1 shift the set point of cell size regulation, but strong size control is retained independent of these factors. Thus, our results integrate the importance of cell size in regulation of G1 length (see Chapter 3) with observations suggesting that asymmetric transcription factors control G1 length (Laabs et al., 2003).

A new link between differentiation and cell cycle in budding yeast. In wild-type homothallic budding yeast, only mother cells express the *HO* endonuclease and switch mating type due to Ash1 repression of *HO* expression in daughters (Bobola et al., 1996; Sil and Herskowitz, 1996). Phylogenetic analysis shows that in fungi, *ASH1* appeared before *HO*. This suggests that Ash1 may have other functions, predating mating type switching by *HO*, that may be important for asymmetrical cell division. It would be interesting to test whether Ash1 functions in cell cycle control in other fungi that can

divide asymmetrically, such as *Candida albicans*, which lacks an *HO* homolog but expresses an Ash1 homolog that localizes specifically to the daughter cells (Inglis and Johnson, 2002; Munchow et al., 2002). Ash1 also is found in *Ashbya gossypii*, which undergoes asynchronous division in a multinucleate syncitium (Gladfelter et al., 2006); it would be interesting to evaluate the role of Ash1 in this asynchrony.

Ace2 controls genes that confer diverse aspects of daughter cell biology (Colman-Lerner et al., 2001; Knapp et al., 1996; Wang et al., 2003); here we show that Ace2 also contributes to differential Start regulation in daughters.

Cell cycle regulation and cell differentiation are inter-regulated in many systems (Buttitta and Edgar, 2007; Jensen et al., 2002; Zhu and Skoultchi, 2001). As the decision of cells to differentiate is often made in G1, cell differentiation and commitment to a stable G1 are often coregulated (Buttitta and Edgar, 2007; Lasorella et al., 2006; Zhu and Skoultchi, 2001). It would be interesting to examine cases in which stem cells produce one proliferating cell and one daughter that differentiates in G1 (Knoblich, 2008); such cells might employ mechanisms similar to those we have uncovered in differential mother-daughter G1 control in budding yeast.

Appendix: Fluorescence-based measurements of cell size

Theoretical considerations. Here, we discuss how to measure single-cell growth using a stable fluorescent reporter expressed from a constitutively active promoter. We take R to be the amount of immature fluorescent protein, R^* to be the amount of fluorescing protein and define $k(R+R^*)$, where k is a constant, as cell size. The kinetics of maturation of R into R^* will be assumed to be first order with time constant τ, not negligible compared to cell doubling time. We concentrate on two simple mathematical models of cell growth: an exponential and a linear model. The exponential model is then the following:

$$\frac{dR}{dt} = \alpha(R + R^*) - \frac{1}{\tau}R$$
$$\frac{dR^*}{dt} = \frac{1}{\tau}R$$

The linear model is the following:

$$\frac{dR}{dt} = \alpha - \frac{1}{\tau}R$$
$$\frac{dR^*}{dt} = \frac{1}{\tau}R$$

The solution of these models requires the knowledge of the initial conditions R(0), $R^*(0)$. The only quantity accessible to experiments is R^*. This implies that a further condition is necessary to solve the models. We impose the condition that the ratio of

fluorescent and non-fluorescent proteins is constant at cell division: $R^*(0)/R(0)=R^*(T)/R(T)$, where 0 and T indicate the two successive division times. It is easy to show that the solution of the exponential model is given by: $R(t)=\alpha \tau R^*(0) e^{\alpha t}$, $R^*(t)=R^*(0) e^{\alpha t}$. This implies that for an exponential model the amount of fluorescent protein is proportional to cell size, defined as $k(R+R^*)$. If growth is exponential, then measures of R^* can be directly used to measure cell size. This is not true for the linear growth model, in which the ratio of R^* to R is not constant during the cell cycle. We will show below that the exponential growth model is a good model for single-cell growth in budding yeast and will therefore use R^* to measure cell size and ignore the correction necessary for linear growth.

Data analysis We measure cell size as the total cell fluorescence from DsRed protein expressed from the constitutively active *ACT1* promoter. Background autofluorescence was measured as the average fluorescence of unlabelled cells for each movie and subtracted from the measured pixel intensities of labeled cells. We observed almost no detectable red auto-fluorescence from unlabelled cells, so that the background could be well approximated by the zero of the camera. The objective depth of field, estimated to be 700-900 nm, was sufficiently large that the total cell fluorescence was only slightly affected (<7%) by displacement of the objective from the plane of focus up to a distance of 2 microns. This distance is larger than the typical error of the auto-focusing routine.

The growth of single cells as a function of time was well approximated by an exponential. Given the limited range of changes in cell size it is hard to distinguish

exactly between different growth laws. Fit to linear growth was slightly but consistently worse than an exponential fit ($\chi^2_{lin} \sim 1.2\ \chi^2_{exp}$) and a fit with two different lines (one from cell birth to bud and the other from bud to cell division, assuming a model in which DNA content is limiting for cell growth) was as good as an exponential fit ($\chi^2_{2lines} \sim \chi^2_{exp}$). However the two-slope fit has two more free parameters than an exponential fit (no continuity condition was imposed on the fit).

The measurement of cell size using total red fluorescence at each time point displayed an appreciable variability probably due to noise in the imaging process and errors in cell body segmentation (average deviation from exponential fit 6% of the average size at budding, Figure A1). The effect of this noise on size measurements was reduced by extracting cell size at a given time point from the fit of exponential cell growth, instead of using the value obtained for cell size at that frame (see Figure A1). To do this, a line was fit to the log of cell size as function of time by the least-squares method (there is no statistically significant deviation from linearity in these plots, as indicated by the fact that fits to higher order polynomials do not perform any better than a linear fit). The points (red points in Figures A1a, b, c) whose distance to the line was bigger than 2 standard deviations (from the distribution of distances from the fitted line) were excluded and the fit was repeated. The residuals of the fit are symmetric around zero and there is no tendency for errors to vary between early and late points. Hence we can conclude that there is no evidence for systematic errors and the error in size at birth or bud can be estimated by the error on the determination of the fit parameters and time frame.

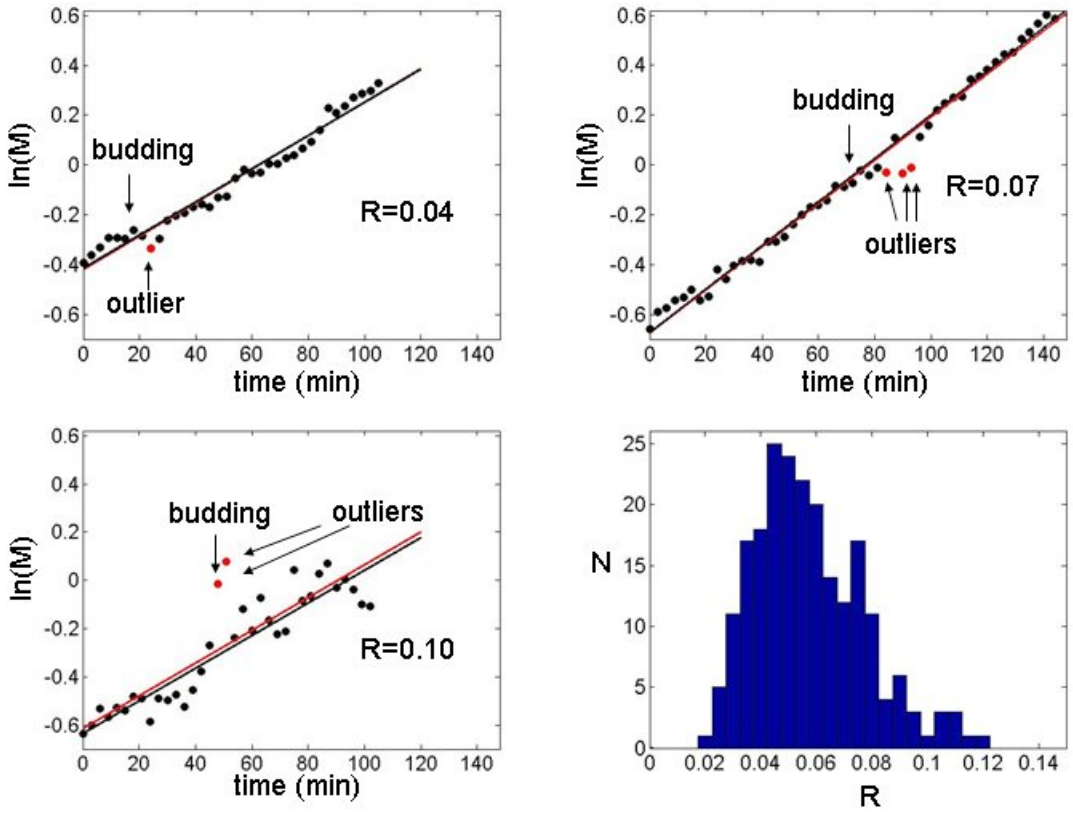

Figure A1 Examples of the linear fit of the logarithm of cell size, M, as a function of time and distribution of residual errors R. a), b) Examples of two fits considered good, c) example of a bad fit that was excluded from final tabulation in the data set. Time of budding is indicated with arrow. d) Distribution of the average distance, R, of points from the fit. The excluded fits with $R \geq 0.10$ account for about 5% of the total number of cells.

This procedure increases the accuracy of cell size determination by 3-fold on average (average error on single points 2% of the average size at budding).

Occasional bad fits (residual error $R \geq 0.10$) were omitted from the data (Figure A1d). Bad fits included about 5% of the data and were mostly restricted to cells at the end of the movie for which the segmentation software had trouble identifying the bud.

Comparison between fluorescence-based and geometrical determinations of cell size. To compare our fluorescence based method of cell size determination with the geometrical determination of cell size based on area (pixel number) within segmented cell boundaries, we computed R^2, the average square residual error, of an exponential fit using the two different measures (see Figures A2a, A2b). We found that the average R^2 of a fit using cell area or volume (estimated as $area^{3/2}$) is about 2.2 times bigger than the R^2 obtained by using total cell fluorescence (Figures A2c, A2d). Furthermore, individual growth rates extrapolated by using an exponential growth model for area or volume are not in perfect agreement with the population doubling time estimated by counting cell bodies. These observations indicate that neither area nor estimated volume is as good a measure of cell size as cell fluorescence using *ACT1pr-DsRed*. We also observe that the fluorescence measurement is more robust to changes in the position of the focal plane, does not necessitate a cell shape model and corrects for variation in vacuole size. We conclude that in our setup it is easier and more accurate to measure cell size with a fluorescent marker. On the other hand, our methods are not geared to the most accurate determination of cell volume from microscopic geometry, and while fluorescence, as we determine it, is a better measure than cell volume extracted directly from the automated segmenter, it is possible that another method measuring cell volume would be equivalent.

We have not explored this because of the ease and simplicity of our method, and its independence of the vacuole issue.

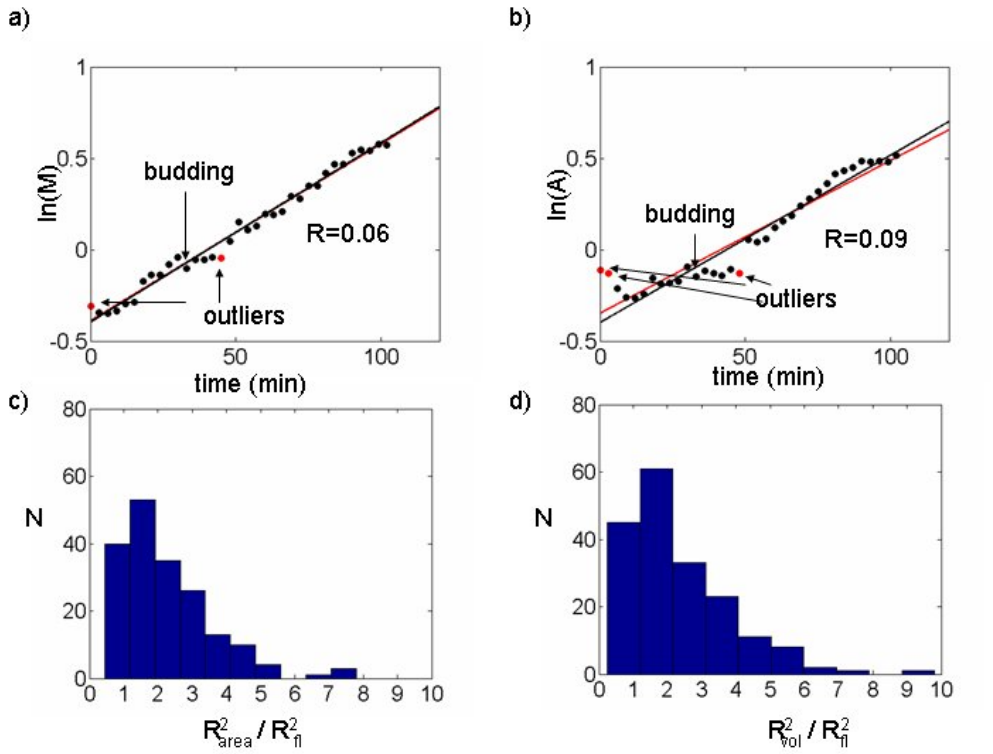

Figure A2 Fluorescence based measurements of cell size are more accurate than geometrical measurements. a) Example of a fit of the logarithm of cell size, M, measured by total cell fluorescence, as a function of time, b) fit of the logarithm of cell area, A, for the same cell as a function of time. c), d) Distribution of the ratio between the average square distance, R^2, of points from the fit of area (c) or volume (d) as a function of time and the average square distance, R^2, of points from the fit using total cell fluorescence, demonstrating almost uniformly better fits using fluorescence.

Variability of single-cell growth rate. The single-cell growth rate α, obtained by fitting ln(M) as a function of time as previously described, is moderately variable but

its average agrees well with the bulk culture growth rate (Table A1), supporting the validity of our fluorescence-based measurements of cell size.

The sources of the variability of α remain unknown. We observe that the variability (measured as standard deviation divided by the mean) is reduced by ploidy (Figure A3). This reduction is statistically significant but less than √2 for each doubling of the ploidy (Table A1). A speculation for the origin of the observed variability is that one or more organelles or macromolecular structures important for cell growth and present in not too high number are produced and partitioned noisily between the mother and daughter cell. The fact that there is not significant correlation between the growth rate of closely related cells (Figure A4) suggests that imprecision in the partitioning of these organelles is unlikely to be the major determinant of this noise. On the other hand, for few cells in which either the mother or the daughter is growing fast the other cell is significantly slower (cells off the diagonal in Figure A4d). This suggests that a fast-growing mother (daughter) may arise at the expense of a slow-growing daughter (mother). This inverse correlation in growth rates between fast mothers (daughters) and slow daughters (mothers) may in part be explained by imprecise partitioning of organelles present in small numbers.

It deserves to be mentioned that while the average growth rate in our setup for cells in glucose is 100 minutes we can observe occasional cells (about 5% in haploids) that double their mass in about 70 minutes. The fact that the fast-growing cells are

accompanied by slow growing ones could explain why yeast do not grow at this faster rate.

	Measured doubling time	**Doubling time predicted from individual cells growth rate**	**Coefficient of variation of growth rates**
wt haploids	99±1	100±1	0.18±0.02
wt diploids	95±1	93±1	0.14±0.01
wt tetraploids	101±2	97±2	0.13±0.01
6xCLN2	104±3	103±3	0.17±0.02
6xCLN3	103±1	105±2	0.21±0.03
6xCLN3 6xCLN2	106±3	107±3	0.17±0.03

Table A1 Comparison between colony doubling time and doubling time predicted from measurements of growth rate of individual cells. The table shows the mean +/- standard error of the mean in minutes.

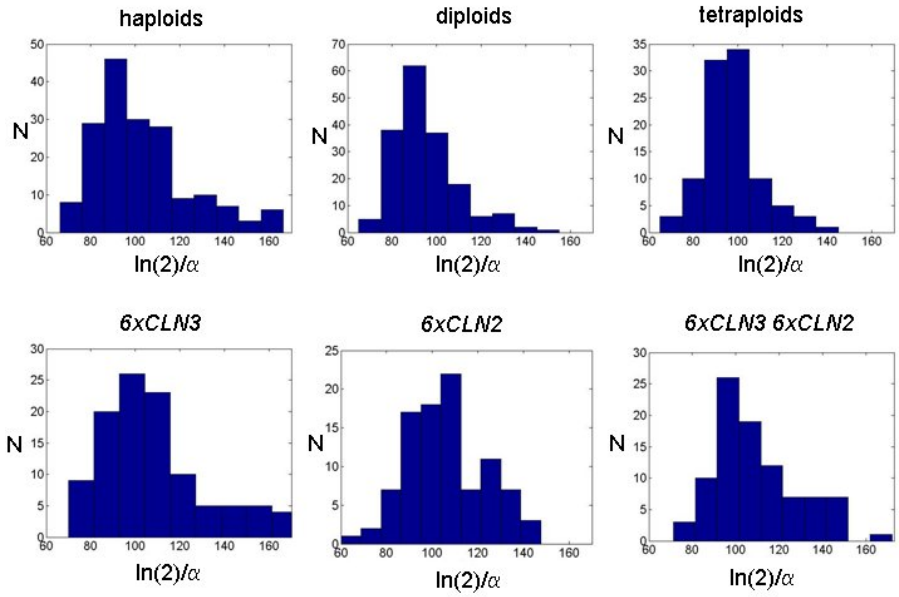

Figure A3 Distribution of growth rates for various strains. The average growth rate <α> agrees well with the colony growth rate (see Table A1).

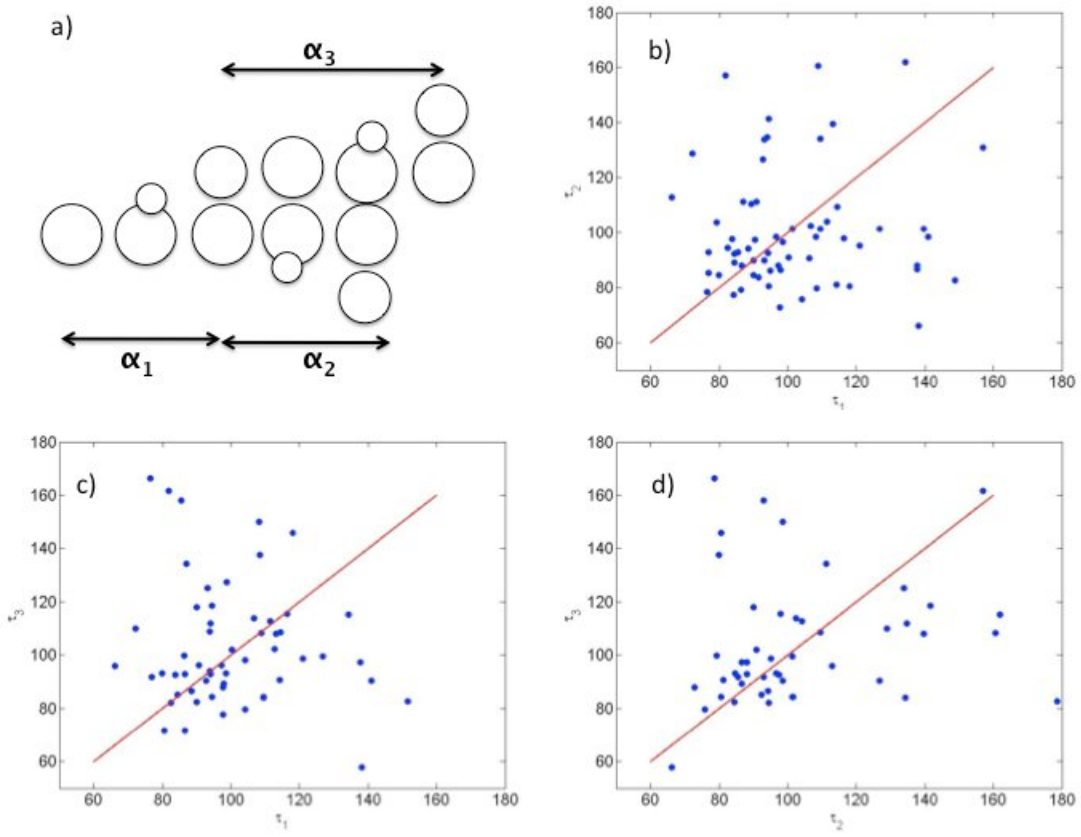

Figure A4 Growth rates of individual cells are not inherited. a) Schematics of growth rate inheritance analysis ($\tau=\ln(2)/\alpha$). b), c), d) Correlation between the growth rates of closely related cells. The red lines are the identity lines.

REFERENCES

Amon, A., Tyers, M., Futcher, B., and Nasmyth, K. (1993). Mechanisms that help the yeast cell cycle clock tick: G2 cyclins transcriptionally activate G2 cyclins and repress G1 cyclins. Cell *74*, 993-1007.

Bean, J.M., Siggia, E.D., and Cross, F.R. (2006). Coherence and timing of cell cycle start examined at single-cell resolution. Mol Cell *21*, 3-14.

Bi, E., Maddox, P., Lew, D.J., Salmon, E.D., McMillan, J.N., Yeh, E., and Pringle, J.R. (1998). Involvement of an actomyosin contractile ring in Saccharomyces cerevisiae cytokinesis. J Cell Biol *142*, 1301-1312.

Bobola, N., Jansen, R.P., Shin, T.H., and Nasmyth, K. (1996). Asymmetric accumulation of Ash1p in postanaphase nuclei depends on a myosin and restricts yeast mating-type switching to mother cells. Cell *84*, 699-709.

Buttitta, L.A., and Edgar, B.A. (2007). Mechanisms controlling cell cycle exit upon terminal differentiation. Curr Opin Cell Biol *19*, 697-704.

Chartrand, P., Meng, X.H., Huttelmaier, S., Donato, D., and Singer, R.H. (2002). Asymmetric sorting of ash1p in yeast results from inhibition of translation by localization elements in the mRNA. Mol Cell *10*, 1319-1330.

Colman-Lerner, A., Chin, T.E., and Brent, R. (2001). Yeast Cbk1 and Mob2 activate daughter-specific genetic programs to induce asymmetric cell fates. Cell *107*, 739-750.

Cosma, M.P. (2004). Daughter-specific repression of Saccharomyces cerevisiae HO: Ash1 is the commander. EMBO Rep *5*, 953-957.

Costanzo, M., Nishikawa, J.L., Tang, X., Millman, J.S., Schub, O., Breitkreuz, K., Dewar, D., Rupes, I., Andrews, B., and Tyers, M. (2004). CDK activity antagonizes Whi5, an inhibitor of G1/S transcription in yeast. Cell *117*, 899-913.

Cross, F.R. (1988). DAF1, a mutant gene affecting size control, pheromone arrest, and cell cycle kinetics of Saccharomyces cerevisiae. Mol Cell Biol *8*, 4675-4684.

Cross, F.R. (1989). Further characterization of a size control gene in Saccharomyces cerevisiae. J Cell Sci Suppl *12*, 117-127.

Cross, F.R. (1995). Starting the cell cycle: what's the point? Curr Opin Cell Biol *7*, 790-797.

de Bruin, R.A., Kalashnikova, T.I., Chahwan, C., McDonald, W.H., Wohlschlegel, J., Yates, J., 3rd, Russell, P., and Wittenberg, C. (2006). Constraining G1-specific

transcription to late G1 phase: the MBF-associated corepressor Nrm1 acts via negative feedback. Mol Cell *23*, 483-496.

de Bruin, R.A., McDonald, W.H., Kalashnikova, T.I., Yates, J., 3rd, and Wittenberg, C. (2004). Cln3 activates G1-specific transcription via phosphorylation of the SBF bound repressor Whi5. Cell *117*, 887-898.

Denis, C.L., Ferguson, J., and Young, E.T. (1983). mRNA levels for the fermentative alcohol dehydrogenase of Saccharomyces cerevisiae decrease upon growth on a nonfermentable carbon source. J Biol Chem *258*, 1165-1171.

Di Talia, S., Skotheim, J.M., Bean, J.M., Siggia, E.D., and Cross, F.R. (2007). The effects of molecular noise and size control on variability in the budding yeast cell cycle. Nature *448*, 947-951.

Dirick, L., Bohm, T., and Nasmyth, K. (1995). Roles and regulation of Cln-Cdc28 kinases at the start of the cell cycle of Saccharomyces cerevisiae. EMBO J *14*, 4803-4813.

Dohrmann, P.R., Butler, G., Tamai, K., Dorland, S., Greene, J.R., Thiele, D.J., and Stillman, D.J. (1992). Parallel pathways of gene regulation: homologous regulators SWI5 and ACE2 differentially control transcription of HO and chitinase. Genes Dev *6*, 93-104.

Donnan, L., and John, P.C. (1983). Cell cycle control by timer and sizer in Chlamydomonas. Nature *304*, 630-633.

Eisen, M.B., Spellman, P.T., Brown, P.O., and Botstein, D. (1998). Cluster analysis and display of genome-wide expression patterns. Proc Natl Acad Sci U S A *95*, 14863-14868.

Elliott, S.G., and McLaughlin, C.S. (1978). Rate of macromolecular synthesis through the cell cycle of the yeast Saccharomyces cerevisiae. Proc Natl Acad Sci U S A *75*, 4384-4388.

Gladfelter, A.S., Hungerbuehler, A.K., and Philippsen, P. (2006). Asynchronous nuclear division cycles in multinucleated cells. J Cell Biol *172*, 347-362.

Han, B.K., Aramayo, R., and Polymenis, M. (2003). The G1 cyclin Cln3p controls vacuolar biogenesis in Saccharomyces cerevisiae. Genetics *165*, 467-476.

Harbison, C.T., Gordon, D.B., Lee, T.I., Rinaldi, N.J., Macisaac, K.D., Danford, T.W., Hannett, N.M., Tagne, J.B., Reynolds, D.B., Yoo, J., *et al.* (2004). Transcriptional regulatory code of a eukaryotic genome. Nature *431*, 99-104.

Hartwell, L.H., and Unger, M.W. (1977). Unequal division in Saccharomyces cerevisiae and its implications for the control of cell division. J Cell Biol *75*, 422-435.

Holstege, F.C., Jennings, E.G., Wyrick, J.J., Lee, T.I., Hengartner, C.J., Green, M.R., Golub, T.R., Lander, E.S., and Young, R.A. (1998). Dissecting the regulatory circuitry of a eukaryotic genome. Cell *95*, 717-728.

Horvitz, H.R., and Herskowitz, I. (1992). Mechanisms of asymmetric cell division: two Bs or not two Bs, that is the question. Cell *68*, 237-255.

Inglis, D.O., and Johnson, A.D. (2002). Ash1 protein, an asymmetrically localized transcriptional regulator, controls filamentous growth and virulence of Candida albicans. Mol Cell Biol *22*, 8669-8680.

Jensen, R.B., Wang, S.C., and Shapiro, L. (2002). Dynamic localization of proteins and DNA during a bacterial cell cycle. Nat Rev Mol Cell Biol *3*, 167-176.

Johnston, G.C., Pringle, J.R., and Hartwell, L.H. (1977). Coordination of growth with cell division in the yeast Saccharomyces cerevisiae. Exp Cell Res *105*, 79-98.

Jorgensen, P., and Tyers, M. (2004). How cells coordinate growth and division. Curr Biol *14*, R1014-1027.

Knapp, D., Bhoite, L., Stillman, D.J., and Nasmyth, K. (1996). The transcription factor Swi5 regulates expression of the cyclin kinase inhibitor p40SIC1. Mol Cell Biol *16*, 5701-5707.

Knoblich, J.A. (2008). Mechanisms of asymmetric stem cell division. Cell *132*, 583-597.

Koch, C., Schleiffer, A., Ammerer, G., and Nasmyth, K. (1996). Switching transcription on and off during the yeast cell cycle: Cln/Cdc28 kinases activate bound transcription factor SBF (Swi4/Swi6) at start, whereas Clb/Cdc28 kinases displace it from the promoter in G2. Genes Dev *10*, 129-141.

Laabs, T.L., Markwardt, D.D., Slattery, M.G., Newcomb, L.L., Stillman, D.J., and Heideman, W. (2003). ACE2 is required for daughter cell-specific G1 delay in Saccharomyces cerevisiae. Proc Natl Acad Sci U S A *100*, 10275-10280.

Lasorella, A., Stegmuller, J., Guardavaccaro, D., Liu, G., Carro, M.S., Rothschild, G., de la Torre-Ubieta, L., Pagano, M., Bonni, A., and Iavarone, A. (2006). Degradation of Id2 by the anaphase-promoting complex couples cell cycle exit and axonal growth. Nature *442*, 471-474.

Lord, P.G., and Wheals, A.E. (1981). Variability in individual cell cycles of Saccharomyces cerevisiae. J Cell Sci *50*, 361-376.

Lord, P.G., and Wheals, A.E. (1983). Rate of cell cycle initiation of yeast cells when cell size is not a rate-determining factor. J Cell Sci *59*, 183-201.

MacKay, V.L., Mai, B., Waters, L., and Breeden, L.L. (2001). Early cell cycle box-mediated transcription of CLN3 and SWI4 contributes to the proper timing of the G(1)-to-S transition in budding yeast. Mol Cell Biol *21*, 4140-4148.

Mangan, S., and Alon, U. (2003). Structure and function of the feed-forward loop network motif. Proc Natl Acad Sci U S A *100*, 11980-11985.

Maxon, M.E., and Herskowitz, I. (2001). Ash1p is a site-specific DNA-binding protein that actively represses transcription. Proc Natl Acad Sci U S A *98*, 1495-1500.

Mazanka, E., Alexander, J., Yeh, B.J., Charoenpong, P., Lowery, D.M., Yaffe, M., and Weiss, E.L. (2008). The NDR/LATS family kinase Cbk1 directly controls transcriptional asymmetry. PLoS Biol *6*, e203.

McBride, H.J., Yu, Y., and Stillman, D.J. (1999). Distinct regions of the Swi5 and Ace2 transcription factors are required for specific gene activation. J Biol Chem *274*, 21029-21036.

McInerny, C.J., Partridge, J.F., Mikesell, G.E., Creemer, D.P., and Breeden, L.L. (1997). A novel Mcm1-dependent element in the SWI4, CLN3, CDC6, and CDC47 promoters activates M/G1-specific transcription. Genes Dev *11*, 1277-1288.

Morgan, D.O. (2007). The Cell Cycle: Principles of control (London, New Science Press).

Mumberg, D., Muller, R., and Funk, M. (1994). Regulatable promoters of Saccharomyces cerevisiae: comparison of transcriptional activity and their use for heterologous expression. Nucleic Acids Res *22*, 5767-5768.

Munchow, S., Ferring, D., Kahlina, K., and Jansen, R.P. (2002). Characterization of Candida albicans ASH1 in Saccharomyces cerevisiae. Curr Genet *41*, 73-81.

Nash, R., Tokiwa, G., Anand, S., Erickson, K., and Futcher, A.B. (1988). The WHI1+ gene of Saccharomyces cerevisiae tethers cell division to cell size and is a cyclin homolog. EMBO J *7*, 4335-4346.

Nurse, P. (1975). Genetic control of cell size at cell division in yeast. Nature *256*, 547-551.

Nurse, P. (1980). Cell cycle control--both deterministic and probabilistic? Nature *286*, 9-10.

Oliva, A., Rosebrock, A., Ferrezuelo, F., Pyne, S., Chen, H., Skiena, S., Futcher, B., and Leatherwood, J. (2005). The cell cycle-regulated genes of Schizosaccharomyces pombe. PLoS Biol *3*, e225.

Racki, W.J., Becam, A.M., Nasr, F., and Herbert, C.J. (2000). Cbk1p, a protein similar to the human myotonic dystrophy kinase, is essential for normal morphogenesis in Saccharomyces cerevisiae. EMBO J *19*, 4524-4532.

Roegiers, F., and Jan, Y.N. (2004). Asymmetric cell division. Curr Opin Cell Biol *16*, 195-205.

Samoilov, M.S., Price, G., and Arkin, A.P. (2006). From fluctuations to phenotypes: the physiology of noise. Sci STKE *2006*, re17.

Sbia, M., Parnell, E.J., Yu, Y., Olsen, A.E., Kretschmann, K.L., Voth, W.P., and Stillman, D.J. (2008). Regulation of the yeast Ace2 transcription factor during the cell cycle. J Biol Chem *283*, 11135-11145.

Schroedinger, E. (1944). What is Life? (Cambridge, Cambridge University Press).

Sil, A., and Herskowitz, I. (1996). Identification of asymmetrically localized determinant, Ash1p, required for lineage-specific transcription of the yeast HO gene. Cell *84*, 711-722.

Simon, I., Barnett, J., Hannett, N., Harbison, C.T., Rinaldi, N.J., Volkert, T.L., Wyrick, J.J., Zeitlinger, J., Gifford, D.K., Jaakkola, T.S., *et al.* (2001). Serial regulation of transcriptional regulators in the yeast cell cycle. Cell *106*, 697-708.

Skotheim, J.M., Di Talia, S., Siggia, E.D., and Cross, F.R. (2008). Positive feedback of G1 cyclins ensures coherent cell cycle entry. Nature *454*, 291-296.

Spellman, P.T., Sherlock, G., Zhang, M.Q., Iyer, V.R., Anders, K., Eisen, M.B., Brown, P.O., Botstein, D., and Futcher, B. (1998). Comprehensive identification of cell cycle-regulated genes of the yeast Saccharomyces cerevisiae by microarray hybridization. Mol Biol Cell *9*, 3273-3297.

Spudich, J.L., and Koshland, D.E., Jr. (1976). Non-genetic individuality: chance in the single cell. Nature *262*, 467-471.

Stuart, D., and Wittenberg, C. (1995). CLN3, not positive feedback, determines the timing of CLN2 transcription in cycling cells. Genes Dev *9*, 2780-2794.

Sveiczer, A., Novak, B., and Mitchison, J.M. (1996). The size control of fission yeast revisited. J Cell Sci *109 (Pt 12)*, 2947-2957.

Tebb, G., Moll, T., Dowzer, C., and Nasmyth, K. (1993). SWI5 instability may be necessary but is not sufficient for asymmetric HO expression in yeast. Genes Dev *7*, 517-528.

Tyers, M., Tokiwa, G., and Futcher, B. (1993). Comparison of the Saccharomyces cerevisiae G1 cyclins: Cln3 may be an upstream activator of Cln1, Cln2 and other cyclins. EMBO J *12*, 1955-1968.

Voth, W.P., Yu, Y., Takahata, S., Kretschmann, K.L., Lieb, J.D., Parker, R.L., Milash, B., and Stillman, D.J. (2007). Forkhead proteins control the outcome of transcription factor binding by antiactivation. EMBO J *26*, 4324-4334.

Wang, Y., Shirogane, T., Liu, D., Harper, J.W., and Elledge, S.J. (2003). Exit from exit: resetting the cell cycle through Amn1 inhibition of G protein signaling. Cell *112*, 697-709.

Weiss, E.L., Kurischko, C., Zhang, C., Shokat, K., Drubin, D.G., and Luca, F.C. (2002). The Saccharomyces cerevisiae Mob2p-Cbk1p kinase complex promotes polarized growth and acts with the mitotic exit network to facilitate daughter cell-specific localization of Ace2p transcription factor. J Cell Biol *158*, 885-900.

Wheals, A.E. (1982). Size control models of Saccharomyces cerevisiae cell proliferation. Mol Cell Biol *2*, 361-368.

Wijnen, H., Landman, A., and Futcher, B. (2002). The G(1) cyclin Cln3 promotes cell cycle entry via the transcription factor Swi6. Mol Cell Biol *22*, 4402-4418.

Wittenberg, C., and Reed, S.I. (2005). Cell cycle-dependent transcription in yeast: promoters, transcription factors, and transcriptomes. Oncogene *24*, 2746-2755.

Xiong, W., and Ferrell, J.E., Jr. (2003). A positive-feedback-based bistable 'memory module' that governs a cell fate decision. Nature *426*, 460-465.

Zhu, L., and Skoultchi, A.I. (2001). Coordinating cell proliferation and differentiation. Curr Opin Genet Dev *11*, 91-97.